OUKA
Osaka University Knowledge Archive

Title	Development of Evaluation Model for Self-Wastage Phenomena in Steam Generator of Sodium-Cooled Fast Reactor
Author(s)	張, 承賢
Citation	大阪大学, 2015, 博士論文
Version Type	VoR
URL	https://doi.org/10.18910/53976
rights	
Note	

Osaka University Knowledge Archive : OUKA

https://ir.library.osaka-u.ac.jp/

Osaka University

Doctoral Dissertation

Development of Evaluation Model for Self-Wastage Phenomena in Steam Generator of Sodium-Cooled Fast Reactor

Sunghyon Jang

JUNE 2015

Graduate School of Engineering,
Osaka University

Development of Evaluation Model for Self-Wastage Phenomena in Steam Generator of Sodium-cooled Fast Reactor

Sunghyon Jang

Abstract

Sodium-cooled fast breeder reactor uses liquid sodium as a moderator and coolant to transfer a heat from reactor core. The main hazard associated with sodium is the vigorous reaction with water. Sodium-water reaction (SWR) takes place when water or vapor leak into sodium side through a crack on a heat transfer tube in a steam generator. The reaction is highly exothermic. Thus, if a water leakage continues, the SWR deteriorates the tube wall by corrosive reaction products such as sodium hydroxide (NaOH). At the same time, a high-pressure water and vapor peel out the weakened material from the surface. As a result the crack is enlarged. This enlargement of the crack is called 'Self-wastage phenomena'. If the tube wall is penetrated by the self-wastage, the leak rate will dramatically increase. It has the possibility that an increased resultant leak damage neighboring heat transfer tubes, it might lead to secondary failure. Therefore, a description of the SWR is an essential issue for safety design of steam generator in a sodium cooled fast breeder reactor.

So far in order to depict the self-wastage phenomena and evaluate the phenomena quantitatively mock-up tests were carried out. However, uncertainties due to immature measurement technology, opacity of liquid sodium and many related parameters made difficult to obtain data with high spatial resolution and accuracy. Thus, an experimental approach is not sufficient to give us a clear understanding about the phenomena.

Accordingly, we have elaborated alternative ways to evaluate the self-wastage phenomena using a computational code of multi-component multi-phase flow involving sodium-water chemical reaction, SERAPHIM (Sodium watEr Reaction Analysis PHysics of Interdisciplinary Multi-phase flow). We compromised an evaluation model which consists of 5 steps of numerical procedures. Based on the developed scheme, a benchmark analysis of SWAT (Small leak sodium-Water reAction Test loop) experiment has been carried out to validate the feasibility of the new method. Numerical results show that the enlarged opening appears to taper inward to a significantly smaller opening on the inside of the tube wall. The outer diameter is 4.72 mm. The outer diameter of SWAT experimental result is 4.96 mm. Also the shape of enlarged nozzle of the SWAT experiment has similarity with the numerical result. Thus, the numerical benchmark

analysis demonstrates the applicability of the self-wastage evaluation model to evaluate the self-wastage phenomena.

Another approach to understand the behavior of the self-wastage, simulated experiment is devised. Since the self-wastage phenomena is attributed to interaction between a wall material and an exothermic chemical reaction which takes place at nozzle exit. We adopt hydrochloric acid and sodium hydroxide solution and paraffin were as candidate materials. We assume that melting of nozzle surface of paraffin wax by the reaction heat released by the neutralization reaction represents the self-wastage phenomena. Through a numerical feasibility analysis, it is demonstrated that the maximum temperature at the surface is high enough to melt paraffin surface. Like the self-wastage phenomena propagation, a propagation of melting also take place around nozzle exist then, it advances through the tube wall toward the inlet direction. The resultant shape of enlarged nozzle of simulant experiment has similarity with the SWAT experiment. Thus, the simulant experiment shows its applicability on evaluation of the behavior of the self-wastage phenomena.

Finally, we consider influence of some parameters on the phenomena. Analyses of the influence of average leak rate and initial leak diameter on the self-wastage behavior are carried out using reference experimental data. It is found that the average leak rate strongly related to the self-wastage rate and both the initial leak diameter and average leak rate has a negative reciprocal relationship with the enlargement ratio.

These studies suggests new approaches to deepen our understanding about the behavior of the self-wastage phenomena and evaluate the self-wastage phenomena. Numerical analysis using SERAPHIM code and simulant experiment is also a good alternative way to expect the self-wastage phenomena behavior. It is expected that further researches through these method deepen our understanding about the self-wastage behavior and give us a chance for quantitative self-wastage evaluation.

Table of Contents

List of Tables

Chapter 1

Chapter 2

Chapter 3

List of Figures

Chapter 1

Chapter 2

Chapter 3

Chapter 4

1. Introduction

1.1 Fast Reactor and Its system

1.1.1 Fast reactor and its coolant

Natural uranium consists of two isotopes: ^{235}U (with an abundance of 0.7%) and ^{238}U (99.3%). Of the two ^{235}U is "fissile", which means that fission can be induced by bombarding it with neutrons of any energy. On the other hand ^{238}U undergoes fission can only if the bombarding neutrons have an energy greater than 1.5 MeV, and even then they are more likely to be captured or scattered inelastically.

Neutrons generated in fission have average energies of about 2 MeV, and cannot sustain a chain reaction in natural Uranium. Since in natural uranium, where the high fission cross-section of ^{235}U compensates for its low abundance, the probability of fission outweighs that of capture for neutrons with energy less than about. 0.1 eV. If a chain reaction is to take place, the kinetic energy of a neutron has to be reduced in energy until it is in thermal equilibrium with the atoms. It is then known as a "thermal" neutron, and at room temperature its most probable energy is about 0.025 eV.

When ^{238}U captures a fast neutron that have an energy greater than 1.5 MeV, the ^{239}U nucleus formed decays in the following way [1]:

$$^{238}U \xrightarrow{\beta^-} {}^{239}U \xrightarrow{\beta^-} {}^{239}Pu \xrightarrow{\alpha} {}^{235}U\ etc \tag{1-1}$$

As far as reactor operation is concerned the long-lived plutonium isotope ^{239}Pu is the end-product of the chain. ^{239}Pu has nuclear properties quite similar to those of ^{235}U, and it can be fissioned by neutrons of all energies. A reactor that utilize the fast neutron to induce the chain reaction is "fast reactor (FR)". The fast reactor has the ability to convert fertile isotopes to fissile raises the possibility of "breeding" new fissile material. The proportion of generation of fissile material to consumption of fissile material (C) is expressed simply as:

$$C \cong \eta - 1 - \mathrm{L} \tag{1-2}$$

η is the average number of neutrons generated per neutron absorbed and it is a function of the neutron energy E, and its variation with E. L is the number of neutrons lost per neutron absorbed in fissile material. In practice, L cannot be reduced below about

0.2, so that breeding is possible only if η is greater than about 2.2. The breeding ratio of Japanese prototype fast reactor, MONJU is about 1.18~1.22 [2].

The fast reactor coolant should meet the following requirements.

- Must not moderate the neutrons emitted from the fission reaction
- Narrow neutron capture cross section
- Effective heat removal from the reactor core

Accordingly, water is unsuitable as a coolant in the FR because it moderates the neutrons effectively. From the neutronic characteristics viewpoint, liquid metals and inert gasses are preferable coolants since it has an excellent thermal property. Sodium, sodium-potassium, lead, lead-bismuth and mercury are considered as a candidate for the coolant. Table 1.1-1 shows the characteristics and thermophysical properties of liquid metals [3].

Among these liquid metals, mercury, lead and lead-bismuth are quite heavy compared with water and it is undesirable from the structural formation view point. For example, it requires a thick reactor vessel to support the coolant and it may bring structural failure due to fluid sloshing. Their heavy toxicity is also an unacceptable disadvantage. Sodium has an excellent thermophysical property as a heat transport material although it has a high chemical reactivity with water and oxygen. Sodium-potassium has more intense chemical reactivity than that of sodium.

Accordingly, liquid sodium is one of the most suitable material as a coolant of a fast reactor. Thus, several countries have researched and developed experimental, prototype and demonstration fast reactors, which use sodium as a coolant. Table1.1-2 shows current fast reactors in the world [4].

In following section, we will briefly consider an overview of the fast reactor system.

Table 1.1-1 Characteristic and thermo-physical properties of liquid metal

	Sodium	Sodium-potassium	Lead	Lead-bismuth	Mercury
Chemical activity	High	High	Low	Low	Low
Corrosivity	Low	Low	High	High	High
Toxicity	Low	Low	High	High	High
Temp [K] /Pres. [MPa]	600 /0.1	600 /0.1	607 /0.1	600 /0.1	550 /0.1
Density [kg/m^3]	874	796	10600	10331	12945
Thermal conductivity [W/m-K]	75.7	26.1	16.3	12.9	12.9
Specific Heat [kJ/kg-K]	1.34	1.028	0.16	0.177	0.135
Melting point [K]	371	262	601	397	234
Boiling point [K]	1155	1057	2010	1943	630
Prandtl number [-]	0.0058	0.011	0.026	0.021	0.01

Table 1.1-2 Current fast reactors in the world

Reactor	Type, coolant	Power thermal/elect	Fuel	Country	Notes
BOR-60	Experimental, sodium	55/10	Oxide	Russia	1969-
BN-600	Demonstration, sodium	1470/600	Oxide	Russia	1980-
BN-800	Experimental, sodium	2100/864	Oxide	Russia	2014-
FBTR	Experimental, sodium	40/-	Oxide	India	1985-2030
PFBR	Demonstration, sodium	1250/500	Oxide	India	2015-
CEFR	Experimental, sodium	65/20	Oxide	China	2010-
JOYO	Experimental, sodium	140/-	Oxide	Japan	1978-2007
MONJU	Prototype, sodium	714/280	Oxide	Japan	1994-96,2010-

1.1.2 Overview of Fast Reactor Plant System

MONJU is a prototype fast reactor, which uses liquid metal (sodium) as a coolant. Its power is 714 MW thermal and 280 MW electric and the fuel is a mixed plutonium and uranium oxide. The reactor cooling system of MONJU consists of three primary and secondary sodium circuits with a steam turbine system (Fig.1.1-1) [5]. MONJU has the intermediate heat transfer system: the secondary cooling circuit between the primary sodium circuit and the steam-water circuit, since the reactor should be protected from the sodium-water reaction. The each circuit is thermally connected by the intermediate heat exchanger (IHX) and the Steam generator. The steam generator consists of and evaporator and a superheater that supplies better quality steam to the turbine. After the reactor shutdown, the decay heat is removed by the air-cooled heat exchangers of the secondary cooling circuits.

The steam generator of MONJU is composed of two generators: the evaporator and the superheater for heating up water to dry steam as shown in Fig.1.1-2 [6]. Specification of Monju is shown in Table 1.1-3 [7]. The evaporator consists of a cylindrical vessel with a bundle of helical tubes inside. The tube material is 2.25Cr-1Mo steel and the tube wall thickness 3.8 mm. The sodium coolant flows through the vessel (outside of the tube) and the water and steam flow through the helical tubes (inside of the tube). The inlet water to the evaporator, which comes from the feed-water heater at 240℃, is heated up to 369℃ and leaves as steam. The sodium coolant comes from the superheater at 469℃ and leaves at 325℃. Then the secondary pump circulates the sodium coolant back to the IHX.

The superheater heats the wet steam, which comes from the evaporator, up to 487℃. The superheater is composed of a cylindrical sodium vessel with a bundle of helical tubes inside. The tube material is type 321 stainless steel and the tube thickness is 3.5 mm. The sodium coolant comes from the IHX at 505 ℃ and leaves the evaporator.

Table 1.1-3 Specification of evaporator and superheater of MONJU

	Evaporator	Superheater
Type	Helical Coil	Helical Coil
Number	3 (one per loop)	3 (one per loop)
Sodium flow rate	3700 tonnes per hour	3700 tonnes per hour
Water/steam flow rate	380 tonnes per hour	380 tones per hour
Operating temperatures		
Sodium inlet	469 ℃	505 ℃
Sodium outlet	325 ℃	469 ℃
Water inlet	240 ℃	
Steam inlet		367 ℃
Steam outlet	369 ℃	487 ℃
Vessel height	15.23m	11.8 m
Vessel diameter	3 m	3 m
Tube number	140/unit	147/unit
Tube diameter	31.8 mm	31.8 mm
Tube thickness	3.8 mm	3.5 mm
Tube length	84 m (approximately)	46 m (approximately)
Tube material	2.25Cr－1Mo	SUS321

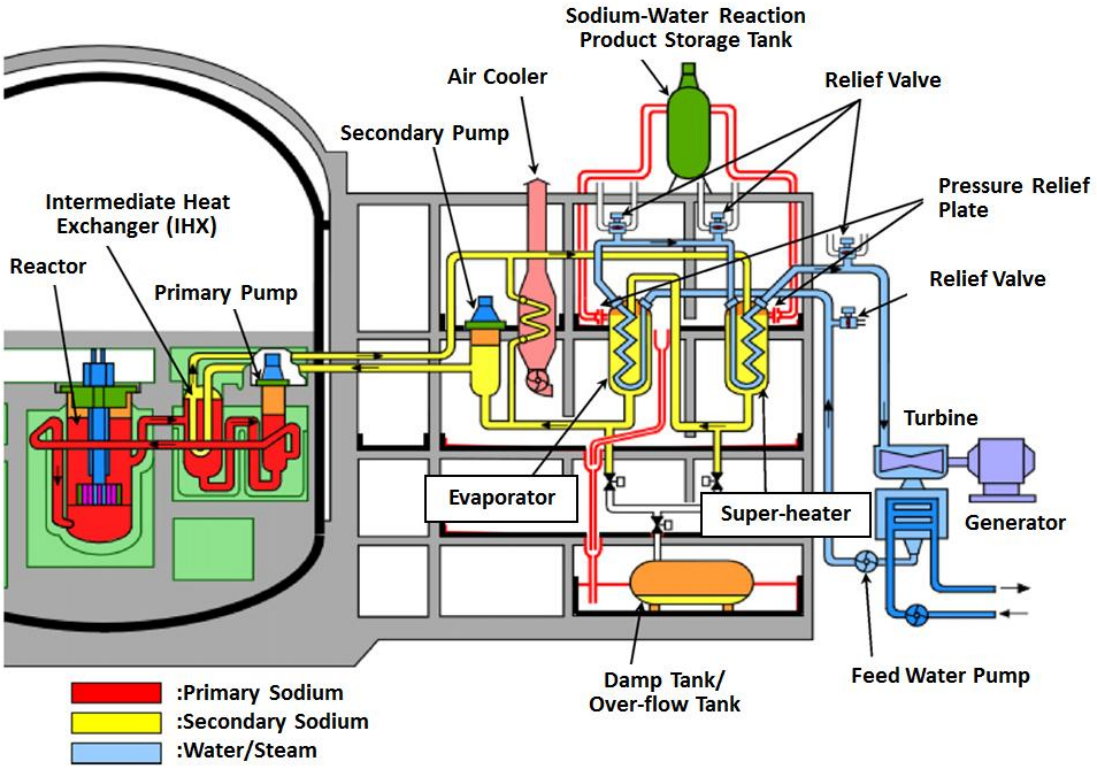

Figure 1.1-1 Overview of MONJU reactor system

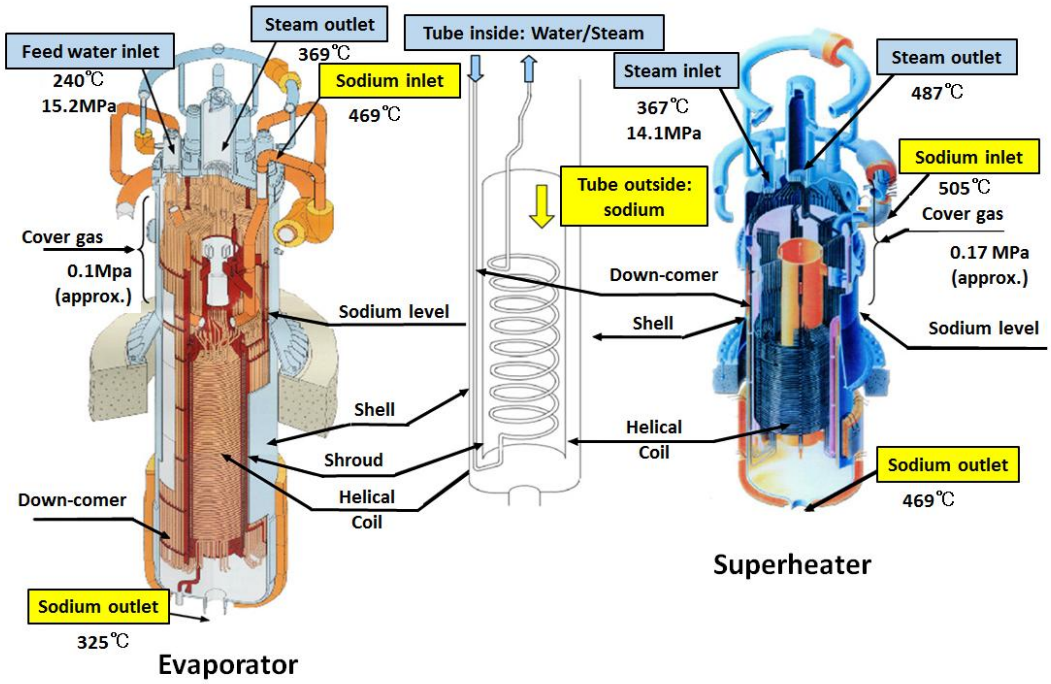

Figure 1.1-2 Evaporator and superheater of MONJU

1.2 Water leak accident in the steam generator

1.2.1 Sodium-water reaction

As seen in Fig.1.1-2, heat transfer tubes are placed in a steam generator system to exchange energy from liquid sodium to water and/or vapor efficiently. In general, high-pressure water and/or vapor flows inside of heat transfer tubes. On the other hand, low pressured liquid sodium flows in the shell side of the steam generator. Therefore, when a heat transfer tube fails in a steam generator, high-pressured water and/or vapor leaks into liquid sodium. Consequently, the following sodium-water reaction will take place as shown in Fig. 1.2-1 [8].

$$Na + H_2O \rightarrow NaOH + {}^1/_2 H_2 \quad (1\text{-}3)$$

$$2Na + 2H_2O \rightarrow 2NaOH + H_2 \quad (1\text{-}4)$$

$$2Na + H_2O \rightarrow Na_2O + H_2 \quad (1\text{-}5)$$

$$Na + NaOH \rightarrow Na_2O + {}^1/_2 H_2 \quad (1\text{-}6)$$

Okano evaluated a composition of the SWR in numerical way under a theoretical adiabatic temperature using the Gibbs free energy minimization method [9]. The proportion of reactant at equal mole rate is summarized in Table 1.2-1. It shows that sodium hydroxide (NaOH) of gas and liquid phase is dominant reaction product, but sodium oxide is a minor product that has a small amount.

A high-temperature area appears due to sodium-water reaction. For instance, the water leakage test that models the steam generator of Monju was conducted and the maximum temperature of 1100-1200 ℃ was measured under when the water leakage rate is not more than 4.5 kg/sec. [10] Under large leak condition (leak rate is 7-15 kg/sec), 1140-1250℃ was observed [11].

Table 1.2-1 Proportion of sodium compounds in sodium-water reaction under an adiabatic

	#1	#2	#3	#4
H2O(g)	251.1	202.5	135.8	97.87
Na(l)	1.662	7.536	6.965	18.94
Na(g)	245.4	185.1	124.1	71.97
Na2(g)	1.082	2.481	0.5657	0.9018
NaOH(l)	79.41	139.6	303.7	356.3
NaOH(g)	165.0	153.3	56.13	40.71
(NaOH)2(g)	1.572	0.8513	0.6037	0.2747
Na2O(l)	1.325	2.915	3.153	3.942
NaH(s)	0.003673	0.03459	0.0274	0.1584
NaH(g)	0.5637	1.959	0.4091	1.059
H2(g)	124.8	149.2	183.5	202.4
Products/Reactants mol ratio	0.872	0.846	0.815	0.759

($\times 10^{-3}$ mol)

(g): gas phase, (l): liquid phase

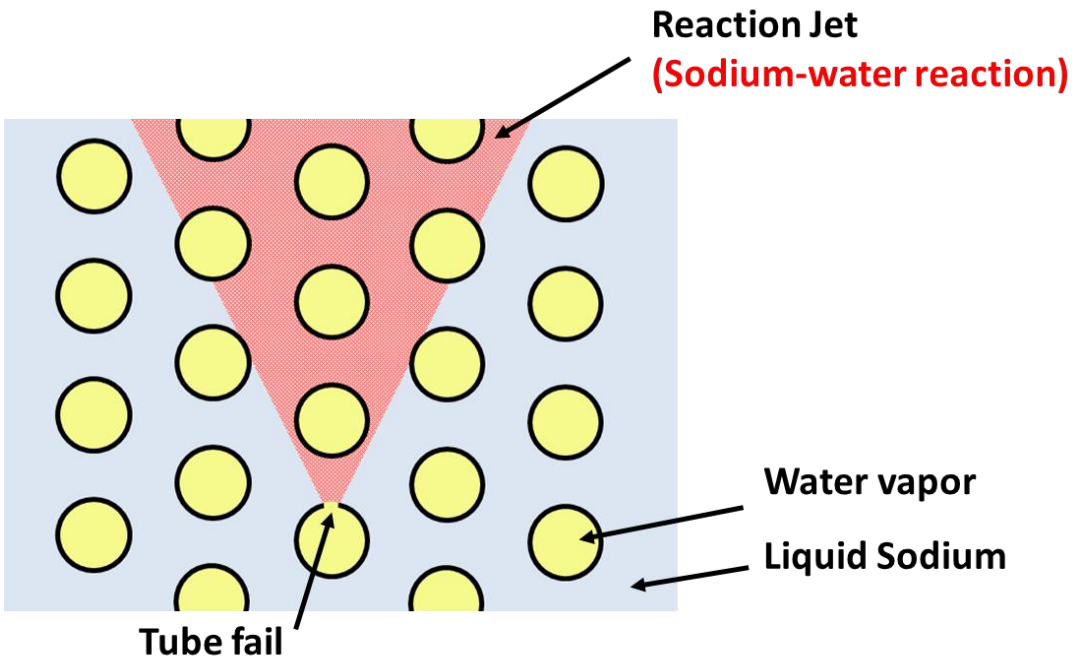

Figure 1.2-1 Scheme of Sodium-water reaction

1.2.2 Classification of water leak

The water leak in the steam generator is classified into the micro, small, intermediate and large leak as shown in Table 1.2-2 and Fig. 1.2-1 [12]. In the micro-leak region, the reaction jet and the heated zone do not extend to an adjacent tube to be damaged. The heated zone and highly concentrated NaOH exist at around the initial defect so that the deterioration of mechanical strength takes place at the initial leak site. High-pressure water vapor peels out the weakened and corroded material at the surface of the tube, and this erosion accelerates the corrosion process. This material damage is the so-called "wastage" phenomenon. As a result, the defect can eventually enlarge to a size that allows a stable reacting jet. The enlargement of the leak is called "Self-wastage phenomena". Figure 1.2-2 shows the cross-sectional morphology of enlarged leak by self-wastage phenomena [13-14]. From the observation on the compositional changes of each element in the tube wall surface, were analyzed to confirm the occurrence of the corrosion phenomena. [15] Sandusky explained the character of the failure of wall material in the process self-wastage phenomena as shown in Fig. 1.2-3 [16]. Self-wastage starts from the sodium side and advances to the water side through the tube wall. As a result of the failure zone propagation, even though the diameter of the leak channel increases, the amount of water leaking out is controlled by the diameter of the original defect which little changes on the water side. So the leak rate stays almost unchanged until the opening of the remaining strap diaphragm would start to increase as a result of a combined corrosion-erosion effect. Also, it takes a few hours even a few days until the failure zone propagation reaches the tube wall on sodium side.

According to experimental studies, reported that the increased leak rate will be at least three orders of magnitude (Fig.1.2-4) [17]. Thus, the resultant leak rate will be in the small leak region. In the small leak region, the leak becomes like a jet, so that the continuous deterioration takes place at an adjacent tube by impingement. It is so-called "target wastage". Consequently, secondary failures might occur, when monitoring system fails to detect the leakage, resulting in a larger leak characteristic of "intermediate leak". The deterioration of adjacent heat transfer tubes, which is called "multi wastage", in the intermediate leak may cause subsequent failure propagations under an undetectable situation or a missing of detection system condition and thus results in "large leak" (Fig.1.2-5). It is noted that the large leak very seldom take place at an initial leak [18].

Accordingly, an investigation of reacting zone and its growth in micro and small leak region is of great importance to estimate the probability of the failure propagation, as

well as the determination of the requirements in the detection system such as sensitivity and response time.

Table 1.2-2 Classification of water leak

Leak categories	Major phenomena	Leak rate
Micro	Self-wastage	Less than 0.05 g/sec
Small	Target wastage	0.05g ~ 10g /sec
Intermediate	Multi wastage	10 g/sec ~ 2 kg/sec
Large	Overheating rupture	More than 2 kg/sec

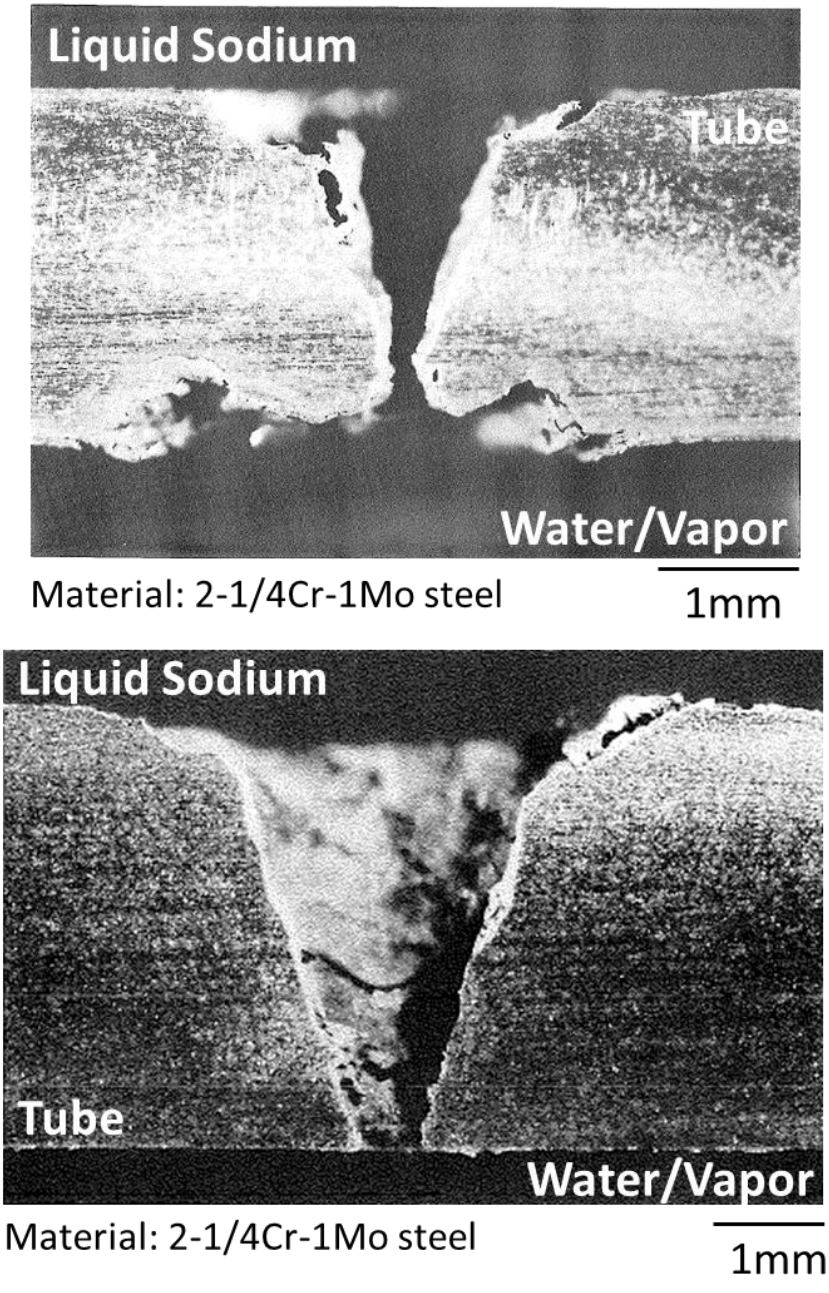

Figure 1.2-2 Sectional morphology on completely self-wasted holes

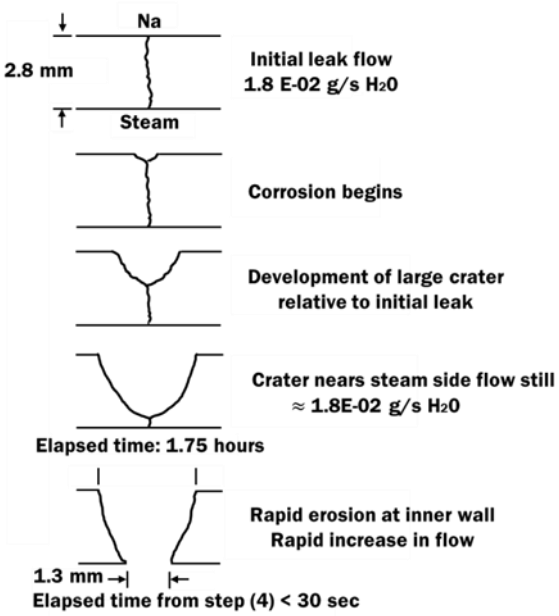

Figure 1.2-3 Process of leak enlargement by self-wastage

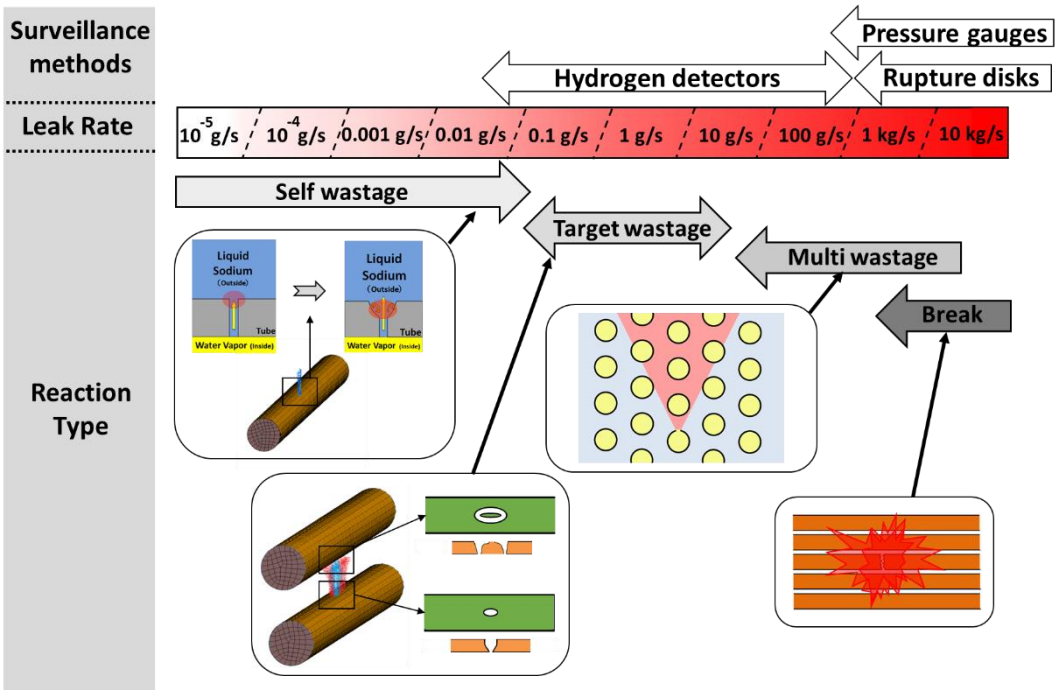

Figure 1.2-4 Types of sodium-water reaction

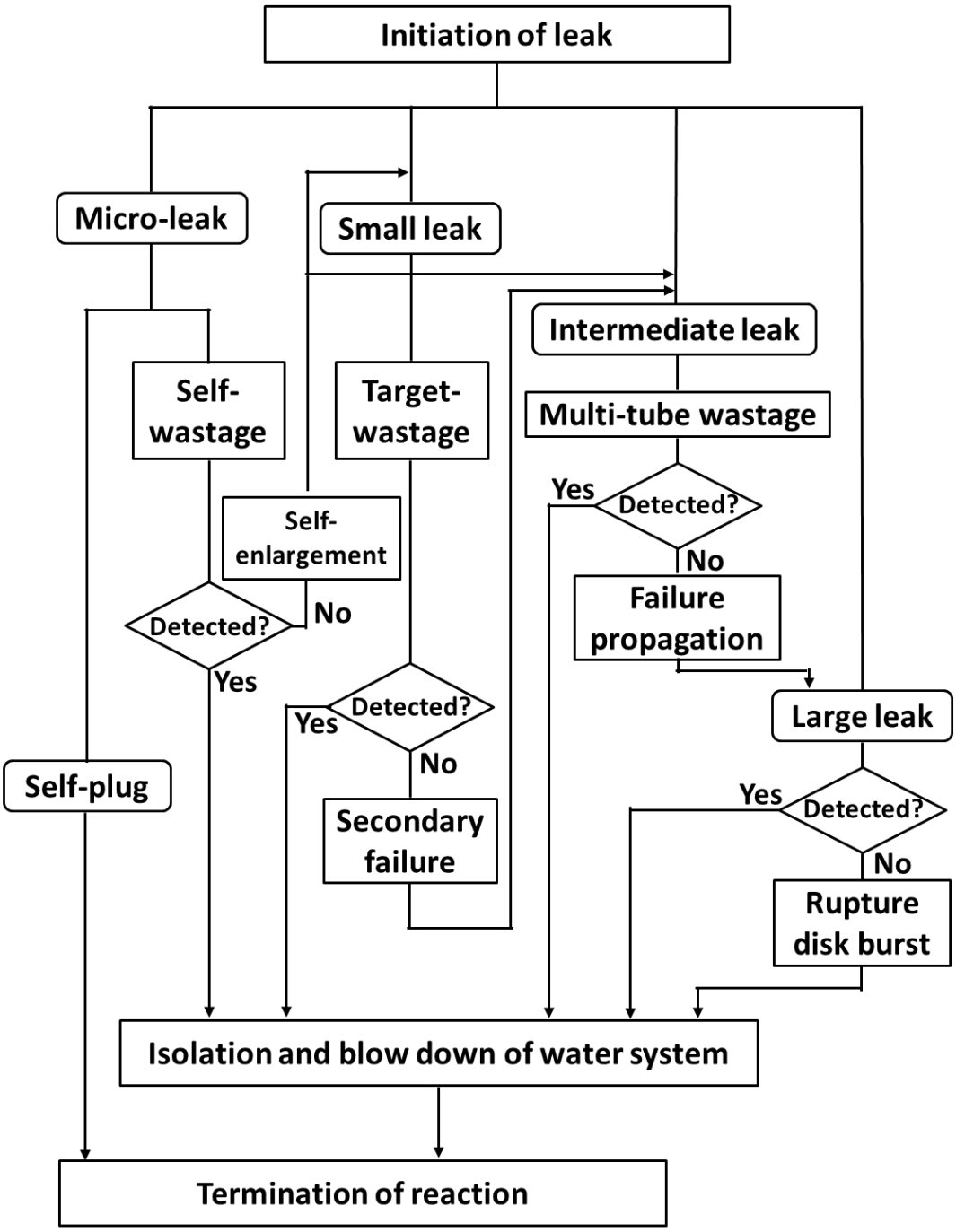

Figure 1.2-5 Flow diagram of leak scenario

1.3 Motivation and Objectives

Liquid sodium is a prospective coolant from the viewpoint of its neutronic and thermo-hydraulic characteristics except the high chemical reactivity with oxygen and water. Therefore when initial leak takes place, it is very important to detect the leakages before they become larger leak, so that prevent the failure propagation and protect reactor system integrity.

In a steam generator, the most of initial crack starts from the micro or small leak, however, it is noted that the detection of the micro-leak is quite difficult because high sensitivity is required to discriminate between the water leakage and noise [19].

Thus, elucidating micro-leak behaviors and characteristic of sodium-water reaction are importnant to improve reactor system safety.

So far, characteristics of sodium-water reaction and self-wastage phenomena has been investigated by mock-up sodium experiments to model the real condition of a steam generator of SFR. For example, Power Reactor and Nuclear Fuel Development Corporation (PNC) Japan, started sodium-water reaction project (SWAT) as one of the projects in the sodium-heated steam generator development program. Small leak sodium-water reaction test loop (SWAT-2) was designed to elucidate the wastage phenomena due to small leak [18]. However, for investigating the thermal-hydraulic characteristics with the chemical process of the SWR, mock-up sodium experiments requires heavy operation cost, so that only limited number of operations were conducted. Also many parameters are related to the phenomena, and it is complex to understand the relationship between the parameters. Moreover, since sodium is opaque, and the sodium-water reaction is vigorous and the measurement technology at that time was not precise to obtain the thermo-physical priorities, it is difficult to evaluate the self-wastage phenomena in quantitative manner.

Since it is difficult to depict the whole picture of sodium-water reaction only with experimental researches, a numerical investigation of sodium reactivity will be an alternative way.

For example, a computational code SERAPHIM (Sodium-watEr Reaction Analysis: Physics of Interdisciplinary Multi-phase flow) was developed to investigate thermal-hydraulics of the SWR based on mechanistic and theoretical modeling on the SWR. Seraphim is based on the semi-implicit method of the Highly Simplified Marker And Cell (HSMAC) [20]. For multi-phase and multi-component calculation, a compressible three-fluid (liquid water, liquid sodium, and mixture gas) and one-pressure model is adopted.

The objectives of the present research are to elucidate the self-wastage phenomena

from microscopic viewpoint and develop the self-wastage evaluation model for quantitative and parametric analysis of the self-wastage phenomena and failure propagation possibility using alternative ways such as numerical simulation and simulant experiment.

For this purpose, the following research projects have been carried out as shown in Fig.1.3-1.

·Development of the self-wastage phenomena evaluation method.
·Parametric analysis of the self-wastage phenomena
·Development of the self-wastage phenomena using simulant material.

- Development of Self-wastage phenomena evaluation method

Using multi-phase computational fluid dynamics calculation code, grasp the thermo-physical properties in the SWR reaction zone and at the crack surface. Then, estimate a self-wastage depth based on the thermal properties at the tube surface. By reflecting the wastage depth to the analytical computational grid, the behavior of the self-wastage phenomena can be evaluated. Validation of the self-wastage evaluation method is carried out through a benchmark analysis of SWAT experiment which is conducted by Japan Atomic Energy Agency.

- Parametric analysis of the self-wastage phenomena

Many parameters are related to the self-wastage phenomena and its relationships between parameters and the phenomena are not clarified. Thus, evaluate the influence of each parameter on the self-wastage rate, leak diameter and leak enlargement ratio. It helps us to classify which parameter has dominant influence on the phenomena.

- Development of the self-wastage phenomena using simulant material

Simulant experiment can simplify the self-wastage phenomena. Simulant experiment is also devised to understand a behavior of the self-wastage phenomena and also to evaluate the influence of parameter on the phenomena.

Self-wastage evaluation model will provides design and safety basis to develop Japanese Sodium Fast Reactor in Fast Reactor Cycle Technology Development Project.

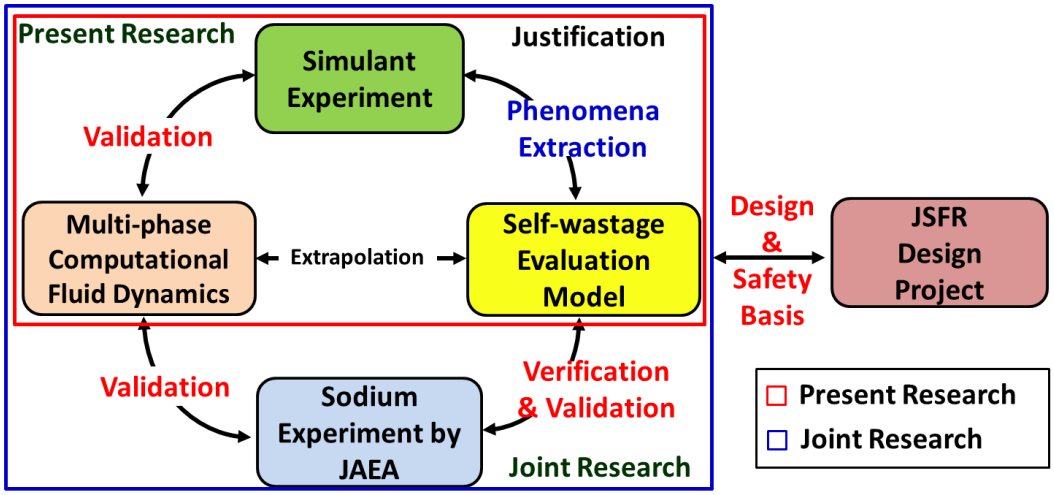

Figure 1.3-1 Composition of this study

[REFERENCES]

[1] A. M. JUDD, 「Fast Breeder Reactors: An Engineering Introduction」, Pergamon press, 1981.

[2] T. Furuyabashi, "Achievements of MOX Fuel Utilization in JNC, Presentation material of Feburary" 18, 2002.

[3] 「JSME Data Book: Heat Transfer (4th Edition)」, Maruzen, Tokyo, 1986

[4] http://www.world-nuclear.org/info/Current-and-Future-Generation/Fast-Neutron-Reactors

[5] M. Matsuura, M. Hatori and M. Ikeda, "Design and modification of steam generator safety system of FBR MONJU", *Nuclear Engineering Design*, 237, pp. 1419-1428, 2007.

[6] Ibid.

[7] http://www.jaea.go.jp/04/monju/EnglishSite/contents02-1.html

[8] T. Takata and A. Yamaguchi, "Numerical Approach to the Safety Evaluation of Sodium-Water Reaction", *J. Nucl. Sci. Technol.* Vol. 40, 10, pp. 708-718, 2003.

[9] Y. Okano and A. Yamaguchi, "Numerical Simulations Study on Sodium-Water Reaction (4) Theoretical Adiabatic Temperature of Sodium-Water Reaction Zone", *2001 Annual Meeting of AESJ*, I4. 2001

[10] H. Tanabe, Y. Wada, K. Hamada, " The Development and Application of Overjeatomg Failure Model of FBR Steam Generator Tubes", *PNC report*, PNC TN9410 98-029, 1998.

[11] C.E. Boardman and M. Hui, H.H. Neely, "Test Results of Sodium-water Reaction Testing in Near Prototypical LMR Steam Generator", *Proc. Of the IAEA/IWGFR Specialists' Meeting on Steam Generator Failure and Failure Propagation Experience, Aix-en-Provence, France*, 1990

[12] http://www.rist.or.jp/atomica/data/dat_detail.php?Title_Key=06-01-02-04

[13] M. Kuroha, K. Sasaki, H. Kawabe, T. Yamada and M. Sato, "Study of Micro-Defect Self-Wastage Phenomena on LMBR Prototype Steam Generator's Tube." *PNC report,* PNC TN941 82-101, 1982.

[14] M. Kuroha and K. Shimoyama, "Micro-Leak Behavior on LMFBR Monju Steam Generator Tube Materials – Studies of Micro-leak Sodium-Water Reaction, *PNC report*, PNC ZN9410 86-027, 1986.

[15] K.Jeong, J.Jeong, B.Kim, T.Kim, J.Choi, D.Hahn and E. Kim, "Sodium-Water Reaction Characteristics with a Speciment and Target Ferrite Steel by Water Leakage

in Liquid Sodium", J. Ind. Eng. Chem., Vol.10, No.4, pp. 524-530, 2004
[16] D. W. Sandusky, "Small Leak Shutdown, Location and Behavior in LMFBR Steam Generators", *Int. Conf. on Liquid Metal Technology in Energy Production*, Seven Springs, PA, USA, May 1976.
[17] M. Matsuura, op. cit.
[18] "Fast Reactor Fuel Failures and Steam Generator Leaks: Transient and Accident Analysis approaches", International Atomic Energy Agency, IAEA-TECDOC-908, 1996.
[19] M. Kuroha, S. Inoue, Y. Daigo and M. Sato, "Preliminal Study of Micro-Defect Self-wastage on 2 1/4Cr-1Mo Steel Nozzles for LMFBR Steam Generators – Studies of Micro-Leak Sodium-Water Reaction (1), PNC Report, PNC ZN941 80-135, 1980.
[20] T. Takata and A. Yamaguchi, "Numerical Thermal-Hydraulics Study on Sodium-Water Phenomena-Development of Computational code 'SERAPHIM'", *Nuclear Cycle Development Institute Techincal Report*, 17, pp. 63-74, 2002

2 Development of Self-wastage Evaluation Model Using SERAPHIM Code

2.1 SERAPHIM code

A new computational code SERAPHIM (**S**odium-wat**E**r **R**eaction **A**nalysis: **Ph**ysics of **I**nterdisciplinary **M**ulti-phase flow) is developed to investigate the sodium-water reaction phenomena [1]. A compressible three-fluid (water, liquid sodium, mixture gas) and one-pressure model is adopted for multi-phase calculation. Two types of reaction model, which are surface reaction model and gas reaction model, are considering for the SWR modeling.

2.1.1 Sodium-water reaction Modeling

In SERAPHIM code, the following two types of reaction models are considered [2].

- **Surface Reaction**

At the beginning of the sodium-water reaction, the temperature is not high enough to vaporize the liquid sodium. In this condition, water vapor reacts with liquid sodium at the gas-liquid interface. It is designated as the surface reaction.

In the surface reaction, it is assumed that

i) The chemical reaction rate is faster than a mass diffusion rate of water vapor toward the surface.

ii) Reaction products such as hydrogen, sodium hydroxide and sodium oxide are emitted to ambient gas.

iii) Reaction heat is allocated to the mixture phase of gas and reaction products

Since the chemical reaction is assumed to be infinitely fast, the surface reaction is controlled by the mass flow rate of the water vapor (γ_{H_2O}) and is given by

$$\gamma_{H_2O} = Sh_g \frac{\rho_g D_{m,H_2O}}{l} \left(Y_{H_2O} - Y_{H_2O,l=0}\right) \times \frac{A_S}{V_G} \tag{2-7}$$

Where, Sh is the Sherwood number, ρ_g the gas density, , D_m the effective binary diffusivity in the gas, l the characteristic length, Y are the mass fraction, As the contact area where the surface reaction occurs and V_G the gas phase volume of each computational cell. $Y_{H2Ol=0}$ is the mass fraction of water vapor at the liquid sodium surface.

Sh_g is estimated from an analogy of mass and heat transfers. It considered that a flow condition near the interface becomes a turbulent state energized by the pressurized water jet stream. Sh_g is related to the Reynolds number Re and Schmidt number Sc as:

$$Sh_G = b1 \times Re_G^{b2} \times Sc_G^{b3} \tag{2-8}$$

$$Re_G = \frac{U_G l}{V_G} \tag{2-9}$$

Where, Re and Sc are the Reynolds number and the Schmidt number respectively. Here, empirical constants $b1$, $b2$ and $b3$ are applied. U_G is the velocity magnitude and V_G the dynamic viscosity in the mixture Gas. Since the characteristic length in Reynolds number is not easy to be defined in a multi-dimensional computation, the following technique is applied to reduce the Reynolds number from Eq.2-2 using the correlation between a mass and heat transfer in the calculation.

Describing the Schmidt number Sc by the Lewis number Le and the Prandtl number Pr, Eq. 2-2 is rewritten as:

$$Sh_G = b1 \times Re_G^{b2} \times \left(Le_g \times Pr_g\right)^{b3} = Le_g^{b3} Nu_g \tag{2-10}$$

$$Le_g = \frac{Sc_g}{Pr_g} = \frac{\lambda_g}{C_{P_g} \rho_g D_m} \tag{2-11}$$

$$Nu_g = \frac{H_g}{\lambda_g / l} \tag{2-12}$$

Here, C_P and Nu are the specific heat and the Nusselt number respectively. H_g is the heat transfer coefficient between the liquid sodium and the gas and is estimated based on the experimental results.

Substituting Eqs. 2-4 and 2-6 into Eq. 2-1, the reaction rate is obtained by

$$\gamma_{H_2O} = Le^{b3-1}\frac{A_S}{V_G}\frac{H_g}{C_{pG}}Y_{H_2O} \tag{2-13}$$

The Lewis number is assumed to be unity for simplicity in the Seraphim code. In this way, the surface reaction rate is rewritten as follows:

$$\gamma_{H_2O} = \frac{A_S}{V_G}\frac{H_g}{C_{pG}}Y_{H_2O} \tag{2-14}$$

Using the stoichiometric coefficient i_{st} that corresponds to a proportion of reactant (sodium) and products in the surface reaction, the consumption rate of sodium and the generation rate of products as follows:

$$\begin{aligned} \text{For reactant(consumption rate)}: \ \gamma_j^{sf} &= -i_{st,j}\gamma_{H_2O} \\ \text{product (generation rate)}: \ \gamma_j^{sf} &= i_{st,j}\gamma_{H_2O} \end{aligned} \tag{2-15}$$

- Gas-Phase Reaction Model

After the liquid sodium is heated up enough by the surface reaction and evaporates vigorously, the gas phase liquid sodium molecules react with water molecules. This reaction process is designated as the gas-phase reaction. For the gas-phage reaction, the reaction rate can be expressed as follows:

$$\text{Chemical reaction } (nA + mB \rightarrow \text{C} + \text{D})$$
$$\gamma = k(T)[A]^{n\prime}[B]^{m\prime} \tag{2-16}$$

Here, $k(T)$ is the rate constant. In the estimation of the rate constant, the investigation results of the MO method such as energy barrier and the grand partition function are used on the basis of the existence of a transition state in the reaction path. When a transition state is found in the reaction path, the rate constant is evaluated by the transition state theory [3]. It is expressed as follows:

$$\mathrm{k}(T) = N_A \frac{k_B T}{h_0} \frac{Q^{\neq}}{Q_A Q_B} exp\left(\frac{\Delta E^{\neq}}{k_B T}\right) \quad (2\text{-}17)$$

Where,

N_A	Avogadro's constant
k_B	Boltzmann constant
h_0	Plank's constant
$Q^{\neq}$	Grand partition function of internal degree of freedom at a transition state
Q_A, Q_B	Grand partition functions of reactants' internal degree of freedom
$\Delta E^{\neq}$	Potential energy difference
T	Temperature

$Q^{\neq}$, Q_A, Q_B and $\Delta E^{\neq}$ are obtained by the MO analysis.

In case of no transition state appears in the reaction, the capture theory is adopted. Concerning the reaction between a dipole and an induced dipole molecules, the rate constant is expressed as:

$$\mathrm{k}(T) = 8.56 \frac{C_6^{1/3}}{\mu_0^{1/2}} (k_B T)^{1/6} \quad (2\text{-}18)$$

$$C_6 \approx \frac{\mu_A^2 \alpha_B}{4\pi\varepsilon_0} \quad (2\text{-}19)$$

Where,

μ_0	Reduced mass
μ_A	Dipole moment
α_B	Polarizability of induced dipole
ε_0	Permittivity of vacuum

Considering reactions given in Eqs (1-3), (1-4), (1-5) and (1-6), the mass generation or consumption rate of sodium gas is obtained as follows:

$$\gamma_{Na}^{gs} = -\alpha_g M_{Na}\left[2k(T)_{1-5}C_{Na}^2 C_{H_2O} + k(T)_{1-3}C_{Na}C_{H_2O} + k(T)_{1-6}C_{Na}C_{NaOH} + 2k(T)_{1-5}C_{Na}^2 C_{H_2O}^2\right] \quad (2\text{-}20)$$

Where,

α	Volume fraction
M	Molecular weight
C	Molar Concentration of gas species

The subscripts of each rate constant represent the equation number and the gas-phase reaction.

2.1.2 Governing and Constitutive Equations

In the present research, two liquids phases of sodium and water and one multi-component gas phase are considered as a set of governing equations. When water leaks into liquid sodium through a crack on heat transfer tube, water vaporizes instantaneously due to the depressurization and is heated up at the liquid sodium surface by the SWR. Thus, it is assumed that liquid water cannot reach the liquid sodium. Thus, the liquid phase only interacts with the gas phase.

The gas phase conservation equations of mass, momentum, energy and mass transfer are shown as following:

$$\frac{\partial}{\partial t}(\alpha_g \rho_g) + \nabla \cdot (\alpha_g \rho_g u_g) = \Gamma_H^e - \Gamma_H^c + \Gamma_S^e - \Gamma_S^c + G^{sf} + G^{dif} \quad (2\text{-}21)$$

$$\begin{aligned}\frac{\partial}{\partial t}(\alpha_g \rho_g u_g) + \nabla \cdot (\alpha_g \rho_g u_g u_g) &= -\alpha_g \nabla p + \alpha_g \nabla \cdot \tau_g + \alpha_g(\rho_g - \rho_0)g + \Gamma_S^e u_S - \Gamma_S^c u_g \\ &+ \Gamma_H^e u_H - \Gamma_H^c u_g - f_S^{ph}(u_g - u_S) - f_H^{ph}(u_g - u_H) \\ &- G^{sf}(u_g - u_S) - f_g^w u_g\end{aligned} \quad (2\text{-}22)$$

$$\frac{\partial}{\partial t}(\alpha_g \rho_g u_g) + \nabla \cdot (\alpha_g \rho_g h_g u_g)$$

$$\begin{aligned} &= \alpha_g \frac{D}{Dt} p + \alpha_g \Phi_g + \alpha_g \nabla \cdot (\lambda_g T_g) + \Gamma_S^e (h_s + i_s) - \Gamma_S^c h y_{Na} \\ &+ \Gamma_H^e (h_H + i_H) - \Gamma_H^c h y_{H_2 0} - \alpha_S \mathrm{H}_S (T_g - T_S) \\ &- \alpha_g \mathrm{H}_H (T_g - T_H) + S^{sf} + S^{gs} - \alpha_H H_g^w (T_g - T_w) + S^{dif} \end{aligned} \tag{2-23}$$

$$\left(\frac{D}{Dt} = \frac{\partial}{\partial t} + u_G \cdot \nabla\right)$$

$$\frac{\partial}{\partial t}(\alpha_g \rho_g Y_j) + \nabla \cdot (\alpha_g \rho_g Y_j u_g) = \nabla \cdot (\alpha_g \rho_g D_{mj} \nabla Y_j) + \Gamma_j^e - \Gamma_j^c + \gamma_j^{sf} + \gamma_j^{gs} \tag{2-24}$$

Where,

α	Volume fraction
ρ	Density
u	Velocity vector
Γ^e	Evaporation rate of liquid sodium and water
Γ^c	Condensation rate
G	Mass generation rate
p	Kinetic pressure
τ	Viscous stress tensor
g	Gravity vector
f^{ph}	Interfacial friction coefficient
f^w	Wall friction coefficient
h	Enthalpy
D	Dissipation function
λ	Thermal Conductivity
i	Latent heat
hy	Enthalpy of gas component
S	Chemical reaction heat source due to the SWR
Y	Mass fraction
D_m	Effective binary diffusivity

Subscripts *G, H* and *S* mean the gas mixture, the liquid water and the liquid sodium,

respectively. Subscripts *J*, *sf* and *gs* represent the gas component, the surface reaction and the gas phase reaction.

Concerning the equation of state in the gas phase, Modified Benedict-Webb-Rubin equation is applied to consider a compressibility of gas with high numerical accuracy. The HSMAC method is implemented for a compressible multiphase flow analysis. The pressure and velocity field are updated so that a divergence of total mass is disappeared in the HSMAC method. The extension scheme of the HSMAC method to a compressible multiphase flow is described as follows. The divergence D is defined as a summation of a differentiated volume fraction of each phase.

$$D = -\sum_{m} \frac{\partial \alpha_m}{\partial t} \tag{2-25}$$

Where subscript m means the fluid type (*G, H* or *S*). A residual divergence ε is obtained by subtracting off a predictor D^* from a subsequent divergence D^{n+1} and is obtained by:

$$\varepsilon = D^{n+1} - D^* = -D^*$$
$$\varepsilon = -D^* = \sum_{m} \left\{ \frac{1}{\rho_m^n} \left(\alpha_m^n \frac{\partial \rho_m}{\partial t}\bigg|^{n+1} + \nabla \cdot \rho_m^n \alpha_m^n u_m^{n+1} - \alpha_m^n \frac{\partial \rho_m}{\partial t}\bigg|^{*} - \nabla \cdot \rho_m^n \alpha_m^n u_m^{*} \right) \right\} \tag{2-26}$$

Where subscript * means the predictor. *n* and *n+1* represent the current and subsequent time step. $\partial \rho_m / \partial t$ in Eq. (2-20) is estimated from equation of state. Then Eq. (2-20) is rewritten as:

$$-D^* = \sum_{m} \left\{ \frac{\alpha_m^n}{\rho_m^n} \frac{\partial p}{\partial \rho_m}\bigg|^{n} \frac{\delta p}{\Delta t} + \right\} \sum_{m} \frac{\alpha_m^n}{\rho_m^n} \frac{\partial T_m}{\partial \rho_m}\bigg|^{n} \frac{\delta T_m}{\Delta t} + \frac{\alpha_g^n}{\rho_g^n} \frac{\partial M}{\partial \rho_g}^{n} \bigg| \frac{\delta M}{\Delta t}$$
$$+ \sum_{m} \frac{1}{\rho_m^n} (\nabla \cdot \rho_m^n \alpha_m^n u_m^*) \tag{2-27}$$
$$(\delta p = p^{n+1} - p^*, \delta T_m = T_m^{n+1} - T^*, \delta \mathrm{M} = M^{n+1} - M^*)$$

M represents the average molecular weight of the gas phase.

Regarding the conservation equation of momentum, only pressure term is treated implicitly, and other terms are treated explicitly in the semi-implicit method. The pressure is treated explicitly in the calculation of the velocity predictor u_m^*, while it is treated implicitly in the estimation of the subsequent velocity u_m^{n+1}. Using the residual value of pressure δp, the velocity predictor u_m^* and subsequent velocity u_m^{n+1}, the conservation equation of momentum can be simplified as:

$$\rho_m^n \alpha_m^n u_m^{n+1} - \rho_m^n \alpha_m^n u_m^* = -\alpha_m^n \Delta t \nabla \delta p \text{ or } \delta U_m = \frac{\alpha_m^n \Delta t}{\rho_m^n} \nabla \delta p$$
$$(\delta U_m = u_m^{n+1} - u_m^*) \tag{2-28}$$

Multiplying the divergence operator to Eq. (2-22), then the following equation is obtained.

$$\nabla \cdot \left(\rho_m \alpha_m u_m^{n+1} - \rho_m \alpha_m u_m^*\right) = -\alpha_m^n \Delta t \nabla^2 \delta p \tag{2-29}$$

The central differences approximation and the super diagonal angle approximation are implemented concerning the Laplacian Eq. (2-23). Eq. (2-23) is finally rewritten as:

$$\nabla \cdot \rho_m^n \alpha_m^n u_m^{n+1} - \nabla \cdot \rho_m^n \alpha_m^n u_m^* = 2\alpha_m^n \Delta t \sum_k \frac{1}{\Delta x_k^2} \delta p \tag{2-30}$$

Where k is the spatial coordinates. Substituting Eq. (2-24) to Eq. (2-21), the residual value of pressure δp is obtained as:

$$\delta \mathrm{p} = -\omega \frac{D^* + \epsilon_\rho^*}{\sum_m \left\{ \frac{\alpha_m^n}{\rho_m^n} \left(\frac{1}{\Delta t} \frac{\partial p}{\partial \rho_m} \right|^n + 2\Delta t \sum_k \frac{1}{\Delta x_k^2} \right) \right\}}$$
$$\varepsilon_\rho^* = \sum_m \frac{\alpha_m^n}{\rho_m^n} \frac{T_m}{\partial \rho_m} \Big|^n \frac{\delta T_m}{\Delta t} + \frac{\alpha_g^n}{\rho_g^n} \frac{\partial M}{\partial \rho_g} \Big|^n \frac{\delta M}{\Delta t} \tag{2-31}$$

Where ω is the relaxation factor ε_ρ^* is the additional residual due to a

compressibility. The numerical procedure is summarized in Fig. 2.1-1.

Takata carried out a benchmark analysis of the Edward pipe blowdown experiment for a code verification. It was reported that comparison of the Seraphim's numerical result and the benchmark data showed good agreement with regards pressure and void fraction in general [4]. Thus, the results indicate that the SERAPHIM code can reproduce the sodium-water reaction and its thermal-hydraulic characteristics.

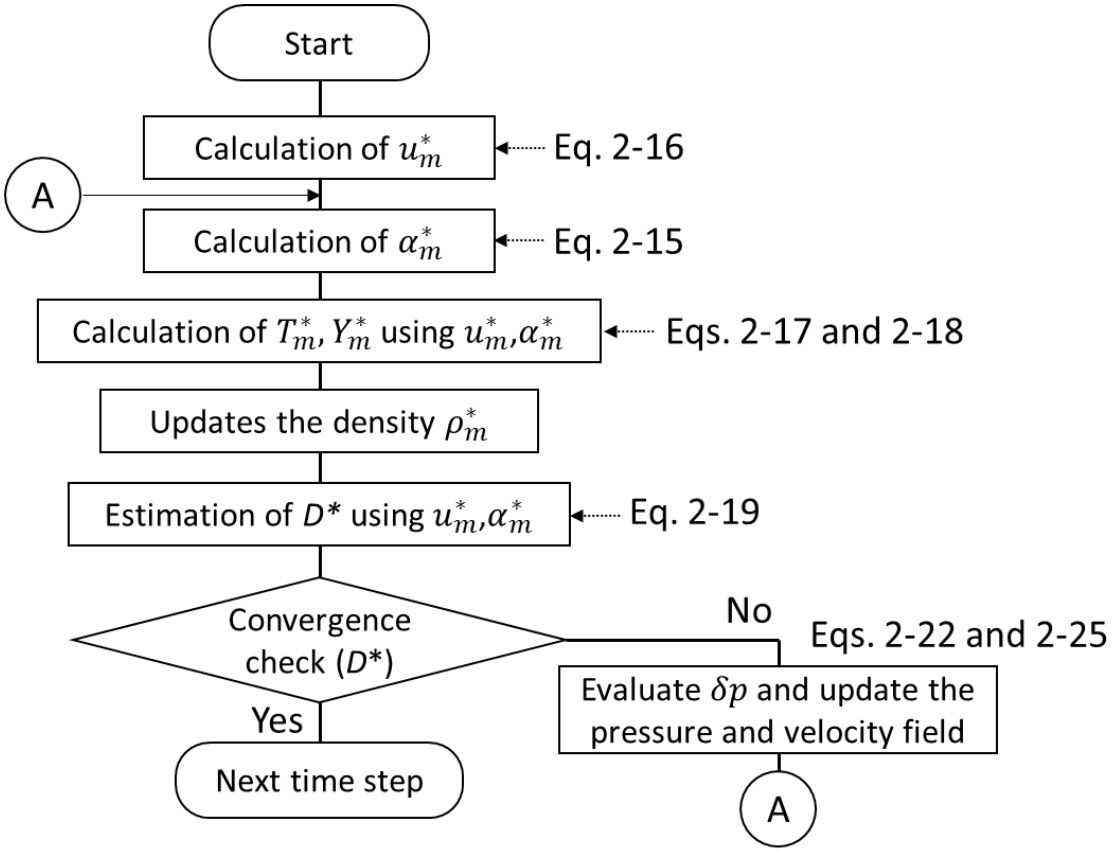

Figure 2.1-1 Numerical procedure of SERAPHIM code

2.2 Self-wastage evaluation model

Self-wastage evaluation model consists of the following two parts. (a) construction of the analytical models (b) wastage rate evaluation by local thermal hydraulic properties physical around the initial crack on the heat transfer tube.

First, we design an analytical model for a heat transfer tube and a crack on the tube wall. Then we carry out a numerical simulation to investigate thermal hydraulic properties using SERAPHIM code. Next, we investigate a self-wastage amount (depth) based on numerical result of thermal properties calculated by SERAPHIM code and reflect the depth to the analytical model, then we can get a new mesh that get the wastage by the self-wastage phenomena. The details are introduced in the following sections.

2.2.1 Numerical procedure

Once again, here we briefly consider the character of a self-wastage phenomena. A gradual failure of steel by the SWR on the side of the water-into-sodium leak issue takes place with the failure front moving deep into the heat transfer wall. As a result of the failure zone propagation, the diameter of the channel increases but the amount of water leaking out is controlled by the size of the original defect which little changes on the water side. The self-wastage continues in such a manner until the opening of the remaining tube wall is removed as a result of corrosion-erosion effects. In this case, a sharp increase of water leak rate occurs.

The behavior of tube wall penetration by self-wastage phenomena requires a long period (few minutes ~ few hours) from its initiation on sodium side to its termination on the water side. According to experimental reports, in some cases, even a few days is required for the tube to undergo the penetration by the self-wastage phenomena. Therefore, a large computation load is necessary to cover the whole picture of the phenomena at one time.

The leak rate stays almost unchanged until the thin edge of the wall is removed. It is called 'Incubation time.' The incubation time lasts for several thousands of seconds during the self-wastage process. During the incubation time, it is expected that the

thermal hydraulic properties are having almost steady condition, so we assume that the self-wastage rate also stays constant during the incubation time. Thus, we devise a stepwise numerical procedure to evaluate the self-wastage phenomena. The detail of the procedure will be depicted as shown in the Fig.2-2.1

- Step 1: set an initial crack width for the initial mesh grid

The initial crack might be a fabrication defects, stress corrosion cracking, fatigue, etc. Thus, it is difficult to model the initial crack shape. However, the shape is expected to be the crevasse shape, since it is noted that in case of leakage through a defect in a tube-to-tube plate attachment, an intensive corrosion failure of the tube wall take place along the generatrix of the leak channel in the region of the direct contact of water leaking out with excessive sodium.

Since the aspect ratio of the crack length and width is large, the crack enlargement dominantly takes place toward the nozzle width and thickness direction. It is assumed that the reproduction of the phenomenon is expected for two-dimensional analysis around the crack center. Thus, the two-dimensional analysis is adopted, two-dimensional crack which as a single with is used as the analytical model.

.

- Step 2: investigation of local thermal properties

A transient two-dimensional numerical simulation is carried out for a particular period until it reaches steady state. To estimate the wastage rate, investigate thermal hydraulic properties such as temperature of the gas mixture, sodium hydroxide concentration.

- Step3: assessment of local wastage rate

The local wastage rate on each cell at the crack surface is evaluated according to the hypothetical Arrhenius model by using the mixture gas temperature and sodium hydroxide concentration.

- Step4: reconstruction of the computational mesh that reflects crack enlargement

The local wastage depth, which is obtained in the former step, is reflected in the original mesh grid by replacing the solid cells (tube wall) to fluid cells in the both crack

width and depth direction on the surface of the tube wall. More detailed about the local wastage evaluation and the reconstruction of the mesh grid are explained in the following sections. Then a further numerical calculation is carried out using the mesh grid. The process of the steps 2 to 4 is repeated until a plastic deformation of material is initiated. Yielding criterion is decided according to Tresca's yield theory [5]. If the principal stress working on the wall is bigger than the 0.2% offset strength of wall, it is regarded as the plastic deformation is initiated.

- Step5: evaluate the geometry of the enlarged crack

Since the crack is completely penetrated by the self-wastage, the leak rate will sharply increase, and it brings a migration of the reaction zone toward the downstream. As a result, the corrosive reactants such as sodium hydroxide, hardly reach the tube wall. Thus, the self-wastage phenomena will be mitigated. In this study, we will focus on the overall shape and geometry of the enlarged leak.

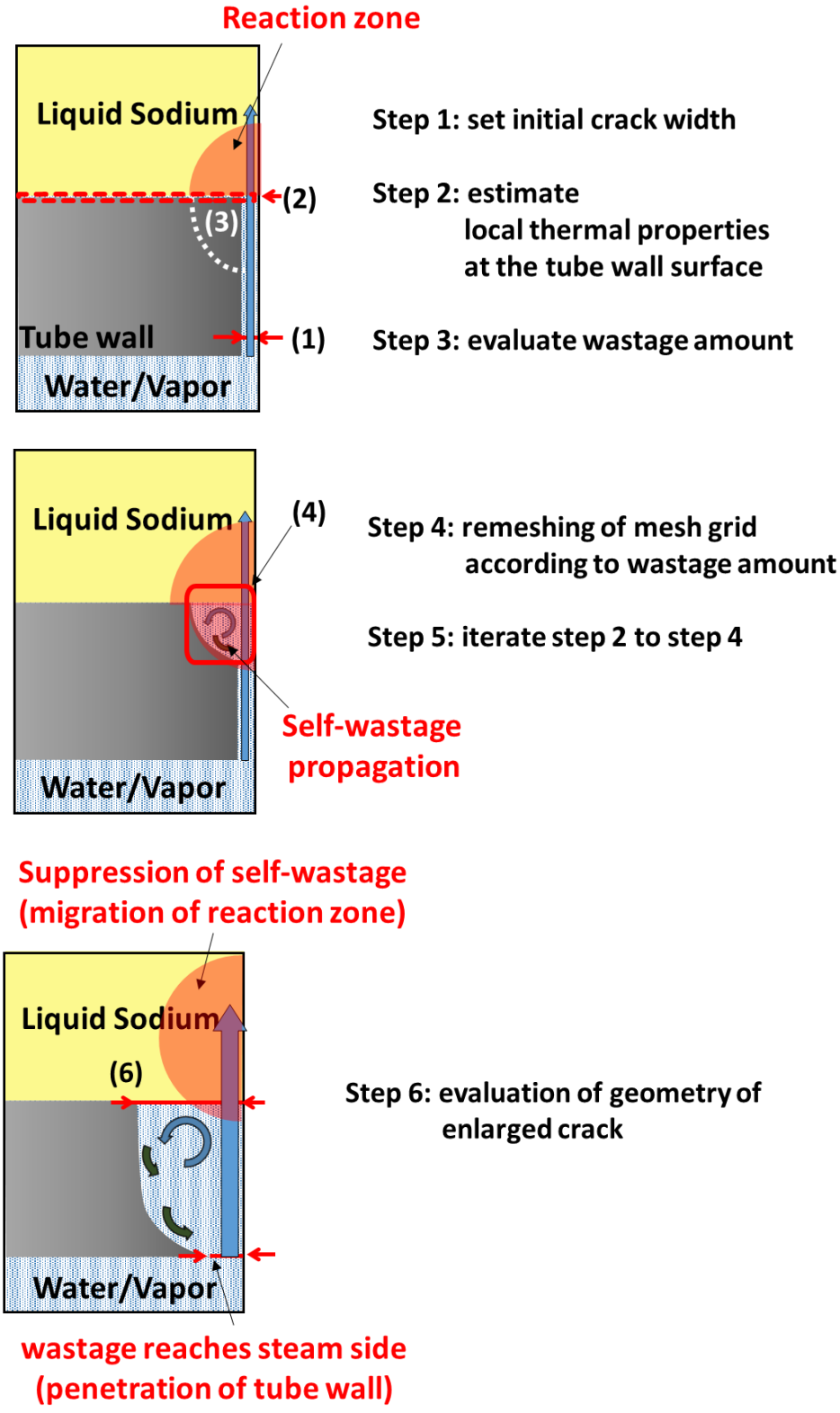

Figure 2.2-1 Concept of Self-wastage evaluation model

2.2.2 Wastage evaluation model

The self-enlargement of the crack is transient phenomena, which last for a several thousand of seconds. Thus, it is difficult to reproduce and evaluate the continuous propagation of the phenomena. Accordingly, we devise the stepwise procedure to evaluate the self-wastage phenomena that mentioned above. To reproduce the crack progression, evaluation of the wastage depth is important to assess the damage that the tube wall undergoes by the self-wastage.

Many experimental researches about the self-wastage phenomena investigated the microscopic inspection of the surface of penetrated crack and found a trace of extensive corrosion of wall material on the surface of the wall except for the center of the crack. In the center of the channel, the less corroded material was found, but, it is expected that the corroded material on the surface of the center of the channel was removed by erosion. We assume that the dominant cause of the self-enlargement of the crack is corrosion by the reaction product, especially sodium hydroxide which is most dominantly produced by the SWR. The sodium oxide is also one of the reaction product, however, according to Takata's analysis, the proportion of the sodium oxide production is less than a few percent [6]. Experimental studies reported that the wastage rate can be expressed by the following form [7]

$$W_R \propto \exp(k_1 - \frac{k_2}{T}). \tag{2-32}$$

Where

W_R	Wastage rate
k_1, k_2	Constant
T	Absolute temperature of sodium or vapor

The temperature of sodium and vapor is one property that affect the wastage rate. The equation has an exponential term.

Therefore, we assume the following wastage rate based on Arrhenius corrosion rate equation in association with Eq. 2-26.

$$WR = A[NaOH]^B exp\left(-\frac{C}{T}\right) \quad (2\text{-}33)$$

Where

WR	Wastage rate [m/s]
A	Exponential Factor
B, C	Experimental constants
$[NaOH]$	Concentration of sodium hydroxide

Constant A is called 'exponential factor' which reflects number of collision between molecules B and C is obtained from the experimental result regarding NaOH corrosion rate experiment performed by JAEA [8].

Unit of Eq.2-27 is [m/sec]. The wastage depth (WD) is obtained by multiplying operating time (t_o) to the self-wastage rate.

$$WD = W_R \times t_o = A[NaOH]^B exp\left(-\frac{C}{T}\right) \times t_o \quad (2\text{-}34)$$

However, in the numerical model, we adopt the stepwise procedure to avoid transient analysis. Accordingly, we assume the maximum wastage depth in each calculation to avoid the influence of A. To dismiss constant A from the Eq. 2-28, the maximum wastage depth for each calculation is decided to become 10 % of the initial tube wall thickness. At this point, the Eq. 2-28 can be rewritten as follow.

$$WD_{Max} = WR_{max} \times t_o = A[NaOH_{max}]^B exp\left(-\frac{C}{T_{max}}\right) \times t_o \quad (2\text{-}35)$$

The WD_{max} is the maximum wastage depth, which is 10 % of the initial tube wall thickness. $NaOH_{max}$ and T_{max} are the concentrations of sodium hydroxide and the gas temperature when the wastage rate is maximum on the mesh at the surface of the crack.

The t_o is decided that the multiplying the wastage rate and t_o, which is the WD max, to become the 10% of the initial tube wall. The wastage depth on each mesh is

decided by taking the ratio of the wastage rate according to the following equation.

$$WD_{(i,j)} = \frac{WR_{(i,j)}}{WR_{max}} \times t_o = \left[\frac{NaOH_{i,j}}{NaOH_{max}}\right]^B exp\left(-\left(\frac{C}{T_{i,j}} - \frac{C}{T_{max}}\right)\right) \quad (2\text{-}36)$$

Where subscription (i,j) means the Cartesian coordinate of the mesh. The wastage depth on a mesh could not exceed the maximum wastage depth. By taking the ratio, the constant A can be ignored.

2.2.3 Remeshing of mesh grid

Remeshing of a computational grid that reflects the leak enlargement is conducted by replacing solid cells to fluid cell according to the local wastage depth that is obtained in the former session. An example of wastage rate estimation and remodeling of computational mesh grid are depicted in Fig.2.2-2 . The red dotted line represents the estimated wastage depth that is obtained from Eq. 2-30. The horizontal axis is the distance from the crack. The black line indicates the initial crack surface. By replacing solid regions to fluid regions according to the wastage depth, new computational mesh grid that reflects the crack enlargement can be obtained. The remeshing procedure is conducted in both the crack width and the thickness direction.

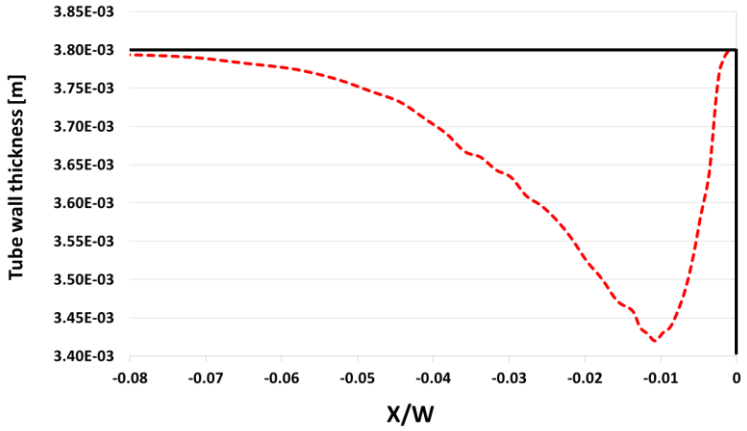

Wastage depth at surface

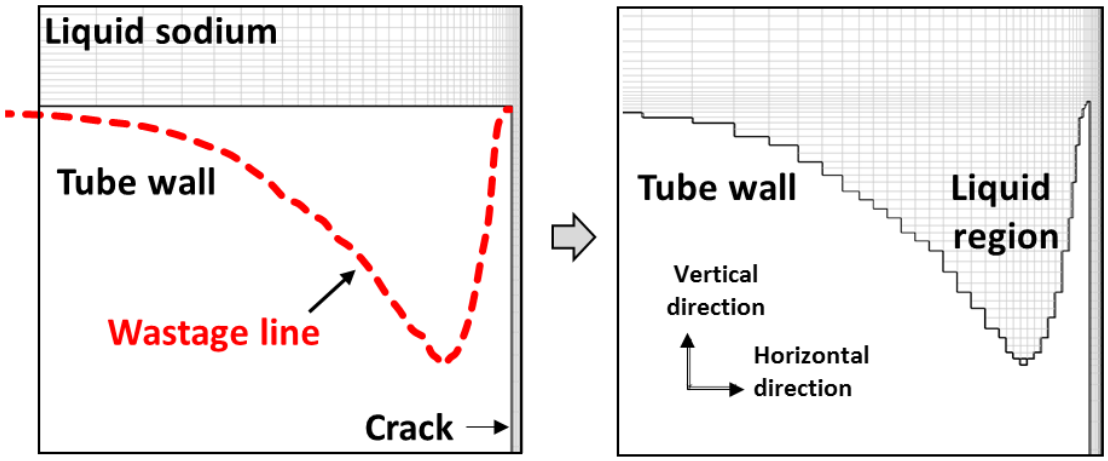

Initial mesh grid (Left) and Remeshed grid (Right)

Figure 2.2-2 Remeshing procedure

2.2.4 Penetration decision

During the incubation stage, the leak rate stay almost unchanged and last for a several thousand seconds. However, a high-pressure works on the water/vapor side, as the self-wastage phenomena progress toward the water/vapor side, the remaining tube wall becomes thinner (Fig. 2.2-3-a and Fig.2.2.3-b). When the tube wall thickness become smaller than a certain size, yielding of the remaining tube wall by the inner pressure is initiated (Fig.2.2-3-c). As a result, the remaining diaphragm is removed and the leak channel is enlarged (Fig.2.2-3-d).

The inner pressure (hoop stress) working on a cylinder is classified according to a tube wall thickness. If the tube wall thickness is thicker than 1/20 of the outer radius, it is regarded thick-wall cylinder (Fig.2.2-4) [9].

$$\sigma_r = \frac{r_{in}^2 P_{in} - r_{out}^2 P_{out}}{r_{out}^2 - r_{in}^2} - \frac{(P_{in} - P_{out}) r_{in}^2 r_{out}^2}{(r_{out}^2 - r_{in}^2) r^2} \tag{2-37}$$

$$\sigma_\theta = \frac{r_{in}^2 P_{in} - r_{out}^2 P_{out}}{r_{out}^2 - r_{in}^2} + \frac{(P_{in} - P_{out}) r_{in}^2 r_{out}^2}{(r_{out}^2 - r_{in}^2) r^2} \tag{2-38}$$

Where, r_{out}, r_{in}, P_{in} and P_{out} are outer, inner radius and outer, inner pressure. According to Tresca's yielding theory, yielding occurs when the equivalent stress is [10]:

$$\sigma_{max} = (\sigma_\theta - \sigma_r) \geq \sigma_Y \tag{2-39}$$

$$\begin{aligned} \sigma_{max} &= 2\frac{(P_{in} - P_{out}) r_{in}^2 r_{out}^2}{(r_{out}^2 - r_{in}^2) r^2} \geq \sigma_Y \\ &= 2\frac{(P_{in} - P_{out})}{k^2 - 1}\frac{r_{out}^2}{r^2} \geq \sigma_Y, \quad k = \frac{r_{out}}{r_{in}} \end{aligned} \tag{2-40}$$

$\sigma_{max}, \sigma_Y, \sigma_\theta$ and σ_r are maximum principal stress [MPa], yield stress [MPa], hoop stress [MPa] and radial stress [MPa], respectively. As the yield stress, 0.2% offset yield strength of 2.25Cr-1Mo steel is adopted.

We assume that the P_{in} and P_{out} are constant during the self-wastage phenomena. Thus, if the wall thickness ($r_{out} - r_{in}$) is decided, the equivalent stress working on the tube wall can be obtained. If the stress working on the tube wall is equal to the 0.2% offset yield strength of the material, it is regarded that the yielding of the tube wall is initiated.

Experimental data of the 0.2% offset yield strength of 2.25 Cr-1Mo is shown in fig.2.2-5. The 0.2% offset yield strength decreases as the temperature increases. The 0.2% offset yield strength at room temperature is 433 MPa and it decrease as the temperature

increases [11]. Since no experimental data that measure surface material temperature in the reaction region is found, the postulated temperature of the surface wall is regarded the same as the temperature of the gas mixture at the surface.

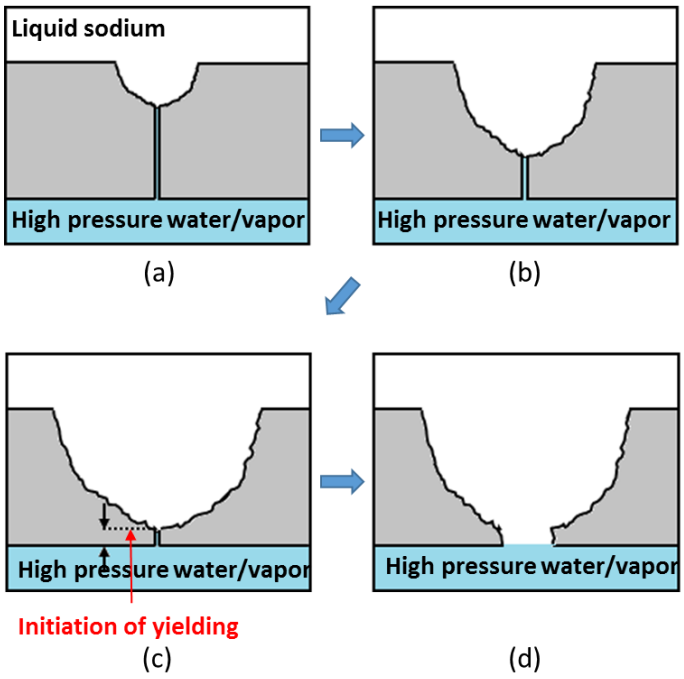

Figure 2.2-3 Self-wastage propagation and yielding of wall by inner pressure

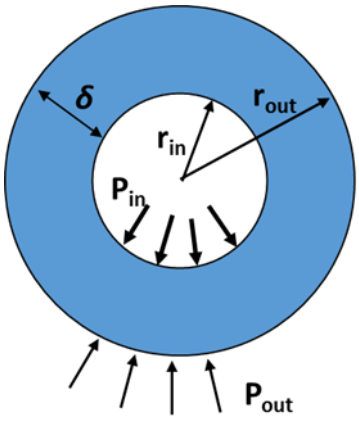

Figure 2.2-4 Stress working on thick-walled cylinder

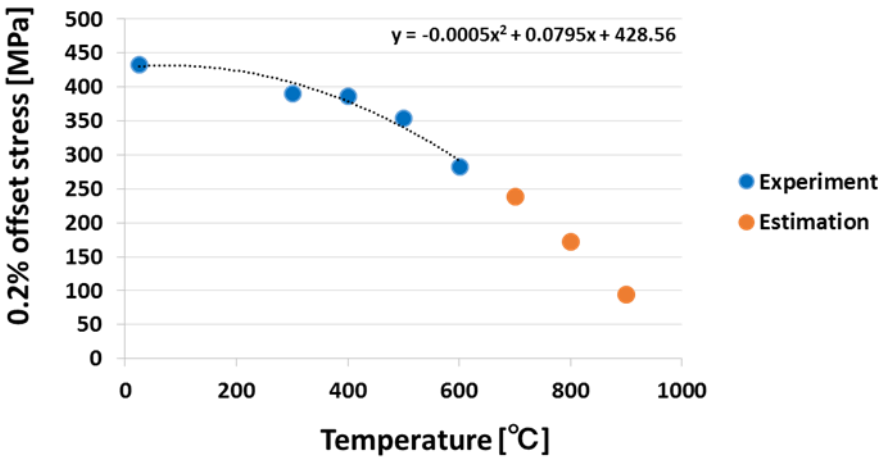

Figure 2.2-5　0.2% offset stress of 2.25Cr-1Mo steel

2.3 Self-wastage evaluation analysis

2.3.1 Analytical conditions

To validate the applicability of the self-wastage evaluation model, numerical simulations are carried out under the same conditions of SWAT experiment

- **SWAT experiment**

Kuroha [12-14] performed a mock-up experiment using SWAT test rig and studied the behavior of the sodium-water reaction and the self-wastage phenomena under the same condition of Japanese prototype FBR Monju's steam generators.

The slit-type nozzle, which was manufactured by pressing a square plate with a drilled hole at the center of it, was used in the experiment. Each slit was constant in the length of approximately 0.05 mm so that the equivalent diameters of leak holes were manufactured in the range of 10 to 100 μm by controlling their widths. The slit has a high aspect ratio. The observation of the vapor blow-off through the slit nozzle indicated that the spread of the vapor differs in the nozzle direction. Table 2.3-1 shows the #2021 experimental condition of the SWAT-2 Experiment. The aspect ratio of the nozzle width (24μm) and the depth (3.48mm) is 1:166 and the equivalent diameter of the nozzle are 0.046 mmφ.

Table 2.3-1 SWAT-2 Experimental conditions

Experimental Conditions	
Experiment Number	: 2020
·Tube Material	: 2.25 Cr-1Mo
·Tube Thickness	: 3.84 mm
·Sodium Temperature	: 470 ◦C
·Sodium Pressure	: 1.47×10^{-1} Mpa
·Steam Temperature	: 470 ◦C
·Steam Pressure	: 12.8 Mpa
·Initial crack width	: 15 μm
·Initial leak rate	: 3.4×10^{-4} g/s
·Average leak rate	: 2.5×10^{-5} g/s

2.3.2 Initial calculation

Figure 2.3-1 shows two-dimensional analytical area and its mesh arrangements. From the observation of the cross section of the enlarged crack, in most case, the penetrated crack has symmetric shape. Thus, to reduce the computational load, a half face grid is used for the calculation. The width of the crack is adopted the same value with the nozzle width of the SWAT-2 experiment. The crack width in the mesh grid (7.5μm) was decided to be divided equally into four cells after considering the effect of the mesh resolution. The height of the analytical region (22 cm) is decided to be as 3 times larger than the reaction jet length which is obtained by Dumm's equation about the jet flame length to cover the reaction zone fully. The width of the analytical region is decided to be a half of the region height. The minimum height of the mesh grid was 10μm, and the whole mesh grid was divided into 49 (I) ×107 (J). Boundary conditions are shown in Fig.2.3-2 As the inlet condition, the constant leak rate is adopted and the constant leak rate of the SWAT experiment, which is the representative value that depict the flow characteristic, is used. Pressure outlet condition is adopted for the top and the left side of the analytical region. Heat transfer between the fluid and the tube wall is ignored in this analysis (Adiabatic condition). Zero gradient concentration is used for the boundary of the interface at the center. Outlet pressure and sodium temperatures are 1.47×10^{-1} [Mpa] and 470 [℃], which are the same value with the SWAT experiment, respectively. Time step is 1.0×10^{-9} [sec].

Figure 2.3-3 shows the void fraction and velocity vector around the crack exit at 1.0×10^{-3}, 5.0×10^{-3}, 1.0×10^{-2} and 2.4×10^{-2} [sec] respectively. It shows that a high-void fraction area is created at the nozzle exit, and it expands toward the down steam as time progresses. Vortex is also created in the liquid sodium area at around crack exit, and it is migrated toward the downstream, then new vortex is created again around nozzle exit. From the void fraction observation, it can be expected that sodium-water reaction occurs around the crack exit, is reproduced by the numerical calculation.

Figure 2.3-4 shows transient data of the gas temperature and NaOH concentration at the surface of the tube top. The horizontal axis indicates the distance from the crack and the axis is adjusted to have a same scale with the Fig.2.3-3. It shows that the gas temperature and NaOH concentration fluctuate in a certain range with the time elapse. It is also noted that the closer position from the crack center, the more changes of the

physical properties are observed. To understand the characteristic of the temperature and NaOH concentration profile, transient data is investigated on a single mesh at the surface (Fig. 2.3-5). As regards the temperature, it sharply increase until 1600 ℃ within 0.1 sec and the temperature goes down to about 500 ℃ after 0.1 sec, and then it fluctuates in the range of 500 ℃ to 1300 ℃. The NaOH concentration sharply decrease in early stage, and it goes up, and then the concentration also changes in a certain range. As we mentioned earlier, after the initiation of the leak, the leak rate stays almost unchanged for a several thousand seconds until the tube is completely penetrated. Therefore, we assume that the physical properties will have the same tendency during the incubation stage. Therefore to investigate the wastage depth, the ensemble averages of the value are taken (Fig.2.3-6).

Using the averaged properties and Eq.2-27 to 2-30, the wastage depth is obtained. Figure 2.3-7 shows the wastage depth on the tube surface. The red dotted line represents the wastage depth on the tube surface, and the black line indicates the tube surface. According to the wastage depth, the solid cells are replaced by the liquid cells (Fig. 2.3-8-a). As a result, the remeshed grid is obtained (Fig.2.3-8-b). The comparison of the shape of remeshed grid and the wastage depth shows good agreement.

The remeshed grid has a projection near the crack center. The width of the projection is about 0.01 cm. If a further calculation is carried out with the projection, it is expected that the reaction products hardly reach the tube wall. Also, the experimental observation of the cross section of enlarged crack shows that the enlarged crack does not have any projection at the surface. Therefore, it is expected that the projection is eliminated while the self-wastage phenomena are progressing. So, we also cut off the projection along the maximum wastage depth and get a new meshed grid (Fig.2.3-9.).

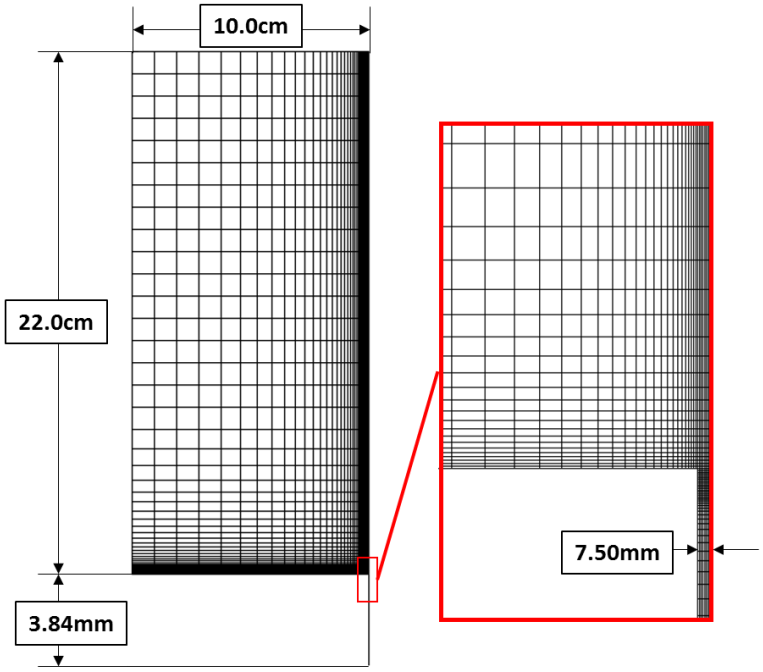

Figure 2.3-1 Initial analytical mesh grid

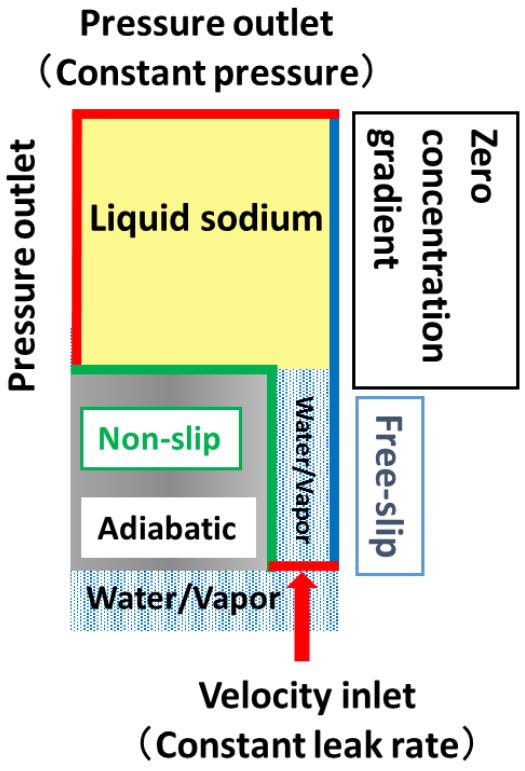

Figure 2.3-2 Analytical boundary conditions

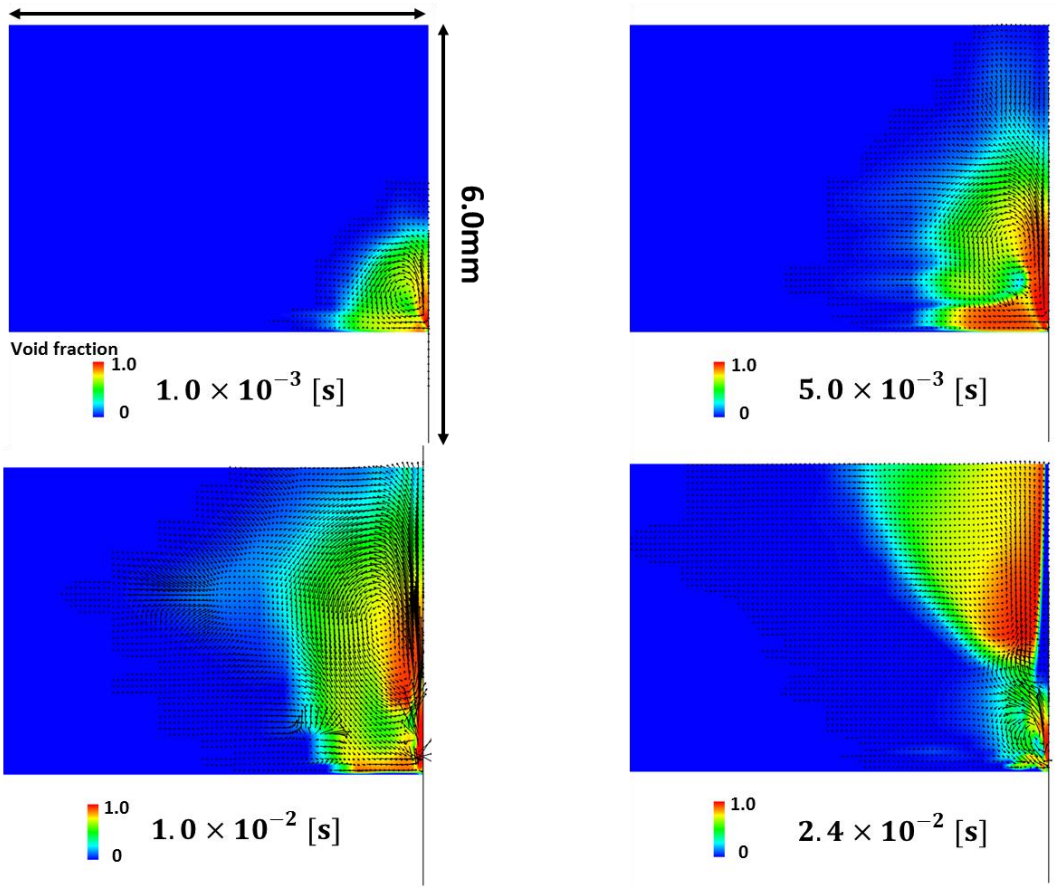

Figure 2.3-3 Void fraction

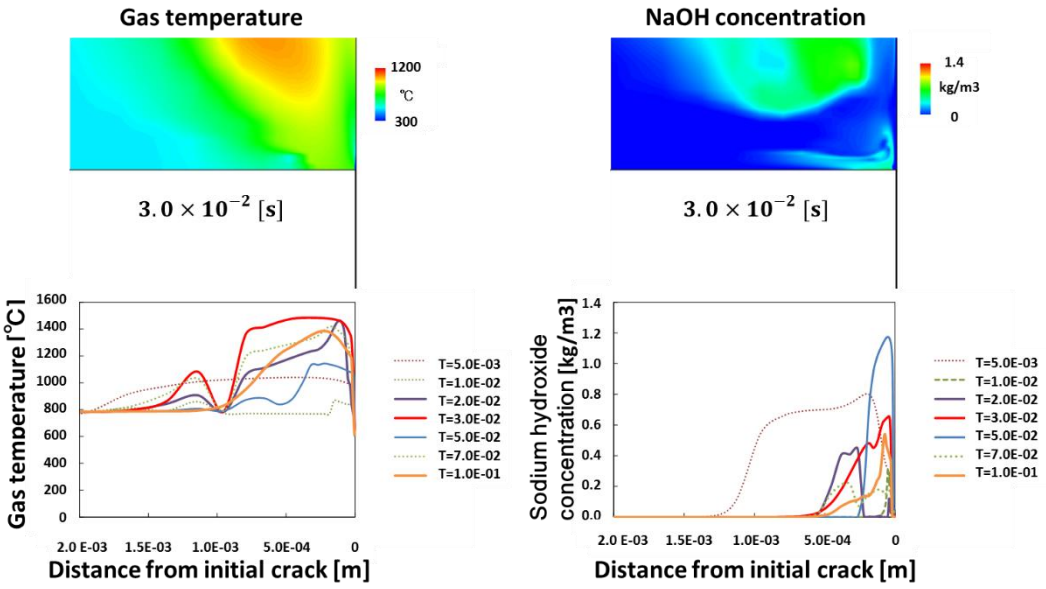

Figure 2.3-4 Transient temperature profile at tube surface

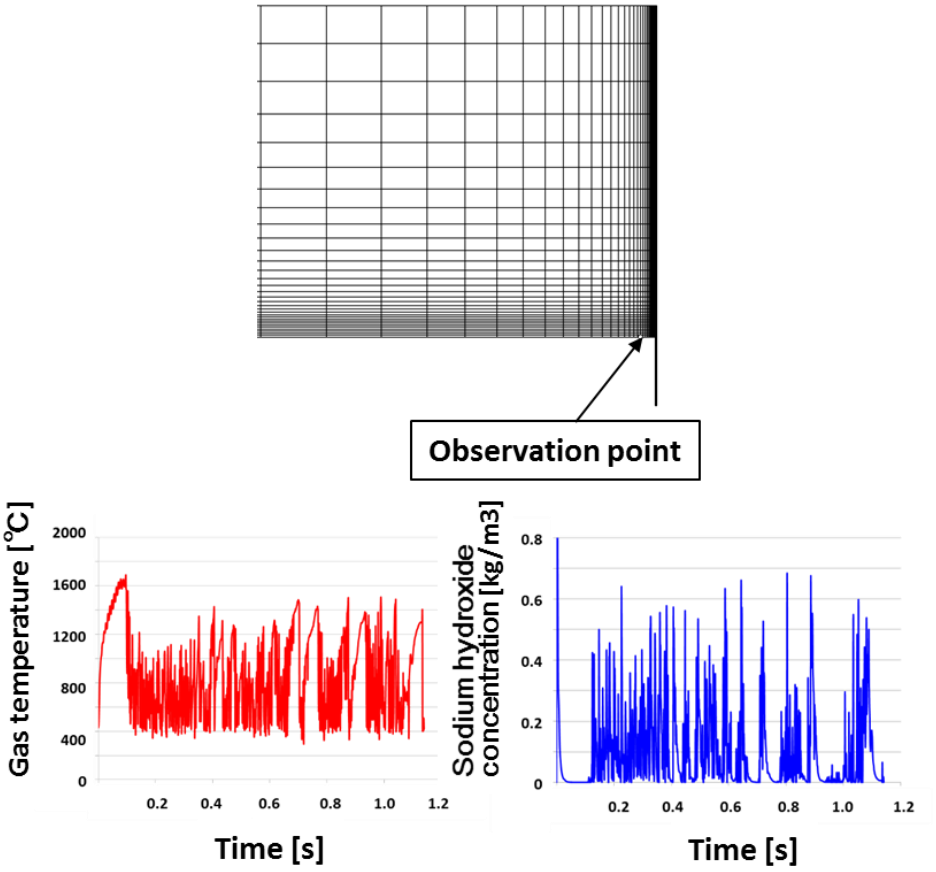

Figure 2.3-5 Transient data profile at tube surface

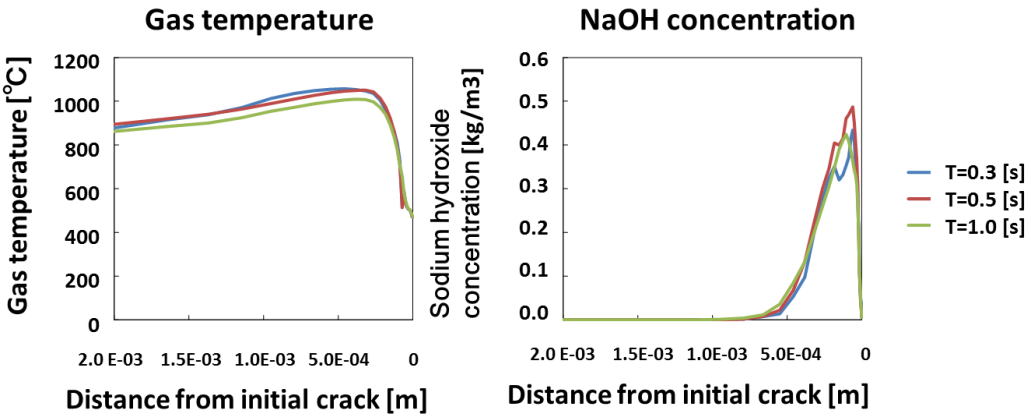

Figure 2.3-6 Averaged temperature and NaOH concentration at tube surface

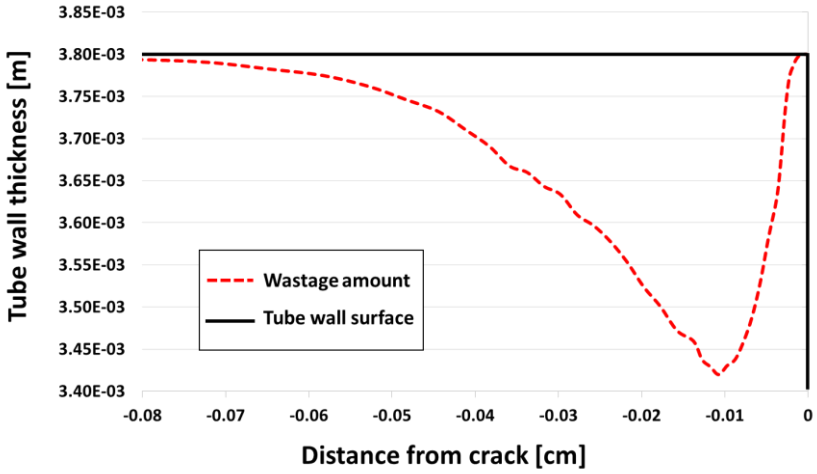

Figure 2.3-7 Wastage depth at tube surface for initial analysis

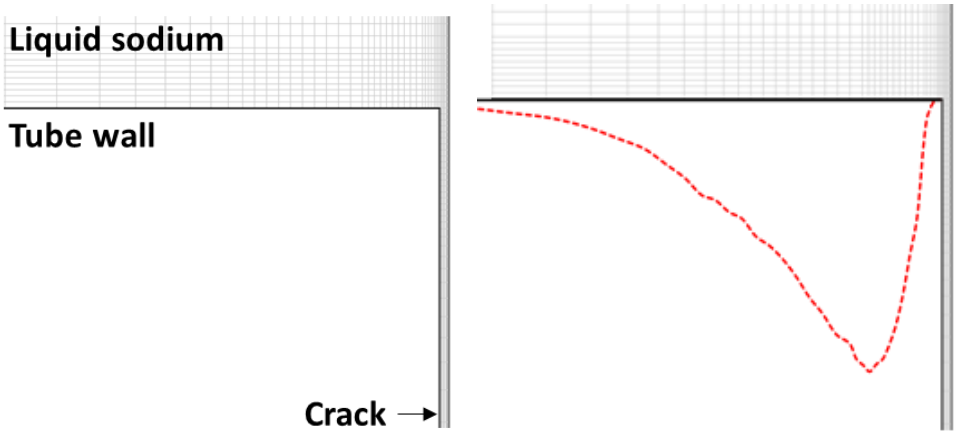

(a) Initial mesh grid (Left) and evaluation of wastage depth (Right)

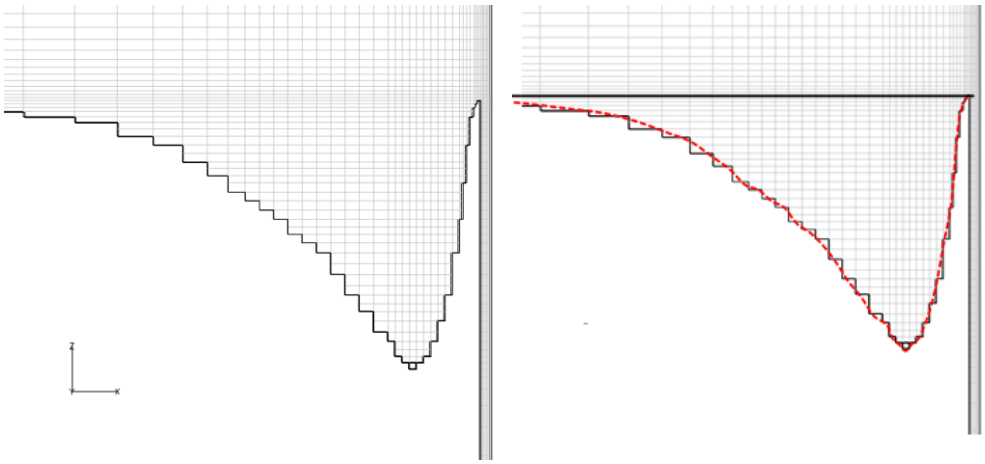

(b) Remeshed grid according to wastage depth and its comparison

Figure 2.3-8 Remeshing procedure in initial analysis

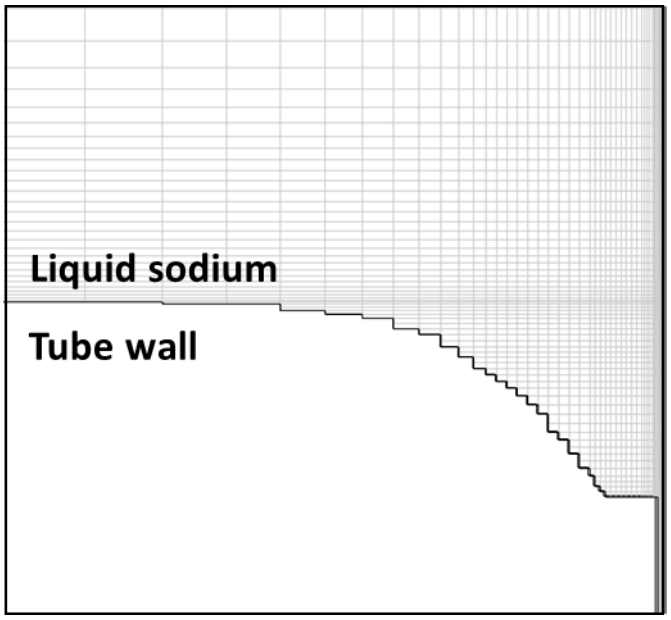

Figure 2.3-9 Remeshed grid after cutting off projection

2.3.3 Second analysis

New numerical simulation is carried out using the remeshed grid in Fig.2.3-9 under the same condition of the initial calculation. Figure 2.3-10 shows the transient temperature profile on four different mesh. As we can see, the temperature and the NaOH concentration change rapidly in an early stage of the leak. However, the properties fluctuate in a certain range. Like the same manner, to evaluate the self-wastage depth, the averaged temperature and NaOH concentration on the tube surface are obtained toward both the horizontal direction and the vertical direction. Based on these averaged properties, the 2nd wastage amount is evaluated, and the remeshing procedure is carried out according to the wastage amount by replacing the solid cells to the liquid cells. As a result, a new mesh for the 3rd analysis is obtained (Fig.2.3-11). Again, a projection is existed near the crack after the remeshing procedure. So, the projection is cut off. Using this mesh grid, a numerical simulation is carried out to check that the calculation is well working with the new mesh grid. The gas temperature, void rate, and NaOH concentration are obtained as shown in Fig.2.3-12. It shows that a high-temperature region is created on the tube wall near the crack center, and NaOH is also located in the same area. So it seems that the new mesh grid is well working with the SERAPHIM code.

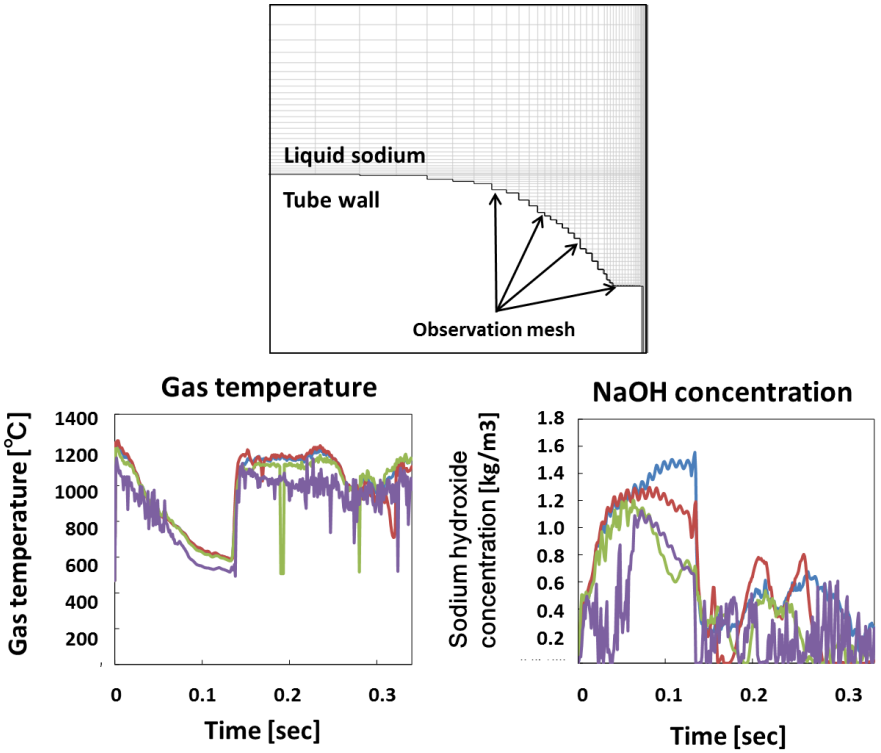

Figure 2.3-10 Gas temperature and NaOH concentration at tube surface in 2nd mesh

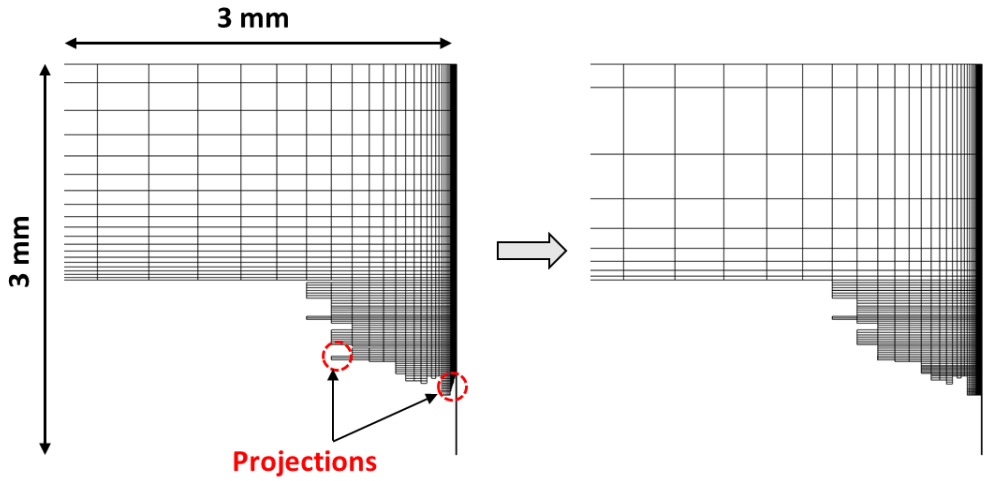

Figure 2.3-11 analytical mesh after remeshing

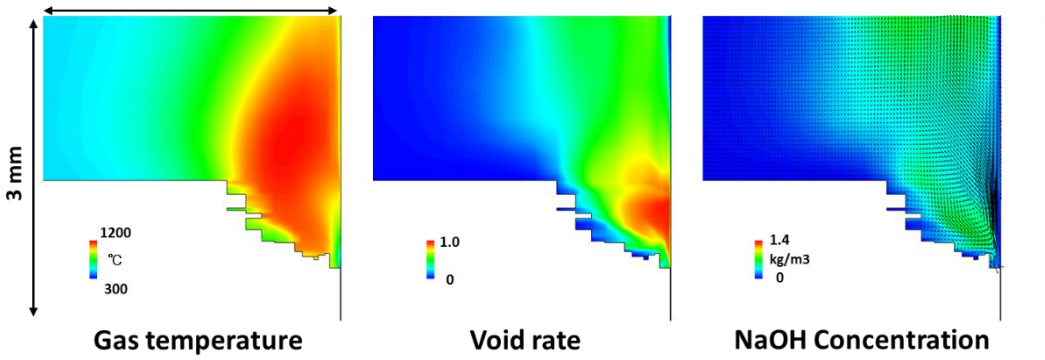

Figure 2.3-12 Thermal hydraulic properties using 2nd analytical mesh

2.3.4 Further calculation

Further calculations are carried out using the remeshed grid to evaluate the self-wastage propagation. Figure 2.3-13 shows the transient gas temperature and NaOH concentration that are investigated on 4 mesh point at the surface of the 3rd mesh grid over 0.4 sec. Both data fluctuate in a certain range after 0.1 sec. Thus, the average of the both data are taken to decide the wastage amount at the surface of the 3rd mesh grid. Further remeshing procedure carried out, consequently a new mesh grid is obtained. Figure 2.3-14 shows 4th, 5th and 6th mesh grid that are obtained from further calculation. As we can see, the self-enlargement of the crack take place toward the both crack width and the thickness direction. It seems that the enlargement rate toward the crack thickness direction is higher than that toward the crack width direction. The enlarged crack has a funnel shape. Also, it can be found that the surface become bumpy after the remeshing process.

Figure 2.3-15 shows the calculation results about the gas mixture temperature, void rate, and NaOH concentration. It can be found that the thermal properties hardly reach a pit on the lumpy surface. Also, as the crack enlarges toward the horizontal direction, the reaction products seldom reach the wall. The blue-colored area near the crack center indicates represents that liquid sodium is dominantly existed in this area. Thus, it is expected that as the crack enlargement advances toward the water/vapor side, the crack enlargement dominantly take place around the crack center on water/vapor side. The transient data of the temperature and the shows same tendency that the value of these properties fluctuates in a certain range in general (Fig.2.3-16). Like the same manner, the remeshing procedure is carried out, and the new mesh grid is generated and it is used for further calculation. The 7th mesh grid and the calculation results is shown in

Fig. 2.3-17. In this case, the liquid sodium dominant are is observed around the crack center. The surface becomes less lumpy than the former mesh. Also based on the gas mixture temperature and NaOH concentration, the wastage amount is calculated, and the wastage amount is reflected the 7th mesh (Fig.2.3-18). As a result, the 8th mesh is generated.

Using the 8th mesh, the wastage amount, and the meshing procedure are performed. Figure 2.3-19 and 2.3-20 shows the 9th mesh and its simulation results. It is observed that the thermal properties hardly reaches the mesh on the wall near the crack exit (A). Thus, the gas temperature is also lower than another mesh point. It is expected that the nozzle enlargement hardly take place on this mesh. Figure 2.3-21 and 2.3-22 shows the 9th mesh and thermal properties in the enlarged crack. It is noticed that as the crack enlargement advances deeper and wider, the reaction zone also migrates toward the upstream of the flow. Therefore, it is expected that the crack enlargement toward the horizontal direction will be mitigated as the diameter become larger.

To decide the thickness of the tube wall, when the plastic deformation initiates, average temperature at the surface is investigated. Average temperature at point A is about 900℃. Since the no measured data about the 0.2% offset stress for 2.25Cr-1Mo steel 900℃, the stress is obtained according to the correlation which is derived from Fig. 2.2-55. The 0.2% offset stress of 2.25Cr-1Mo steel at 900℃is about 95.11 MPa. According to the Eq.2-40, when the tube wall thickness become 15% of the initial thickness, the principal stress working on the tube wall become 108 MPa. Thus, when the tube wall thickness become 0.58 mm, which is 15% of the initial thickness, it is assumed that the yielding of the material take place according to the Tresca's yield theory.

After 10th remeshing procedure, the thickness of the remaining tube wall become 0.56 mm which is 14.5% of the initial tube wall thickness. It is regarded that the remaining diaphragm of the tube wall will be removed, and the tube become penetrated. In other words, the crack enlargement is terminated. Figure 2.3-23 shows the completely enlarged crack. The mesh grid has a funnel shape that the diameter become larger toward the crack exit. The maximum diameter is 2.36 mm. As regards the geometry, we compare the numerical result with the SWAT experimental data as shown in Fig.2.3-24. Overall, as regards with the shape of the enlarged leak the crack has a funnel shape in the both case. The equivalent diameter of the numerical result is 4.72 mm, and the diameter of the SWAT experimental nozzle is 4.96 mm, respectively. It seems that a curvature of the surface of the enlarged crack is slightly different, but it is expected that it caused by the mesh sensitivity. Either, the difference depends on the maximum wastage amount of an each analysis.

The wastage amount of each calculation according to its direction (horizontal and vertical) is compared in Fig. 2.3-25. The vertical axis indicates an accumulated ratio of wastage amount toward the initial thickness and the horizontal axis represents a non-dimensional time that is the ratio of number of a current trial to the total number of remeshing trials. It demonstrates that the speed of wastage propagation in the vertical direction is faster than that in the horizontal direction. Thus, it is expected that the maximum diameter of enlarged crack has a converged value when the wastage rate and the thickness of the tube wall are decided.

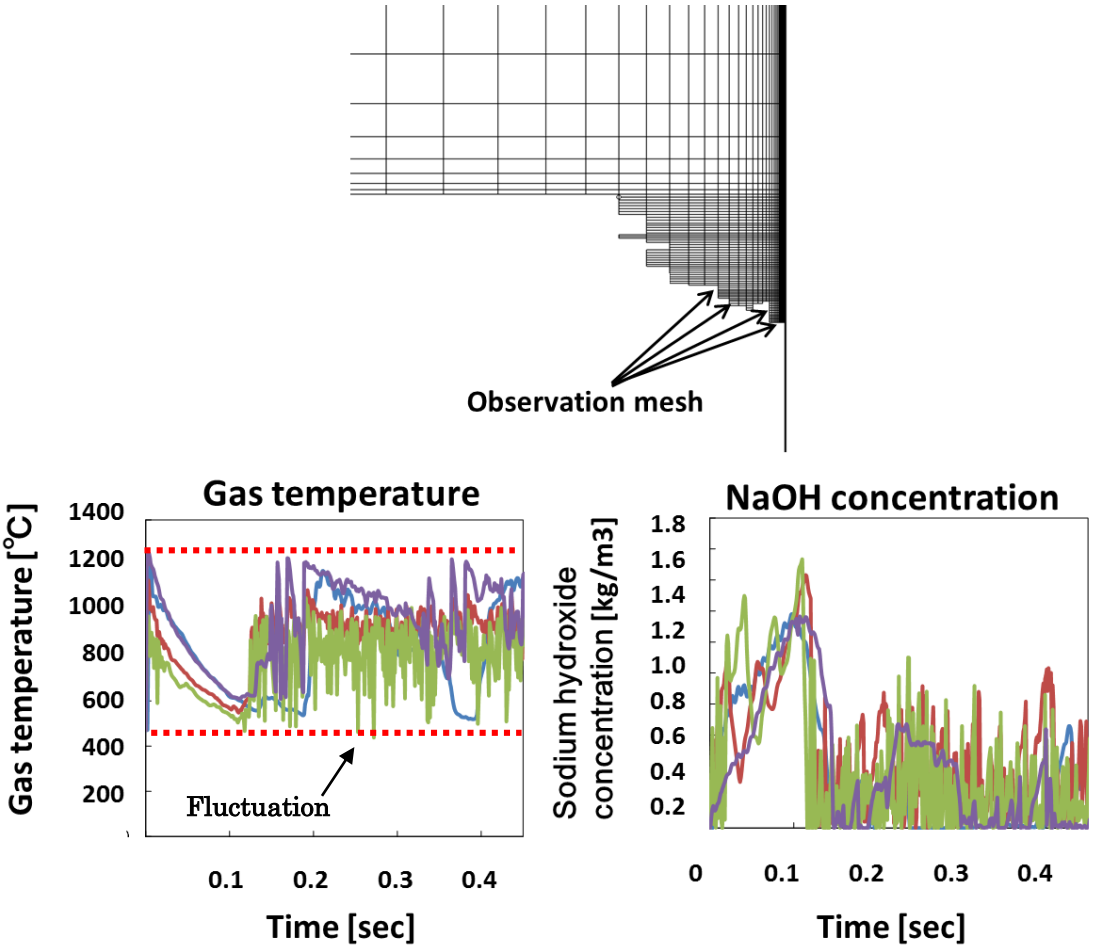

Figure 2.3-13 Gas temperature and NaOH concentration at tube surface in 3rd mesh

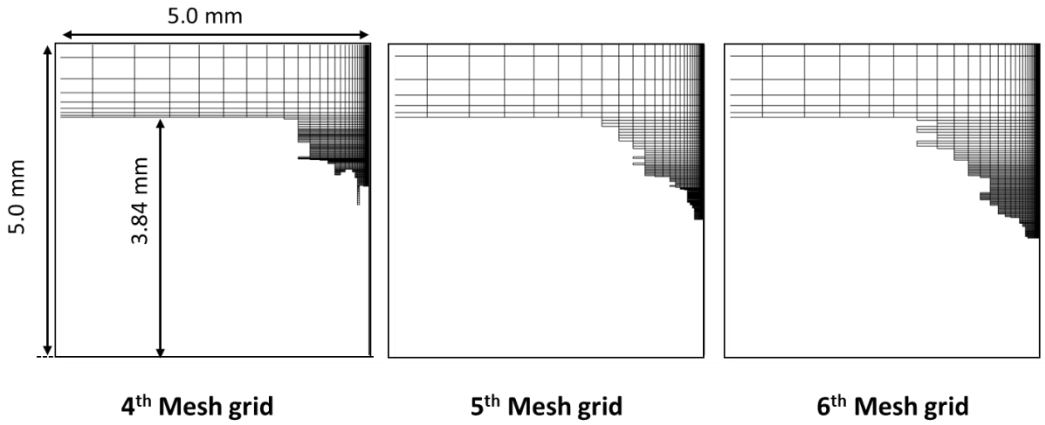

Figure 2.3-14 4th, 5th and 6th mesh grid after remeshing

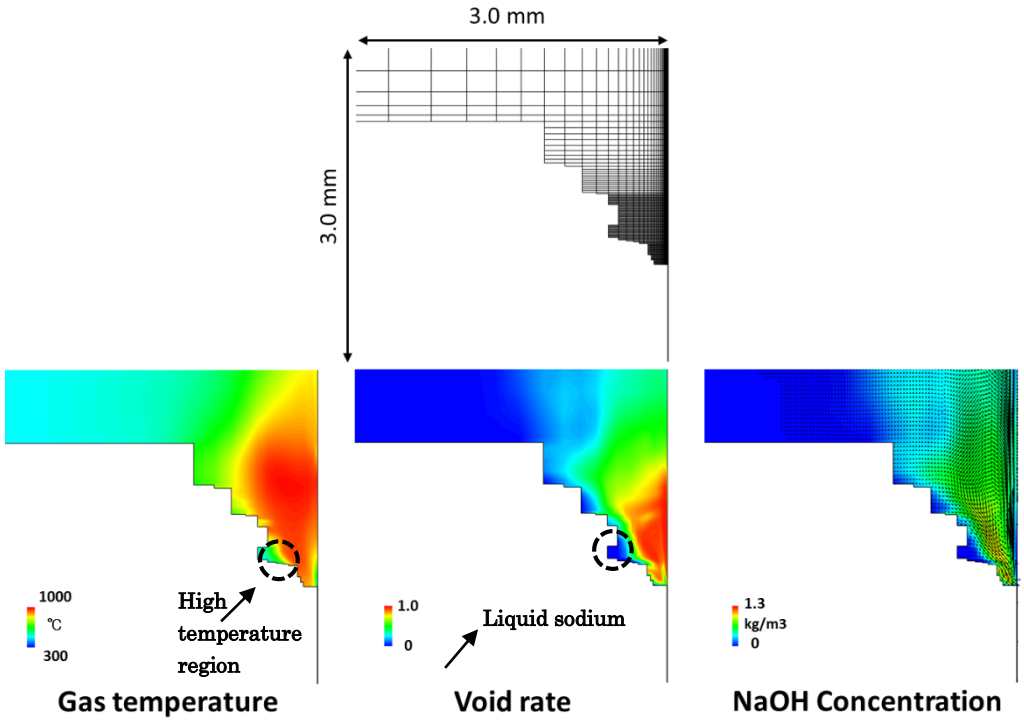

Figure 2.3-15 Thermal hydraulic properties using 6th analytical mesh

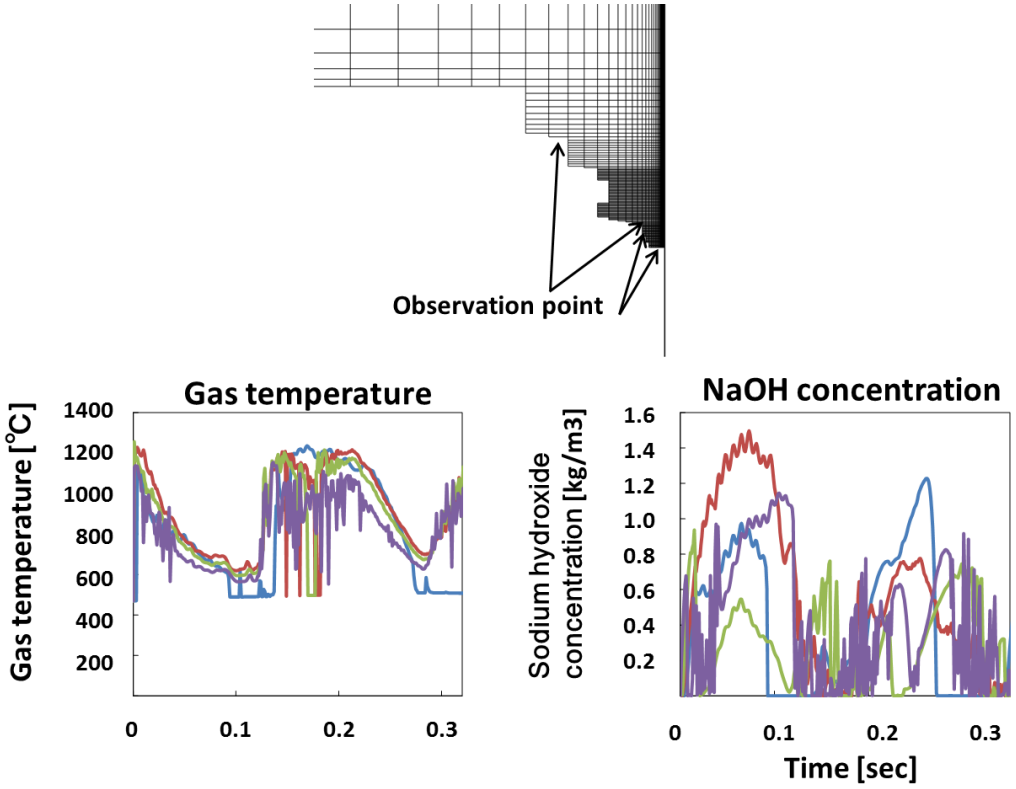

Figure 2.3-16 Gas temperature and NaOH concentration at tube surface in 6th mesh

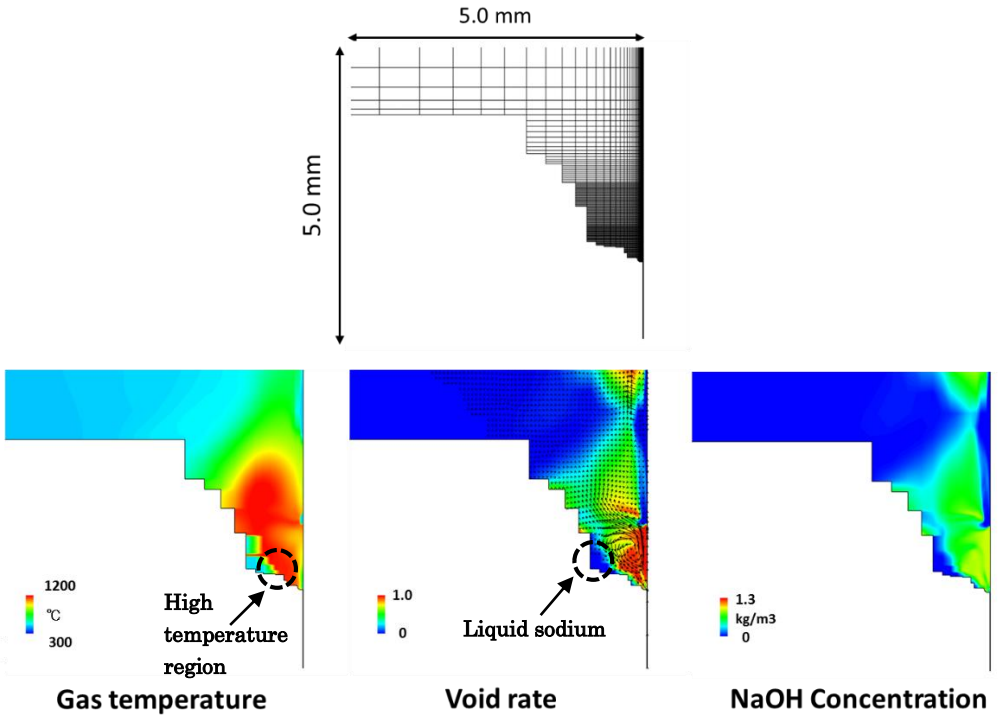

Figure 2.3-17 Thermal hydraulic properties using 7th analytical mesh

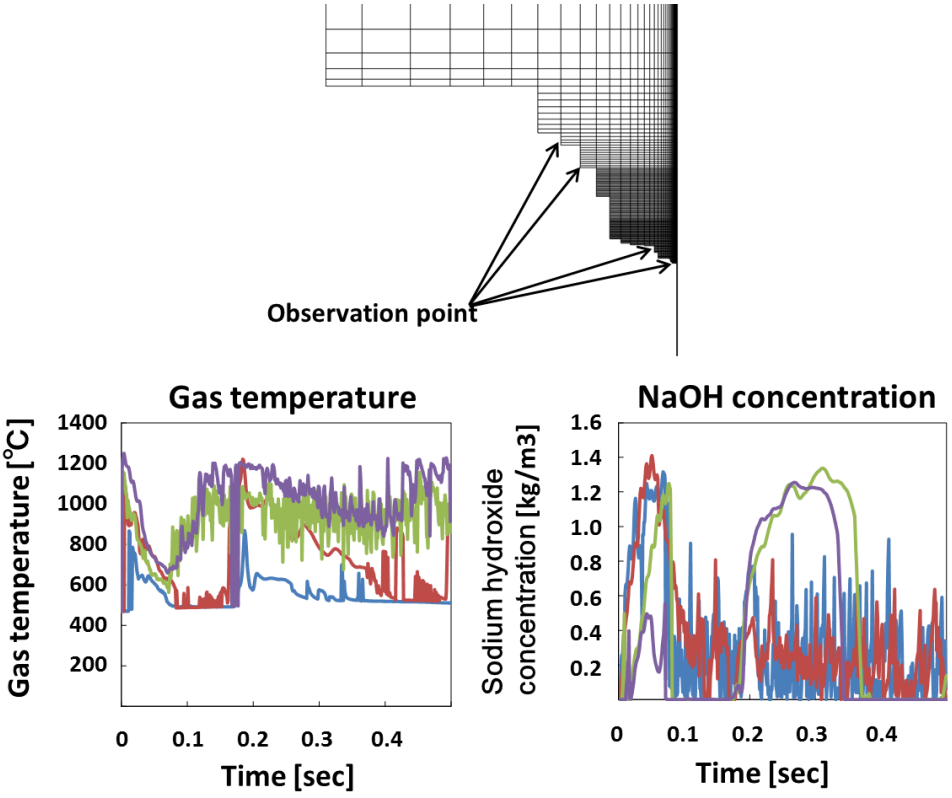

Figure 2.3-18 Thermal hydraulic properties using 7th analytical mesh

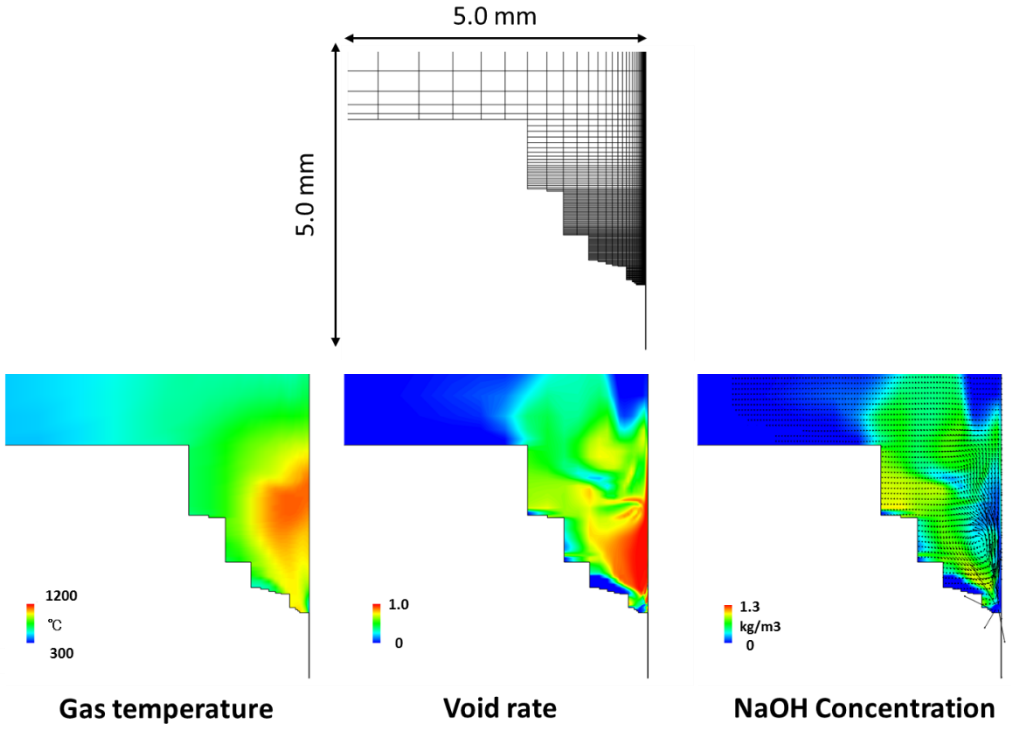

Figure 2.3-19 Thermal hydraulic properties using 8th analytical mesh

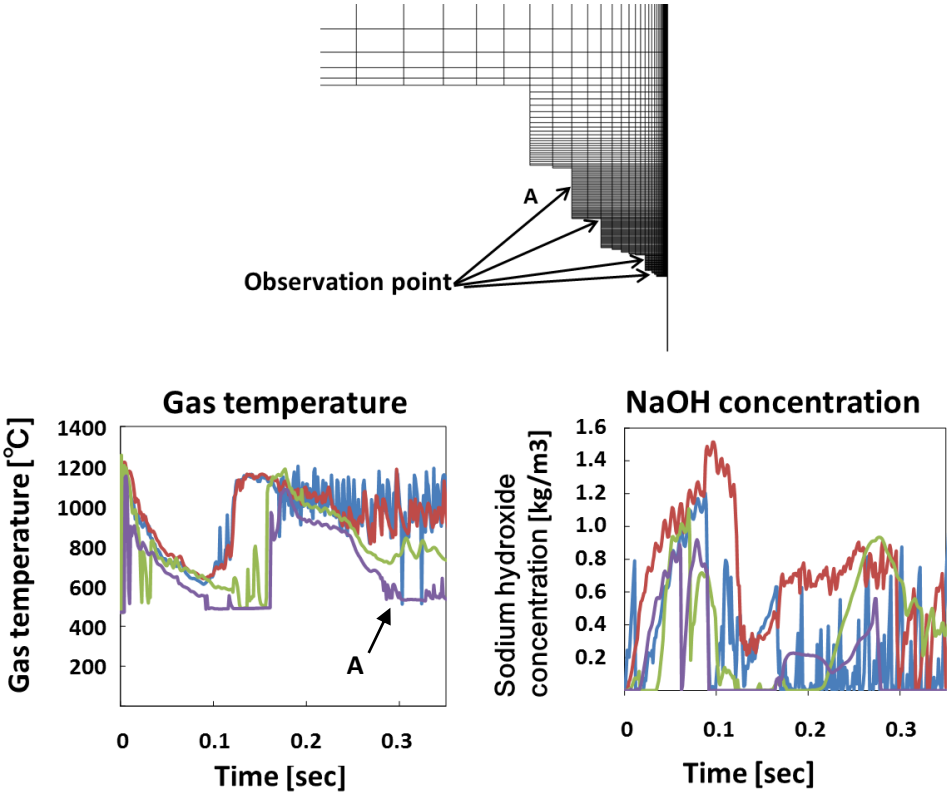

Figure 2.3-20 Thermal hydraulic properties using 8th analytical mesh

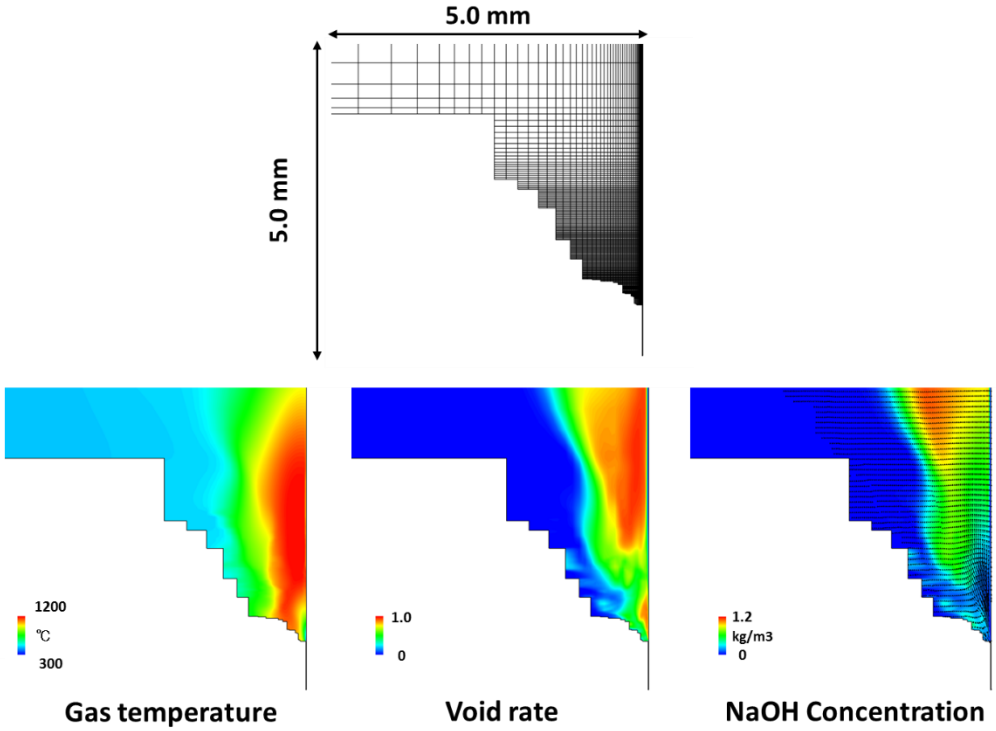

Figure 2.3-21 Thermal hydraulic properties using 9th analytical mesh

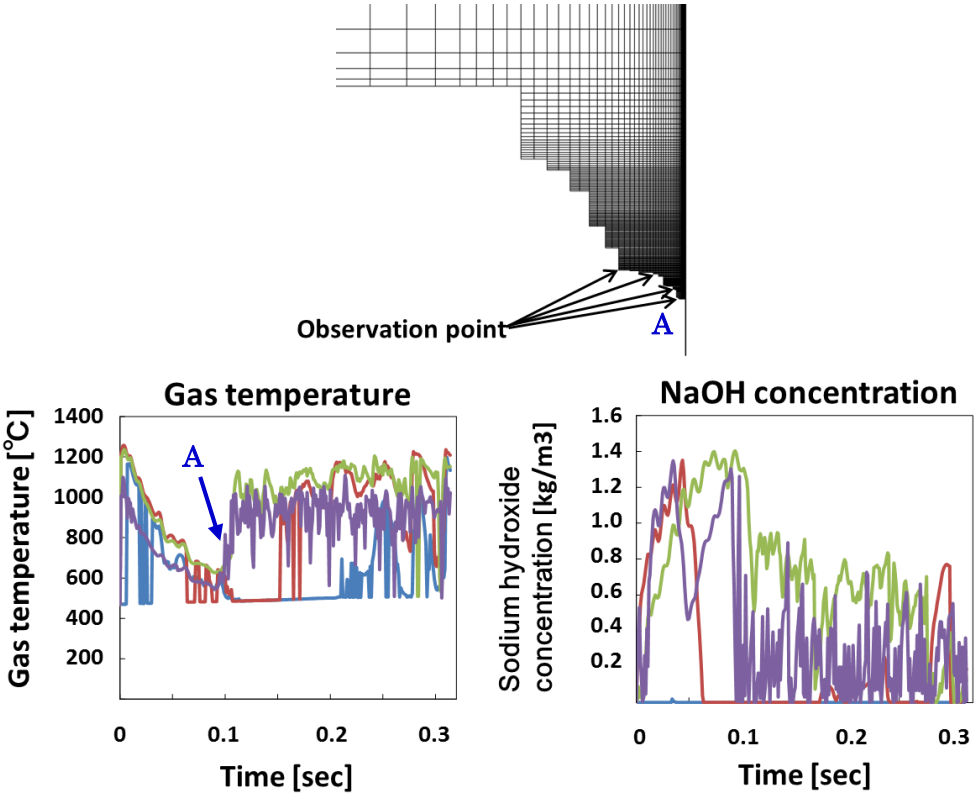

Figure 2.3-22 Thermal hydraulic properties using 9th analytical mesh

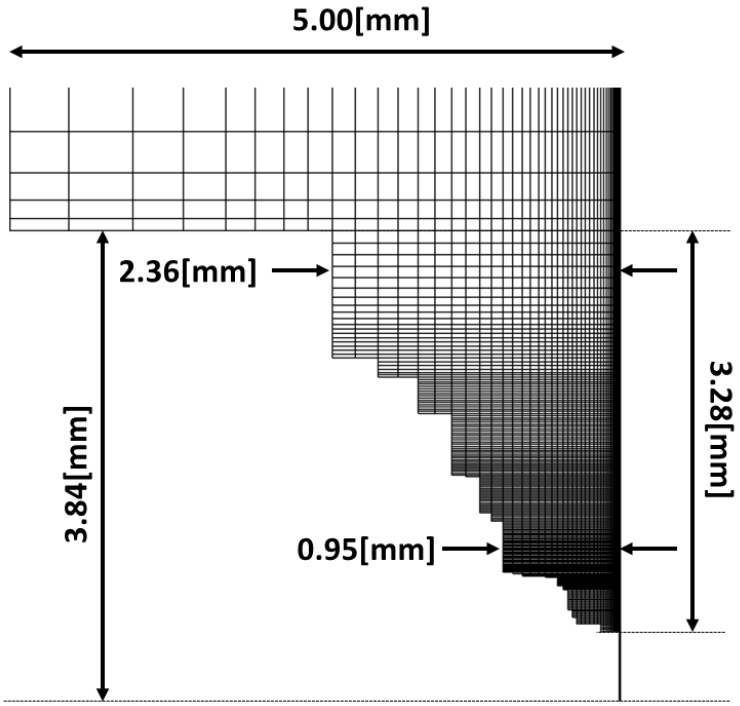

Figure 2.3-23 Completely enlarged crack mesh after remeshing

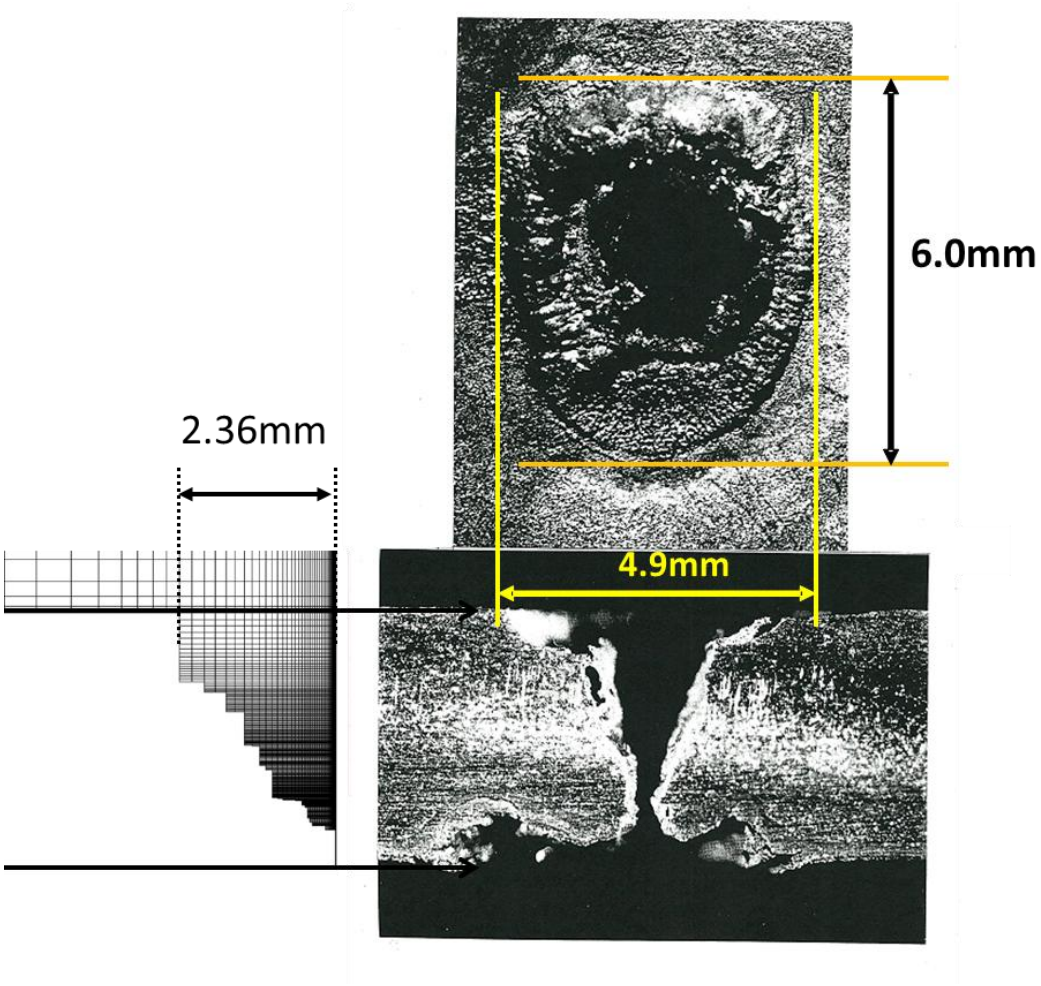

Figure 2.3-24 Comparison of numerical result and SWAT experiment result

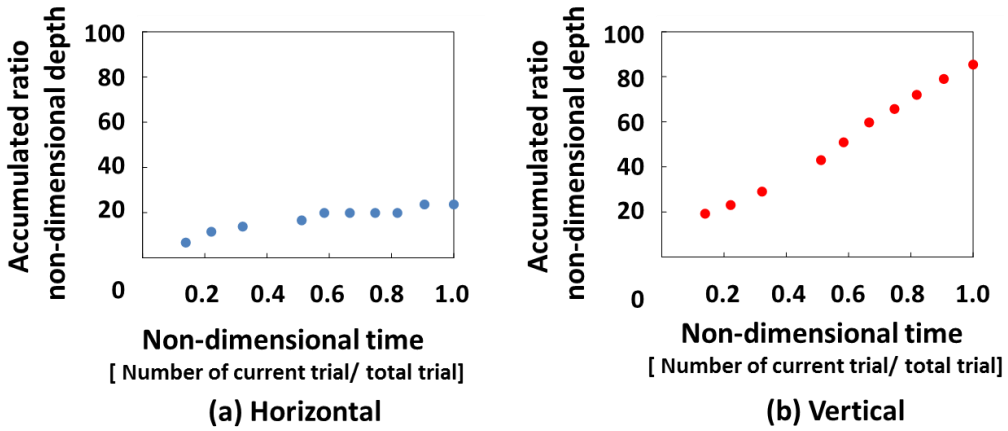

Figure 2.3-25 Self-wastage propagation speed according to its direction

[REFERENCES]

[1] T. Takata and A. Yamaguchi, “Numerical Approach to the Safety Evaluation of Sodium-Water Reaction”, *J. Nucl. Sci. Technol.* Vol. 40, 10, pp. 708-718, 2003.

[2] T. Takata and A. Yamaguchi, “Numerical Thermal-Hydraulics Study on Sodium-Water Phenomena-Development of Computational code ‘SERAPHIM’”, *Nuclear Cycle Development Institute Techincal Report*, 17, pp. 63-74, 2002.

[3] M.J. Pilling, “Reaction Kinetics”, Clarendon Press, Oxford, 1974.

[4] T. Takata and A. Yamaguchi, “Computational Sensitivity Study on Sodium-Water Reaction Phenomenon", *J. Nucl. Sci. Technol.* Vol. 43, 5, pp. 514-525, 2006.

[5] R.L. Mott, Applied Strength of Materials, Prentice Hall, New Jersey,Ohio, 2002

[6] T. Takata and A. Yamaguchi, “Numerical Approach to the Safety Evaluation of Sodium-Water Reaction”, *J. Nucl. Sci. Technol.* Vol. 40, 10, pp. 708-718, 2003.

[7] Hori, M. "Sodium/Water Reactions in Liquid Metal Fast Breeder Reactions," Atomic Energy Review, 183, pp.707-778, 1980.

[8] A. Kurihara, R. Umeda, S. Kikuchi and H. Ohshima, “Study on Sodium-water Reaction Phenomena in Steam Generator of Sodium-cooled Fast Reactor - (6) Thinning Evaluation due to High-temperature Sodium-hydroxide Impinging Experiment”, Proceeding of AESJ 2011 Fall Meeting, P09, p.781, 2001.

[9] J. Perry, J. Aboudi, “Elastic-plastic stresses in thick-walled cylinders”, ASME J. Pressure Vessel Technology, Vol. 125, pp. 248-252, 2003.

[10] A. B. Ayob, M. N. Tamin, and M. Kabashi Elbasheer, “Pressure Limits of Thick-Walled Cylinders”, Proceedings of the International MultiConference of Engineers and Computer Scientists 2009 Vol IIIMECS 2009, March 18 - 20, Hong Kong, 2009.

[11] Metallic material database – KINZOKU (http://metallicmaterials.nims.go.jp/)

[12] M. Kuroha, K. Sasaki, H. Kawabe, T. Yamada and M. Sato, "Study of Micro-Defect Self-Wastage Phenomena on LMBR Prototype Steam Generator’s Tube." *PNC report,* PNC TN941 82-101, 1982.

[13] M. Kuroha and K. Shimoyama, "Micro-Leak Behavior on LMFBR Monju Steam Generator Tube Materials – Studies of Micro-leak Sodium-Water Reaction, *PNC report*, PNC ZN9410 86-027, 1986.

[14] K. Shimoyama, T. Kobasyashi, M. Usami, S. Hagi, H. Tanabe and E, Yoshida, “ Wastage Characteristics of Welds of High-Chrome stee Heat Transfer Tube of steam Generator (Micro-leak and Small leak Sodium-Water Reactions)”, PNC report, PNC TN

9410 91-288, 1991.

3 Parametric Analysis of Self-wastage Phenomena

3.1 Related parameter

Self-wastage phenomena are very complicated phenomena that many parameters are related in. Sodium temperature, gas temperature, injection pressure, leak diameter, leak direction, leak rate, and wall materials are considered as a parameter that is related to the self-wastage phenomena. Figure 3.1-1 shows some aspect of enlarged crack from the sodium-water reaction experiment [1-3]. As we can see, the cross section of the enlarged nozzle varies according to parameters. Uncertainties exits in the self-wastage phenomena due to parameters. Therefore, to understand the self-wastage phenomena more clearly, the influence of each parameter on the phenomena is necessary to be clarified. In this study, we focus on the influence of leak rate and leak diameter on the self-wastage phenomena.

3.1.1 Leak rate

Leak rate is a parameter that closely relates to the sodium water reaction rate. It is expected that when the leak rate increase, it makes more sodium-water reaction take place, and it results in the more self-wastage phenomena. Micro-leak behaviors can be classified into the following 3 cases [4].

Case 1: in the initial leak rates of more than 1.0×10^{-2} g/sec, the leak rate is kept comparatively constant as shown in Fig. 3.1-2 (a) and consequently develops rapidly owing to the self-wastage penetration (without incubation time case).

Case 2: in the case of the leak rate less than 10^{-2} g/sec, it reduces for the short period to the range of 10^{-4} to 10^{-5} g/sec. In such cases of the 2-1/4Cr-Mo steel nozzle, the leak rate frequently reduces further with time to approximately 10^{-7} g/sec owing to the self-plugging in the leak hole. This leak rate is kept for the long period, and it almost never returns to the initial value with a few exception as shown in Fig. 3.1-2 (b) (Self-plugging).

Case 3: the micro-leak behaviors can be classified into some cases. For example, On the other hands, when the micro crack chokes partially, the leak rate become reduced for a period (incubation time) then, the leak rate finally returns to a level of initial one, and results to develop rapidly as shown in Fig.3.1-3 (c) (with incubation time case).

In SWAT experimental reports, the proportion of each case was evaluated according to the material and slit-type. The result is shown in Table 3.1-1 [5].

Therefore, to depict the overall flow characteristic, the initial leak rate is not proper. The average leak is a good parameter to represent the flow characteristic during the propagation of the self-wastage propagation.

However, according to the SWAT experimental data which depicts the relationship between the average leak rate and the enlarged leak diameter, it seems that there is no remarkable relationship between these two parameters. Figure 3.1-3 shows total 41 experimental results. The horizontal axis is average leak rate, and the vertical axis indicates the orifice diameter of the enlarged hole. It seems that there is no strong relationship between the average leak rate and enlarged orifice diameter. The figure shows that in most case, the resultant diameter of enlarged crack exists smaller than 1.2~1.3 mm regardless of averaged leak rate. Also, it shows that for the case 1 has larger leakage than the case 3. Because, the reduction of leak rate is caused by a plugging by the reaction product that is more likely happened with a small leak hole.

Figure 3.1-4 shows an enlargement ratio of leak hole according to the average leak rate. A tendency between the case 1 and case 3 are distinct. For the case 1, it has a larger average leak rate and a smaller enlargement ratio than the case 3. Generally, it seems that a reciprocal relationship exists between the average leak rage and the enlargement ratio. It is assumed that if the leak rate is large, an erosive effect will be dominant. On the other hand, if the leak rage is small, a corrosive effect will be more dominant than the erosive.

For the case 3, even though the average leak rate is almost same, the resultant enlargement ratio has different value.

Figure 3.1-5 shows self-wastage rate according to average leak rate. The overall

tendency of the data shows that as the average leak rate is larger, the self-wastage rate also become bigger. The reason is assumed that if the leak rate is increased, erosive effect will be stronger by increased flow, and the reaction rate also increases, thus corrosive effect also become stronger, this brings the faster self-wastage rate. However, the leak rate is decided by a crack diameter, an injection velocity and plugging degree, the influence of this parameter on the leak rate is also needed to be considered.

3.1.2 Leak diameter

It is generally anticipated that a micro-defect in the heat transfer tube of the actual plant will occur in the form of a crack rather than in the circular hole. It is also seemed that the behaviors of the self-wastage and the self-plugging are different in the both type. For crack type nozzle, it is difficult to define a diameter of the crack. Thus an equivalent diameter is estimated by measuring the time when it took for argon to discharge through the crack from the small tank to the atmosphere until the pressure in the tank reduced from a certain value to another one.

Generally, the larger initial diameter produces, the bigger leakage rate under the same operating pressure. Therefore, the larger initial diameter results, the faster self-wastage rate and the larger enlarged orifice diameter.

Figure 3.1-6 shows the enlarged orifice diameter according to the leak diameter. It seems that the result has a similar tendency with Fig.3.1-3. Any distinct relationship between the two parameters can be founded. From these results (Fig. 3.1-3 and 3.1-6), it can be said that the enlargement diameter does not affect the average leak rate and the initial leak diameter. In other hands, that the enlarged orifice diameter does not exceed a certain scale.

Figure 3.1-7 shows the enlargement ratio according to the leak diameter. It seems that strong negative correlation is existed between the enlargement ratio and the leak diameter for both the enlargement ratio and the leak diameter. This results can be explained from the fact that the enlarged diameter has an upper limit. Thus, for a small diameter nozzle has the large enlargement ratio and a big diameter nozzle has the small enlargement ratio. The orifice leak diameter is determined and able to be evaluated by the tube wall thickness if the vertical wastage rate and the horizontal wastage rate are

clarified.

Figure 3.1-8 shows the self-wastage rate, according to the leak diameter. It shows different tendency with the fig. 3.1-5. It seems that the self-wastage is not influenced by the leak diameter.

Figure 3.1-9 shows the relationship between the leak diameter and self-wastage rate. As shown in the figure, generally as the initial leak diameter increase, the average leak rate also increase in whole.

From this analysis, it can understand that the self-wastage rate is closely related average leak rate. The average leak rate and the leak diameter also influence the enlargement ratio. From the figure 3.1-5 and the figure 3.1-8, it can be expected that another parameter, which affects the average leak rate such as flow velocity, also may relate to the self-wastage rate. Influence of the flow velocity is necessary to be evaluated.

The fact that the enlarged nozzle diameter is not subject to the influence of the leak diameter and the average leak rate. It might be affected by the thickness of the tube wall.

To understand the influence of the average leak rate and the leak diameter more clearly, the following analyses are devised.

▷ Analyses that vary only the flow velocity with a single-diameter nozzle to evaluate the influence of flow velocity.

▷ Analyses that vary only the leak diameter with a constant flow velocity to evaluate the influence of leak diameter.

▷ Analyses that vary the flow velocity and the leak diameter while the total leak rate is constant.

Table 3.1-1 Classification of micro-leak behavior in SWAT experiment

Material	Crack type	Case 1	Case 2	Case 3	Total
High Chrome alloy steel	Fatigue	10	6	32	45
Mod. 9Cr-1Mo	Artificial	4	4	1	9
SUS 321	Artificial	11	7	1	19
2-1/4Cr-1Mo	Artificial	4	23	5	32

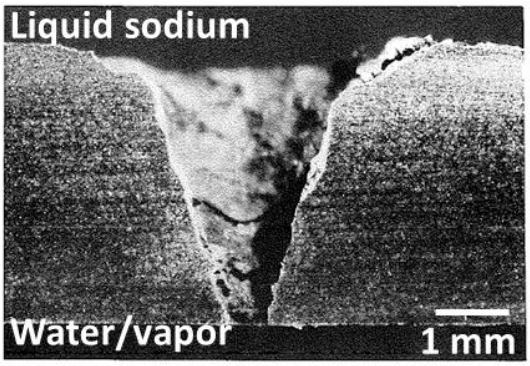

Material: 2-1/4Cr-1Mo steel

Average leak rate: 5×10^{-4} g/sec
Self-wastage rate: 3×10^{-4} mm/sec
Sodium temp: 470℃

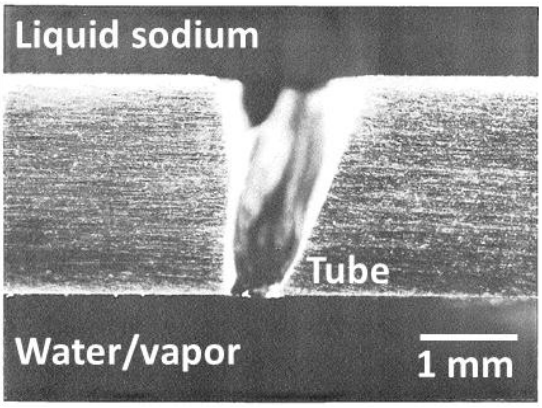

Material: 321 Stainless steel

Average leak rate: 4×10^{-2} g/sec
Self-wastage rate: 3.12×10^{-3} mm/sec
Sodium temp : 505℃

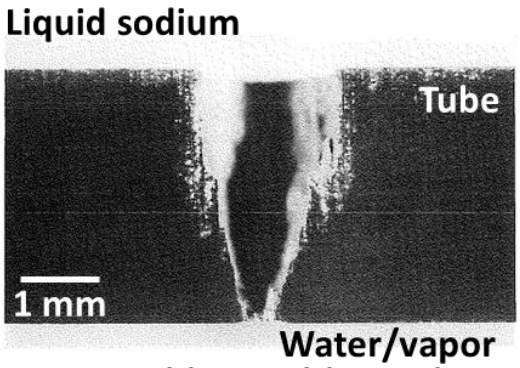

Material: 321 Stainless steel

Average leak rate: 8×10^{-5} g/sec
Self-wastage rate: 4×10^{-5} mm/sec
Sodium temp : 460℃

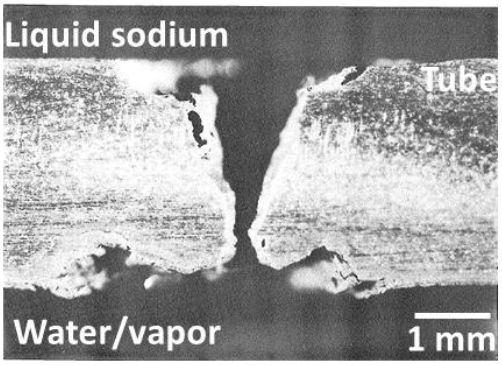

Material: 2-1/4Cr-1Mo steel

Average leak rate: 2.35×10^{-5} g/sec
Self-wastage rate: 6.23×10^{-6} mm/sec
Sodium temp : 470℃

Fig. 3.1-1 Various aspect of enlarged crack (continued)

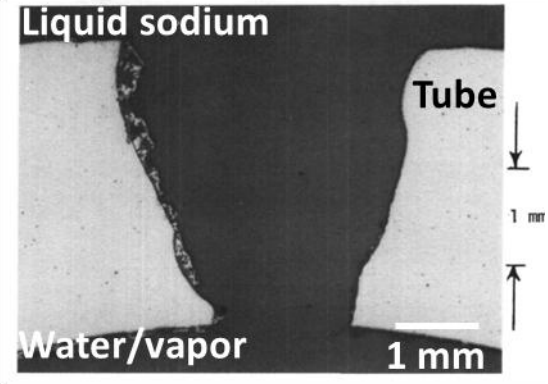

Material: 2-1/4Cr-1Mo steel

Average leak rate: 8×10^{-5} g/sec
Self-wastage rate: 5.17×10^{-4} mm/sec
Sodium temp : 493℃

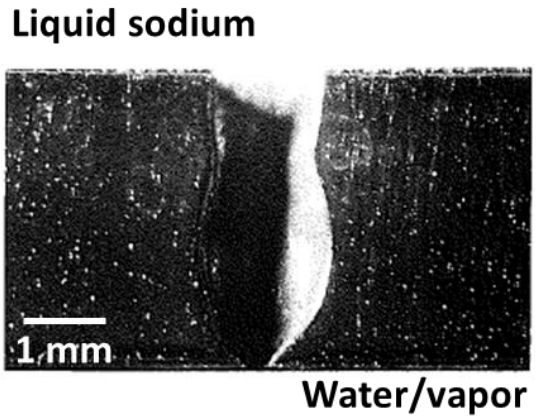

Material: 321 Stainless steel

Average leak rate: 3.5×10^{-2} g/sec
Self-wastage rate: 3.22×10^{-3} mm/sec
Sodium temp : 505℃

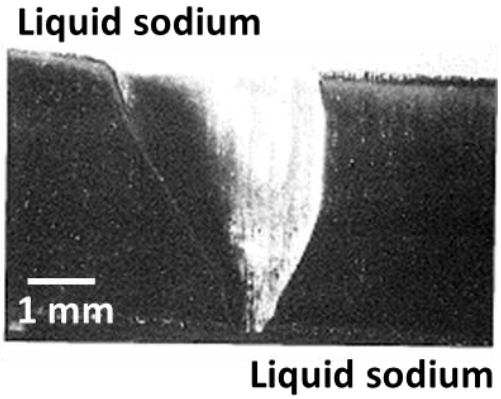

Material: 321 Stainless steel

Average leak rate: 2.4×10^{-3} g/sec
Self-wastage rate: 4.1×10^{-4} mm/sec
Sodium temp : 505℃

Figure 3.1-1 Various aspect of enlarged crack

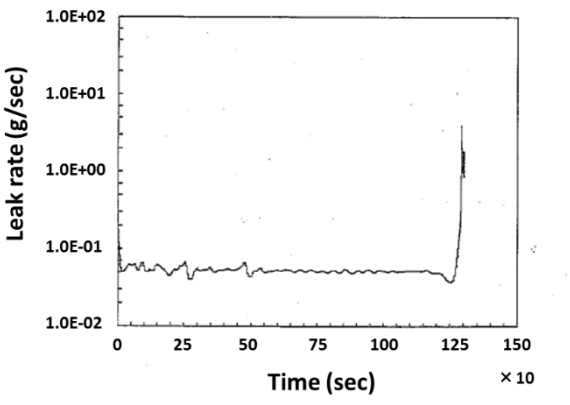

(a) Case 1: without incubation time

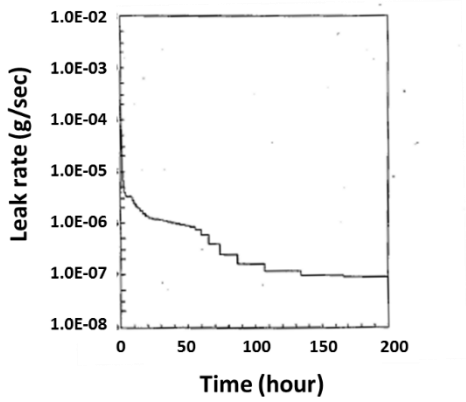

(b) Case 2:self-plugging

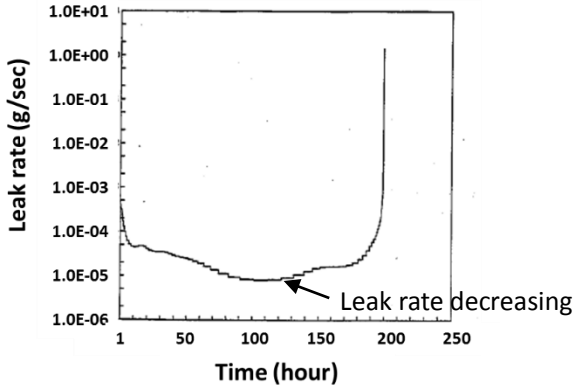

(c) Case 3: with incubation time

Figure 3.1-2 Micro-leak behaviors

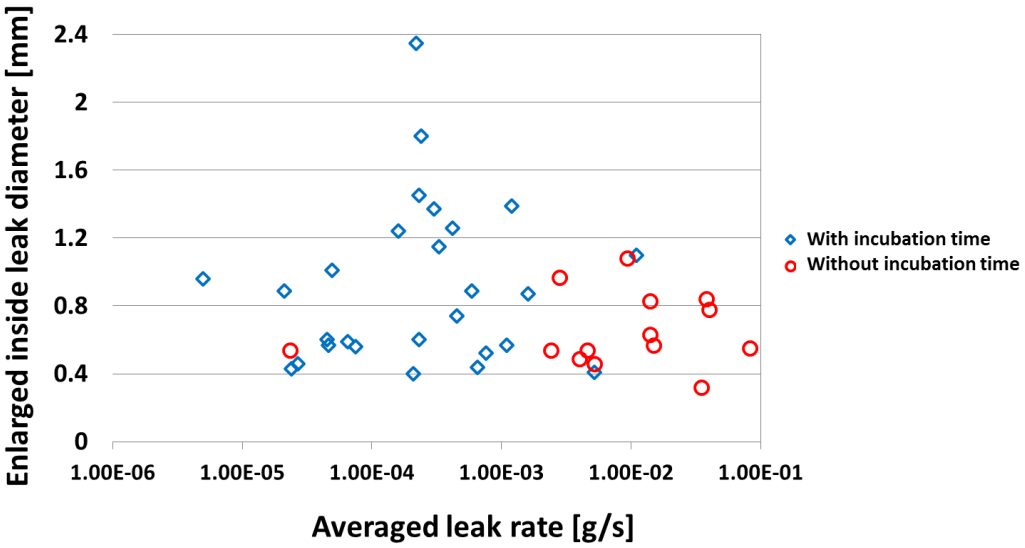

Figure 3.1-3 Orifice diameters of the self-enlarged holes

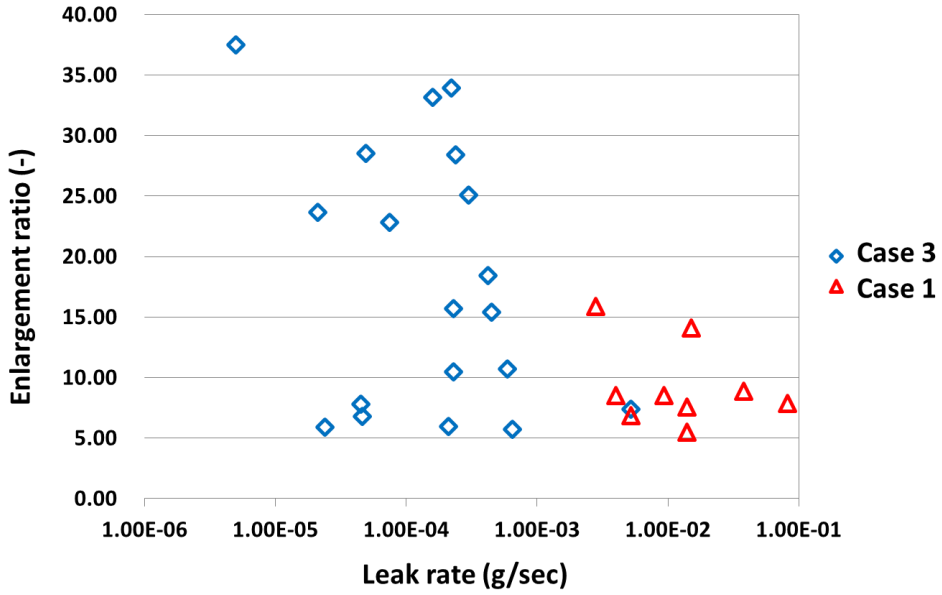

Figure 3.1-4 Enlargement ratio of self-enlarged holes

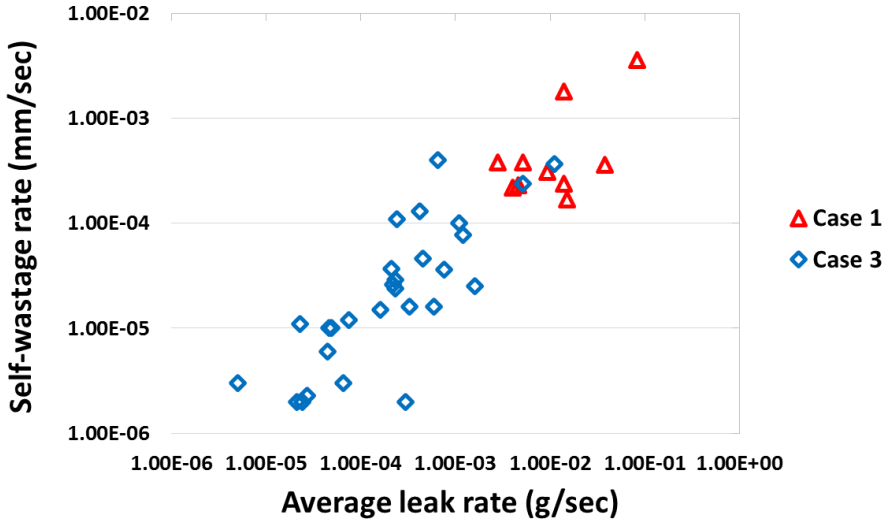

Figure 3.1-5 Self-wastage rate according to average leak rate

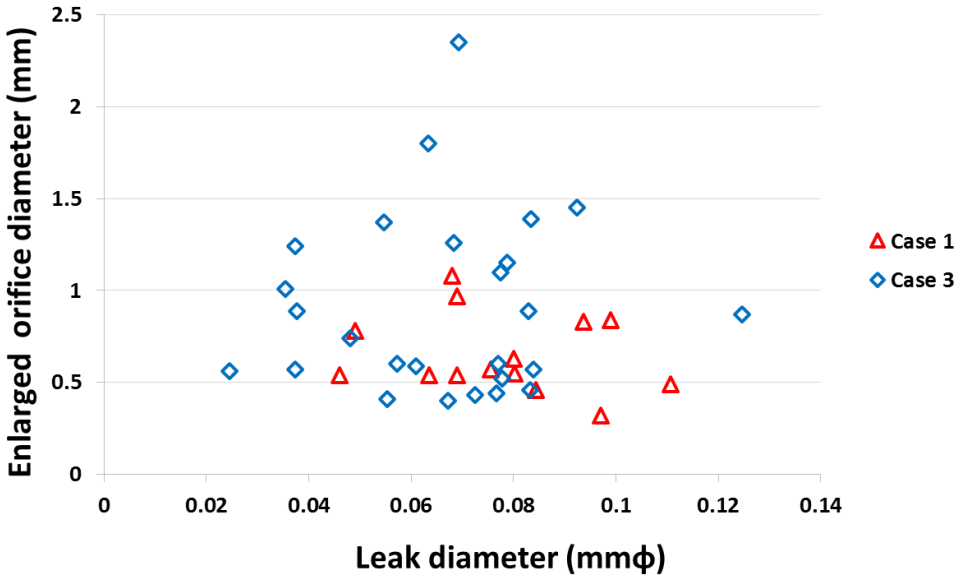

Figure 3.1-6 Enlarged orifice diameter according to leak diameter

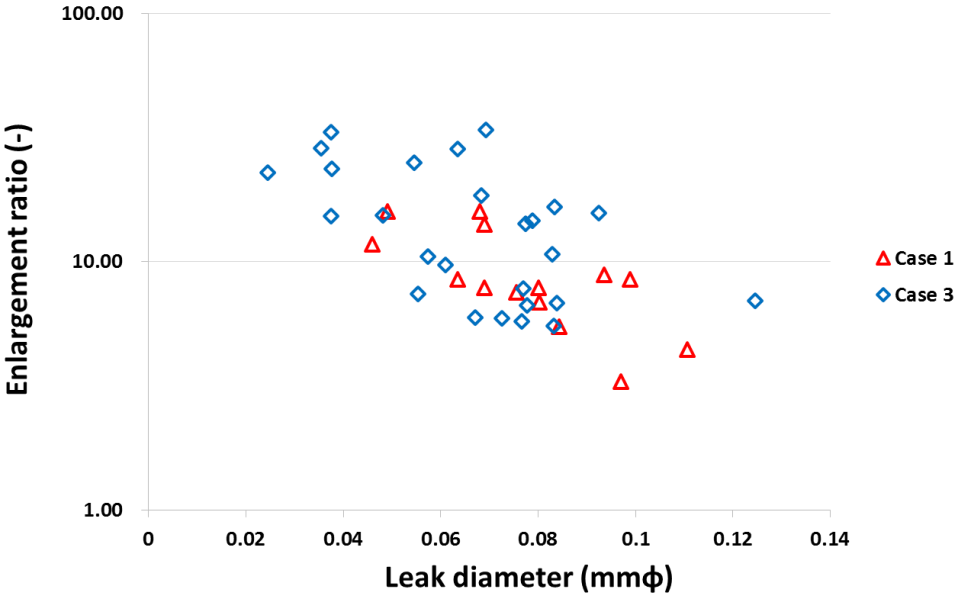

Figure 3.1-7 Enlargement ratio according to leak diameter

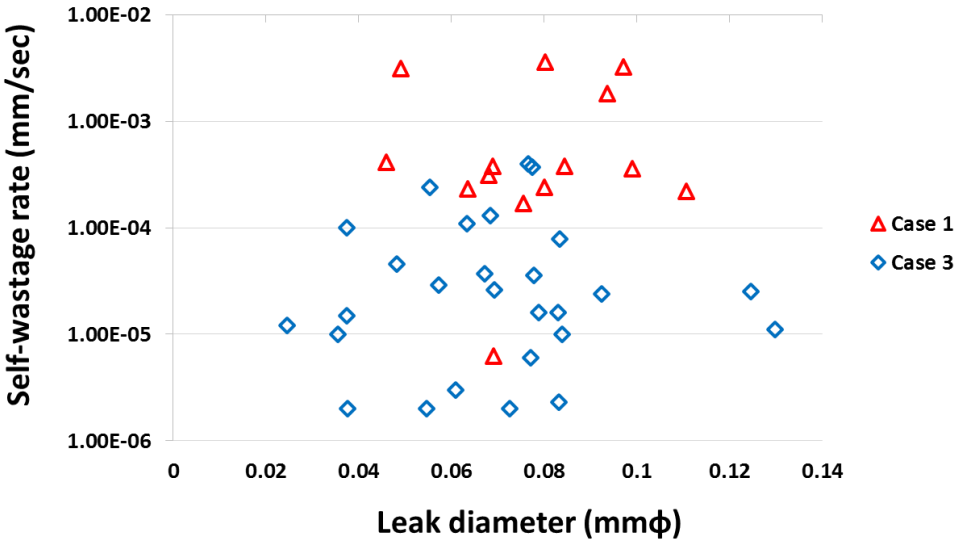

Figure 3.1-8 Self-wastage rate according to leak diameter

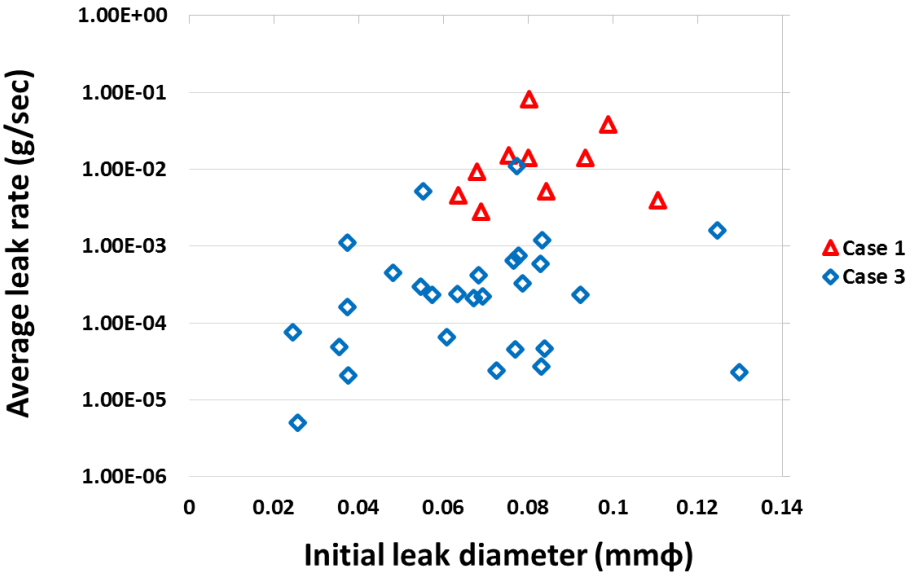

Figure 3.1-9 Average leak rate according to initial leak diameter

3.2 JAEA experiment analysis

In the early section, the influences of the average leak rate and the initial leak diameter on the self-wastage phenomena are considered. From the analysis regarding the enlarged orifice diameter, it is found that the orifice diameter does not affect the average leak rate and the initial diameter. Rather the tube thickness may affect the enlarged diameter. Therefore, to verify these new understanding an extra numerical analysis using SERAPHIM code is carried out. In this calculation, recent experimental data (SWH-5) and results of the self-wastage phenomena are used [6].

3.2.1 Analytical conditions

The same numerical procedure, which is mentioned in Ch.2, is adopted for the new analysis. The details about the experimental conditions are listed in Table 3.2-1. In this experiment, the tube wall thickness is 0.8 mm, and it is thinner than the tube wall thickness of the SWAT experiment mentioned in Ch.2. The initial nozzle diameter is 57.1 μm, and it is smaller than the equivalent diameter that is used in the former calculation. The average leak rate of SWH-5 is larger than that of the SWAT-2 experiment. Figure 3.2-1 shows the analytical grid for a numerical simulation. In this time, since the leak rate and the steam pressure increases the height and width of the analytical grid become twice in scale. The time step is 2.0×10^{-9} sec.

3.2.2 Numerical results

Figure 3.2-2 shows void fraction, velocity vector and NaOH concentration around the nozzle exit at 2.0×10^{-2} sec. It shows that high-temperature region is appeared above the tube wall around the nozzle exit. The width of the reaction zone is much narrower than the reaction zone obtained from Fig.2.3-3. In this case, the injected leakage jet tends to flow straight forwardly toward downstream. These differences are caused by the flow velocity. SWH-5's leak rate is 2.58 times larger than that of SWAT experiment. The leak area measured by the diameter of SWAT experiment is 1.5 times larger than that of SWH-5 result. Thus, the flow velocity of SWH-5 is almost 4 times larger than the velocity of SWAT experiment. The high velocity caused by high-pressure brings different on the

reaction region.

Figure 3.2-3 shows transient gas temperature and NaOH concentration profile on 4 different mesh. As we can see both the properties fluctuate in a certain rage. No significant difference can be found in the tendency between Fig.3.2-3 and Fig.2.3-5. It seems that the NaOH concentration in Fig.3.2-3 is slightly smaller than that in Fig.2.3-5. It is caused by the fact that the injected jet flow into the liquid sodium straightly rather than spread toward the surrounding region.

Figure 3.2-4 shows the estimated wastage depth according to the thermal properties at a different time. A slight variation exists between each wastage depth. However, overall shape and depth are coincident. As we considered in Ch.2, a projection appears near the nozzle. In this analysis too, this projection is removed by the same way we used in Ch.2.3. According to self-wastage depth, remeshing procedure is carried out. Remeshed mesh grid with a projection and the mesh removing the projection are shown in Fig.3.2-5. The projection is removed that the remaining depth is equal to the maximum wastage depth.

Using the newly remeshed grid, another calculation is carried out. Figure 3.2-6 shows void fraction, velocity vector and NaOH concentration around the nozzle exit at 2.0×10^{-2} sec. The figure shows that a high-temperature and a high-void fraction region is appeared above the newly generated surface of enlarged leak. It can be expected that the self-wastage phenomena will be continued.

Figure 3.2-7 shows the transient NaOH concentration profile, gas temperature and wastage depth that is estimated by using the temperature and the NaOH concentration. Wastage depth is reflected on the 2nd mesh in Fig.3.2-5 by remeshing the mesh grid. As a result, newly mesh grid is obtained. (Fig.3.2-8). After the 2nd remeshing, the newly remeshed 3rd grid has a lumpy surface with a thick projection near the crack. Thus, like the same manner, this projection is removed, and the 3rd grid is obtained.

The 4th calculation is carried out using the 3rd mesh grid. Again the wastage depth on each cell are estimated using the average thermal properties on the mesh. Figure 3.2-9 shows the horizontal and vertical estimated wastage depth. The self-wastage depth is also reflected by the remeshing procedure, after the 3rd remeshig procedure, the penetrated mesh grid is obtained (Fig.3.2-10). The opening appeared to taper in ward to

a significantly smaller opening on the inside of the tube wall. The inner diameter is 321 μm, and the outer diameter is 884μm. The experimental results have 601μm for outer diameter and 444μm for inner diameter. The difference between the numerical results and the experimental data is caused by estimated maximum wastage depth. 30% of the initial depth is a slightly coarse amount for each estimation. More small wastage depth for each calculation is desirable to get a more accurate numerical result. Still, there is a necessary to decide the best level for the maximum wastage depth estimation for each step. Further evaluation is needed.

Table 3.2-1 SWH-5 and SWAT-2 (#2022) experimental datat

	JAEA(SWH-5)	SWAT-2(#2022)
Material	9Cr-1Mo	$2^{1}/_{4}$Cr-1Mo
Tube wall thickness (mm)	0.8	3.84
Sodium temperature (°C)	520.5	470
Sodium pressure (Mpa)	0.133	0.147
Steam temperature (°C)	516.86	470
Steam pressure (Mpa)	4.093	12.8
Initial nozzle diameter [μm]	57.1	69.0
Average leak rate [g/s]	8.0×10^{-3}	3.4×10^{-3}

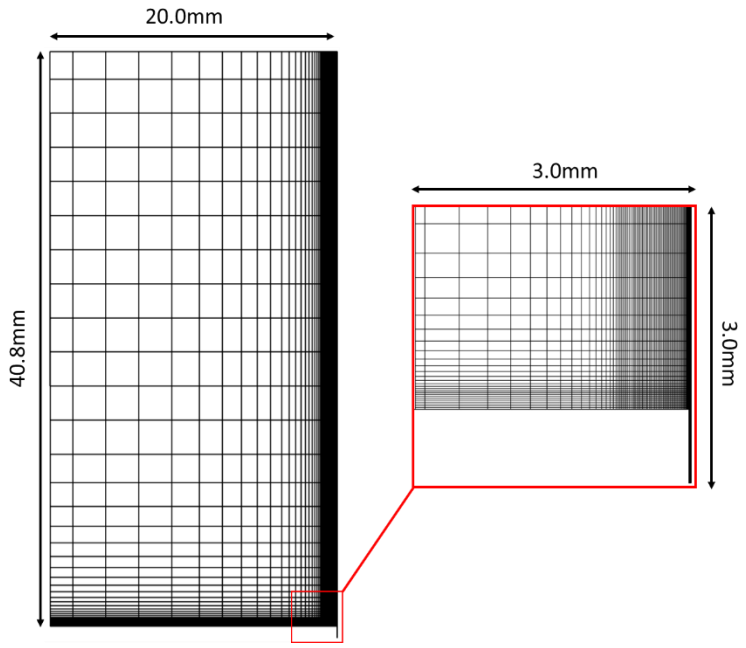

Figure 3.2-1 Initial analytical mesh grid

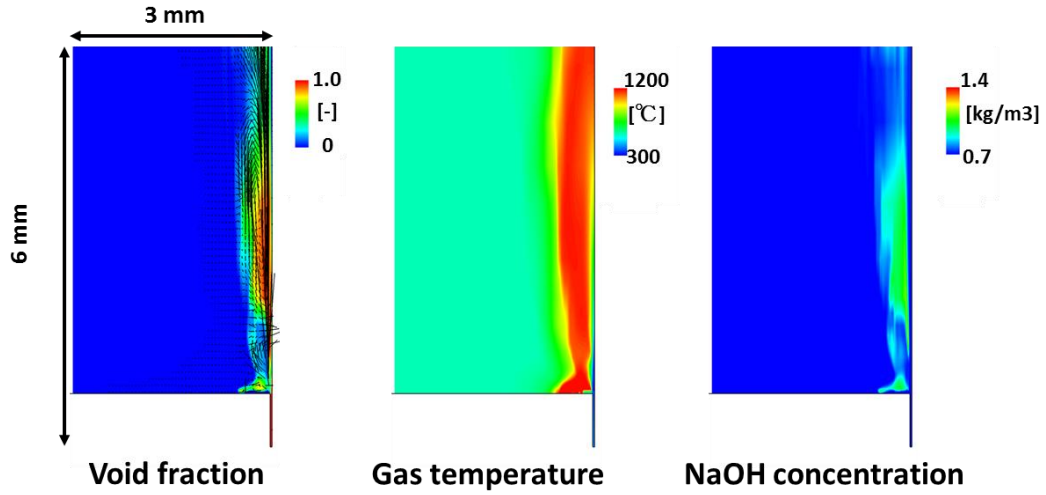

Figure 3.2-2 Void fraction, gas temperature and NaOH concentration around nozzle exit (T=0.2 sec)

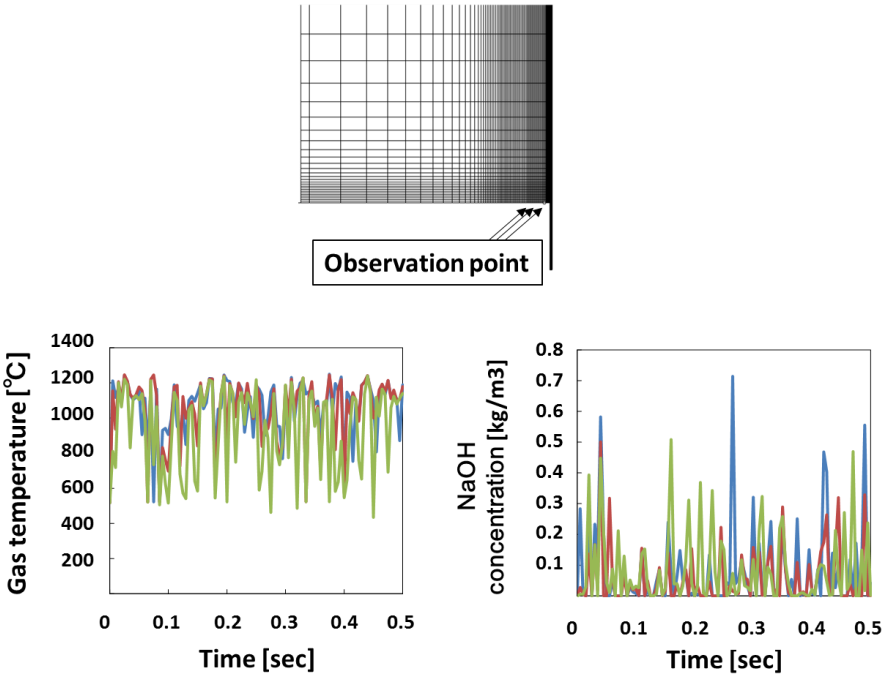

Figure 3.2-3 Transient temperature and NaOH concentration profile at tube surface

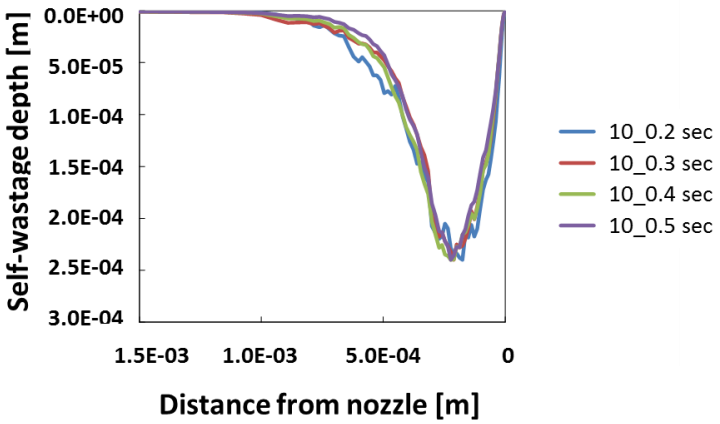

Figure 3.2-4 Estimation of vertical wastage depth at tube surface

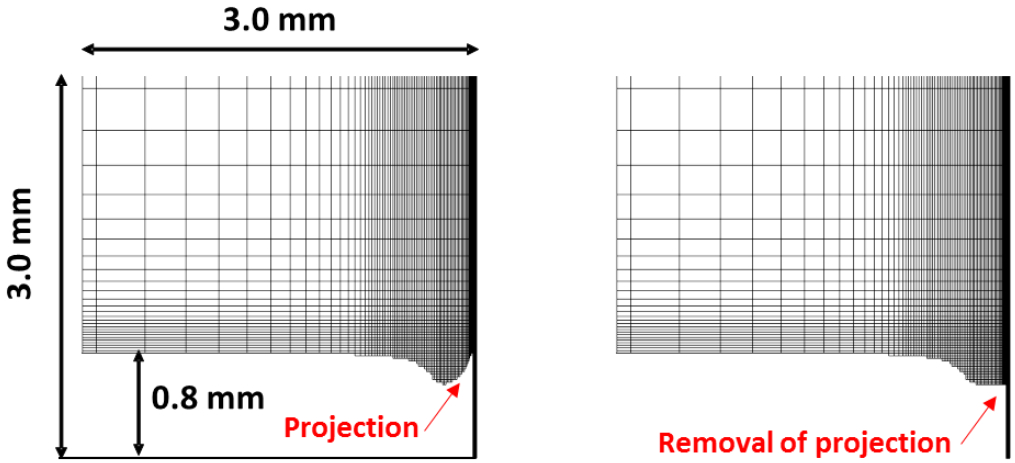

Figure 3.2-5 Remeshed mesh grid before and after removal of projection

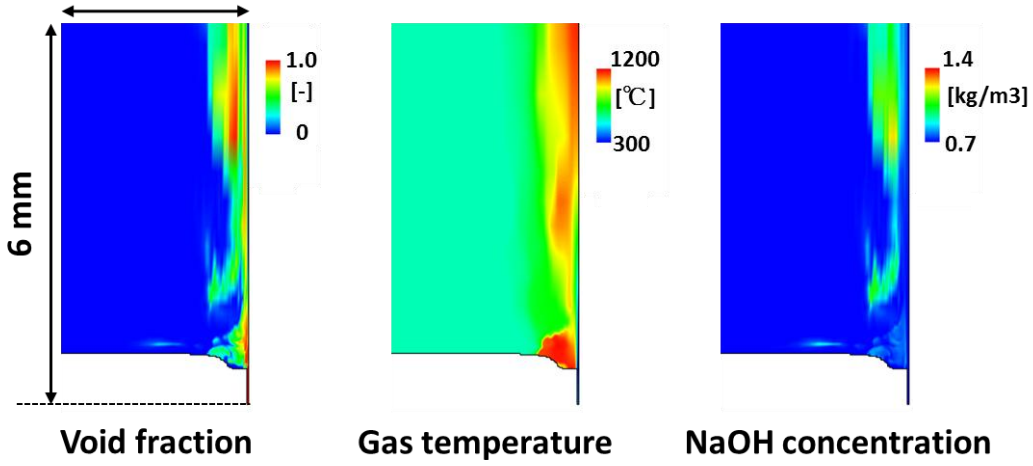

Figure 3.2-6 Void fraction, gas temperature and NaOH concentration around nozzle exit

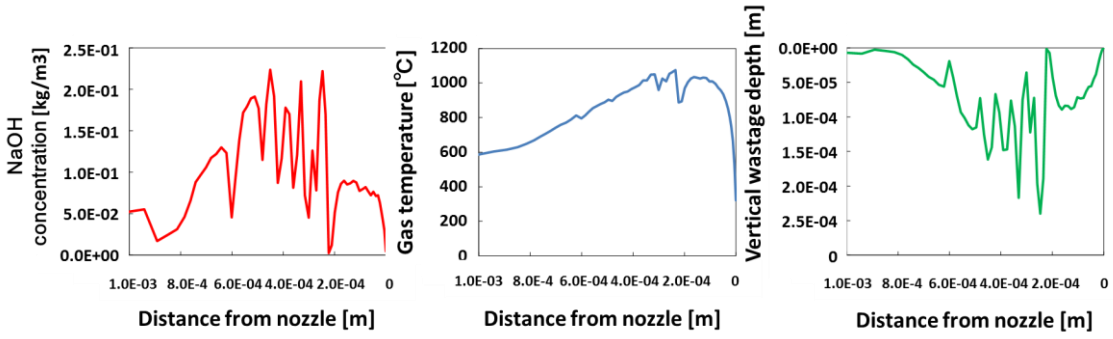

Figure 3.2-7 Estimation of vertical wastage depth and distribution of NaOH concentration and gas temperature at tube top

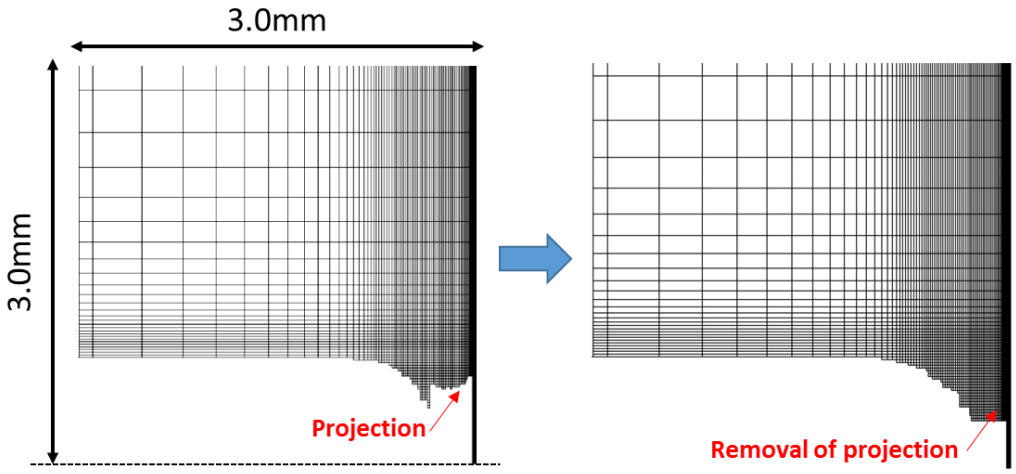

Figure 3.2-8 Remeshed 3rd mesh grid (left) before projection removal (right) after removal

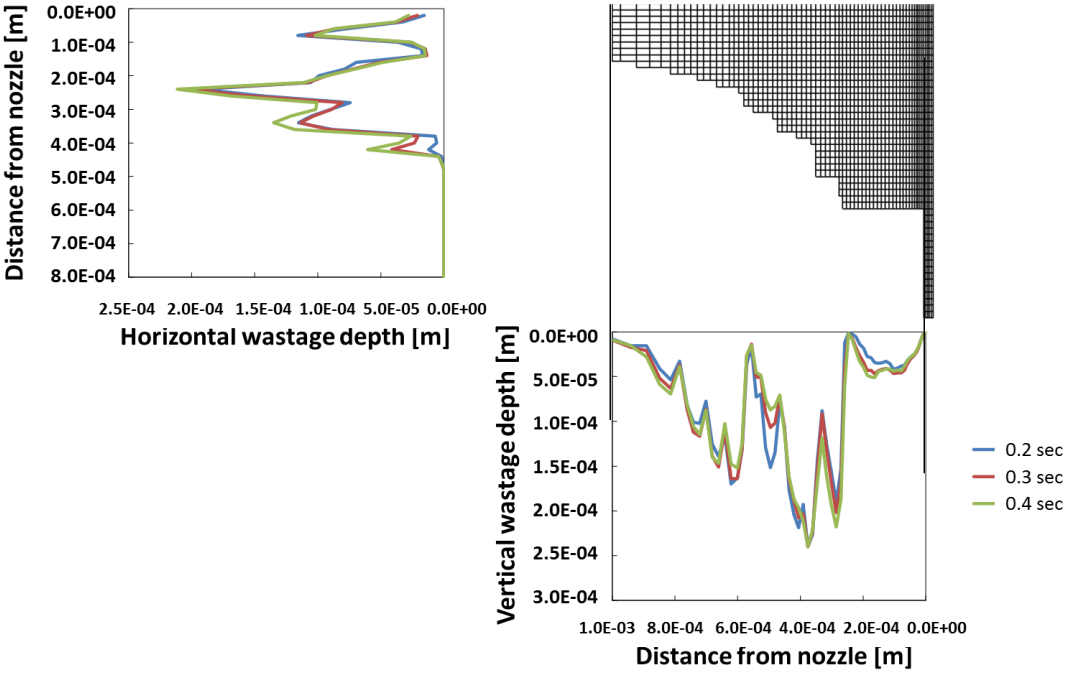

Figure 3.2-9 Estimation of horizontal and vertical wastage amount

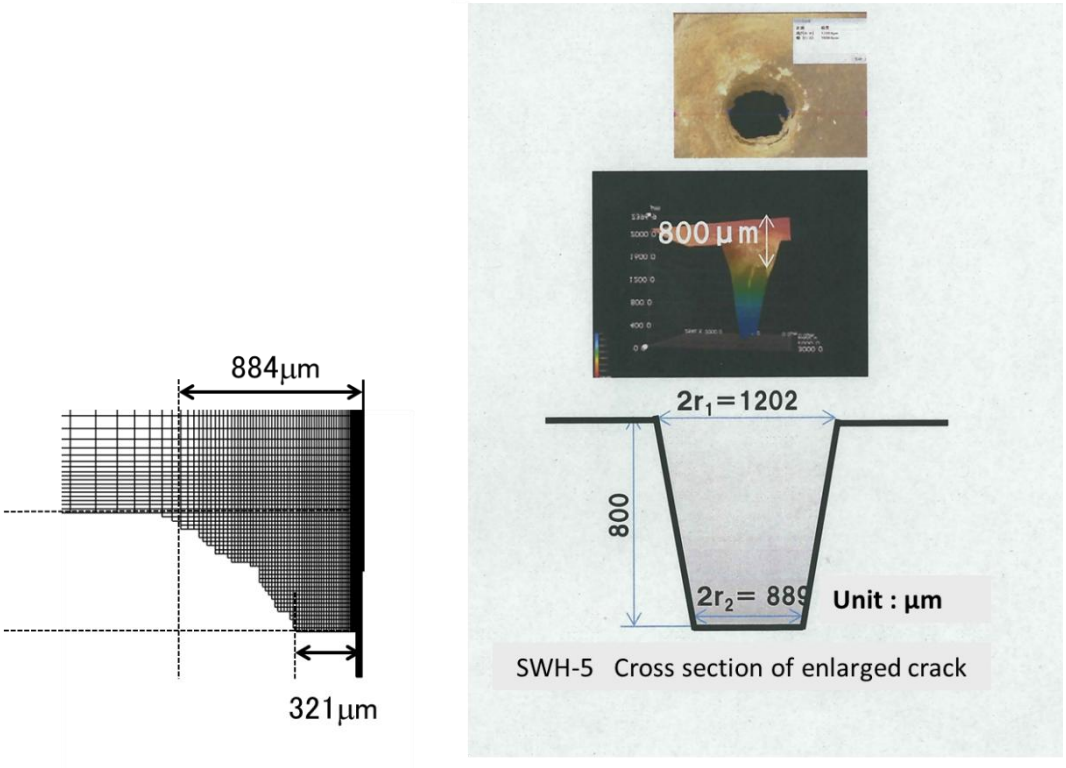

Figure 3.2-10 Comparison of penetrated crack from numerical analysis and experimental result

[REFERENCES]

[1] M. Kuroha, K. Sasaki, H. Kawabe, T. Yamada and M. Sato, "Study of Micro-Defect Self-Wastage Phenomena on LMBR Prototype Steam Generator's Tube." *PNC report,* PNC TN941 82-101, 1982.

[2] M. Kuroha and K. Shimoyama, "Micro-Leak Behavior on LMFBR Monju Steam Generator Tube Materials – Studies of Micro-leak Sodium-Water Reaction, *PNC report*, PNC ZN9410 86-027, 1986.

[3] D.W. Sandusky, "Small-Leak Behavior Summary Report on Scoping Tests", NEDM 14063, General Electric, 1975.

[4] M. Kuroha and K. Shimoyama, op.cit, 1986.

[5] K. Shimoyama, H. Tanabe, Y. Himeno, "Self-Wastage Behavior of High-Chromium Content Steel for FBR Steam Generator tube – Studies of Micro-Leak Sodium-Water Reactions (4)", PNC ZN9410 88-140, 1988.

[6] Internal report not for publication

4 Simulant experiment for Self-wastage phenomena

4.1 Concept of Simulant Experiment

As mentioned earlier in the Ch.1, mock-up test was a major way to evaluate the self-wastage phenomena. However, this conventional approaches have the following limitations [1].

- Liquid sodium is opaque so that observation during the self-wastage phenomena is difficult
- Measurement technology at that time (1970s to 1980s) was immature so that measurement of thermal hydraulic properties is difficult
- Mock-up test consumes a large operating cost, not enough trials were conducted to understand the phenomena.
- Many parameters are related to the phenomena; it is difficult to evaluate the relationship between the parameters with a limited numbers of tests

For example, to understand the behavior of the self-wastage in early stage, the operation is needed to step during the propagation of the self-wastage phenomena and the microscopic inspection of the cross section of tube wall is necessary. However, such data hardly exists.

So we devise a new approach to assessing the self-wastage phenomena through a simulant experiment. This new method focuses on the quantification of the diameter of the enlarged crack by the self-wastage phenomena and the relationship between parameters.

4.1.1 Simulant

Since the self-wastage phenomena are attributed to an exothermic and corrosive chemical reaction that takes place near the outside of the crack, we assumed that it can evaluate the damage on the surface of the crack by making an exothermic reaction such

as the Neutralization reaction with hydrochloric acid (HCl) solution and sodium hydroxide (NaOH) solution [2].

$$HCl_{(aq)} + NaOH_{(aq)} \rightarrow NaCl_{(aq)} + H_2O_{(aq)} + \Delta H \qquad (4\text{-}41)$$

When HCl solution and NaOH solution are mixed, the following neutralization reaction occurs, and the reaction heat is released.

The amount of reaction heat released from the above reaction is 55.6kJ/mol (ΔH= 55.6kJ/mol). Therefore it is expected that when the neutralization reaction takes place, surrounding environment is heated up by the reaction heat. If the temperature in reaction zone, exceeds the melting point of a material, it is imagined that the material would be melted by reaction heat.

So we find that the paraffin wax 115F is a material that has a low melting point (115F, 46.11℃, 319.26K) [3]. So we decide HCl, NaOH, and paraffin wax as a simulant and devise an experiment using this simulant. The following section, the detail of the experiment is introduced.

4.1.2 Concept of Simulant experiment

The self-wastage phenomena is a result of interaction between tube material and an exothermic chemical reaction that takes place around the tube wall. Therefore, if the neutralization reaction that takes places at the nozzle exit, the temperature in the reaction zone will increase. And if the temperature in the reaction zone proceeds the melting point of paraffin wax, it is expected that the surface of paraffin wax melts and the nozzle will be enlarged. We assume that this procedure may reproduce the self-enlargement of the nozzle.

Figure 4.1-1 shows the concept of the experiment phenomena [6].

(a) The self-wastage phenomena are attributed to a chemical reaction followed by reaction heat and corrosive effect of the reactant that takes place at the initial crack site.

(b) The wastage starts from the sodium side and advances through the tube wall. As

the failure propagation advances by the self-wastage, the reaction zone would migrate toward the water/vapor side. The corrosive reactant becomes easily reaches the tube wall. Thus, the self-wastage phenomena would be accelerated. In this stage, the leak rate would be stable in a certain range.

(c) If the wastage reaches the water side, resultant leak rate will sharply increase then the sodium water reaction zone moves to the sodium side so that the corrosive reactants seldom reach the tube wall. Thus, the self-wastage phenomena will be mitigated.

(d) In the experiment, hydrochloric acid solution (HCl) and sodium hydroxide solution (NaOH) are used as the simulant. Paraffin wax ($C_{25}H_{52}$) which has a low-3 point (115oF, 319.26 K) is chosen as simulant for the nozzle that represents the heat transfer tube. In the experiment, HCl solution is injected to the reaction tank that is filled with NaOH solution so that the neutralization reaction would take place in the leaked exit and the reaction heat would be released.

(e) The temperature of the surface of the wax would increase, and if the temperature exceeds the melting point of the paraffin wax, the surface of the wax will be melted. Thus, the size of the nozzle would be enlarged. The resultant leak rate is controlled by the minimal diameter of the nozzle. So investigating the minimal width and the shape of the enlarged nozzle hole, the effect of the self-wastage on the heat transfer tube wall are evaluated.

A schematic experimental apparatus is shown in Fig.4.1-2. The experimental setup consists of a reaction tank, a paraffin wax nozzle and a solution supply system. HCl solution is injected to NaOH solution through a paraffin wax nozzle.

To evaluate the feasibility of the simulant experiment, a numerical simulation is carried out as a scoping phase of the study.

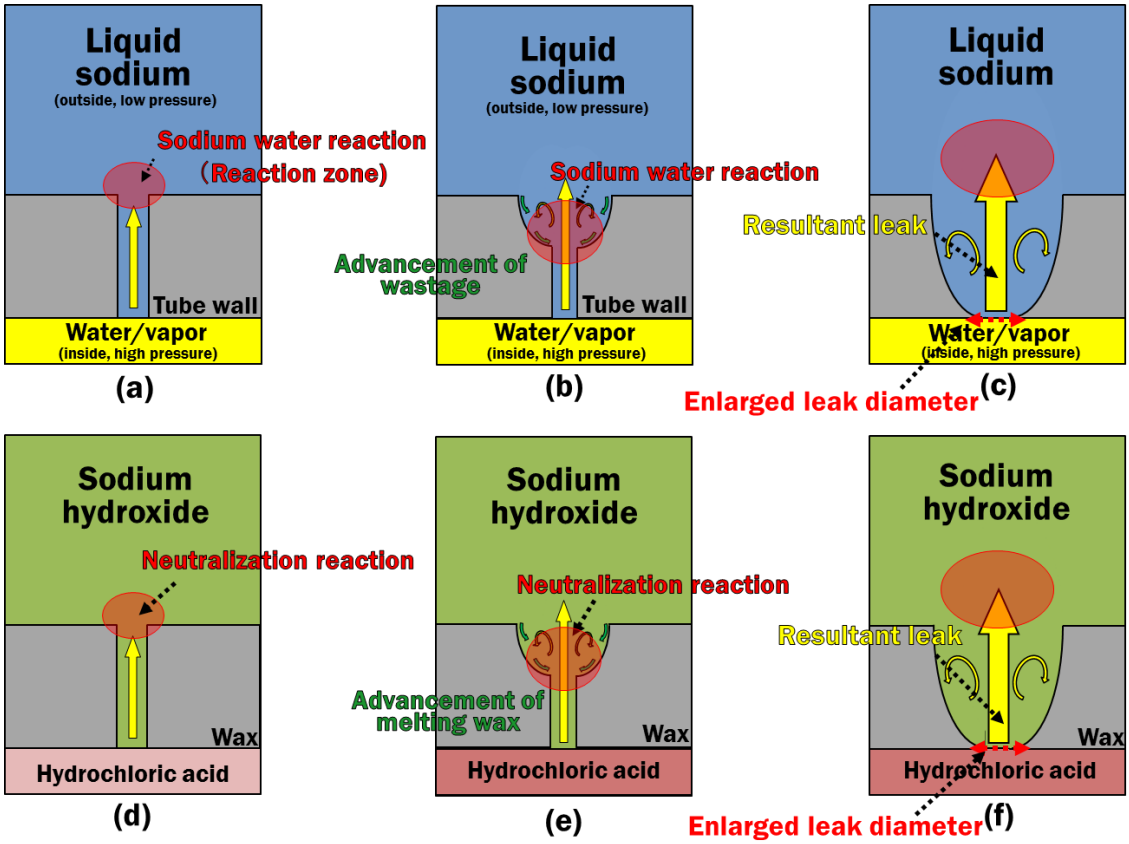

Figure 4.1-1 Concept of simulant experiment

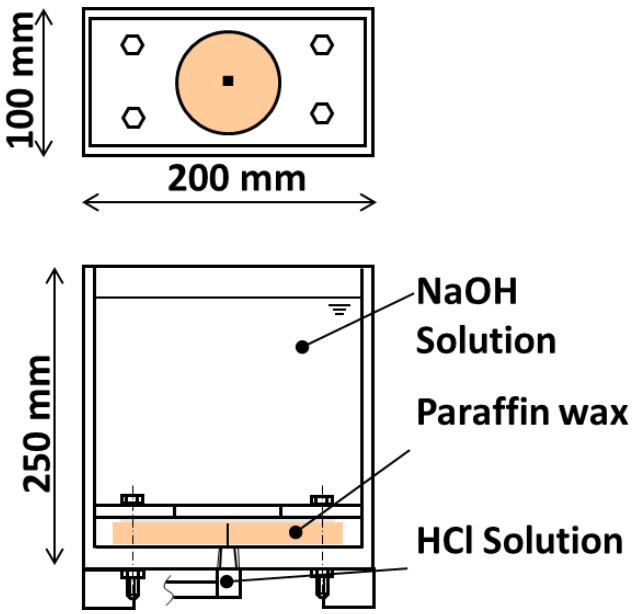

Figure 4.1-2 Experiment apparatus of simulant experiment

4.2 Feasibility analysis of Simulant experiment

To evaluate the feasibility of the new approach and decide experimental condition, 2 dimensional analysis is devised. The detail will be explained in the following section.

4.2.1 Governing equation

In this study, a two-dimensional transient flow with the chemical reaction is considered. The conservation equation for chemical species is given by the following [5]

$$\frac{\partial}{\partial t}\left(\rho Y_i\right)+\nabla\cdot\left(\rho\vec{v}Y_i\right)=-\nabla\cdot\vec{J}_i+R_i \tag{4-42}$$

Where

R_i : net rate of production of mass of species

Y_i :molar concentration of species j in reaction r

$\vec{J}_i$: diffusion flux of species i

In Eqn. (10), $\vec{J}_i$ is the diffusion flux of species i, which arises due to concentration gradients, under the diffusion flux can be written as

$$\vec{J}_i=-\rho D_{i,m}\nabla Y_i \tag{4-43}$$

Here,

$D_{i,m}$: molecular diffusion coefficient for species i in the mixture

In aqueous solution, the diffusion coefficient $D_{i,\mathrm{m}}$, which is called Electrolyte diffusion coefficient, can be given as

$$D_i=\frac{|z_1|+|z_2|}{|z_1||z_2|}\left(\frac{1}{|z_1|D_1}+\frac{1}{|z_2|D_2}\right)^{-1} \tag{4-44}$$

D_1, D_2 : molecular diffusion coefficients of the individual ions

z_1, z_2 : valences of the ions

The D_1, D_2 can obtain from the Stokes-Einstein equation as shown below [7].

$$D_{i(i=1,2)} = \frac{kT}{6\pi\mu R_i} \tag{4-45}$$

The viscosity of the m (in this study, it is water), and R_i is the radius of solute.

For the reaction rate, the laminar finite-rate model is adopted. This computes the chemical source terms using the Arrhenius expression. The net source of chemical species i due to reaction is computed as the sum of the Arrhenius reaction sources over the N_R reaction that the species participate in

$$R_i = M_{w,i} \sum_{r=1}^{N_R} R_{i,r} \tag{4-46}$$

Where $M_{w,i}$ is the molecular weight of species i and $R_{i,r}$ is the Arrhenius molar rate of creation/destruction of species i in reaction r. The reaction may occur in the continuous phase at wall surfaces.

The molar rate of creation/destruction of species i in reaction are given by

$$R_{i,r} = k_F \left[C_{j,r} \right]^{\left(\eta'_{j,r} + \eta''_{j,r}\right)} \tag{4-47}$$

Where

k_F :rate constant for reaction

$C_{j,r}$:molar concentration of species j in reaction r

$\eta'_{j,r}$:rate exponent for reactant species j in reaction r

$\eta''_{j,r}$:rate exponent for product species j in reaction r

For the neutralization reaction with HCl and NaOH, the rate exponents are 1

respectively. Thus, the molar rate of creation/destruction can be written as

$$R_{i,r} = k_r [HCl][NaOH] \tag{4-48}$$

The rate constant (k_r) is defined according to Arrhenius equation, like the following. Eqmentioned earlier in Ch.2 does not depend on the concentrations of reactant but the temperature. It is computed using the Arrhenius equation.

$$k_r = A_r \exp\left(-\frac{E_a}{RT}\right) \tag{4-49}$$

Where

k_F :rate constant for reaction

A_r :pre-exponential factor (mol-1m3s-1)

E_a :activation energy for the reaction (Jmol-1)

R :universal gas constant (Jmol-1K-1)

One similarity between the simulant experiment and the self-wastage phenomena is that considering the reaction mechanism of the neutralization reaction and the sodium water reaction, the reaction rate is expressed by the Arrhenius equation as Eq 2-10 and Eq 4-7. And it is also expected that the melting of paraffin wax and the self-wastage phenomena are proportional to the reaction rate.

In the following section, the numerical procedure for the feasibility analysis is introduced.

4.2.2 Numerical procedure

Figure 4.2-1 explains a concept and a numerical procedure of the simulant experiment.

In the feasibility analysis, 2-dimensional analysis is also adopted since the nozzle enlargement dominantly takes places toward nozzle horizontal and vertical direction

The numerical approach is estimating the self-enlargement of the nozzle consists of the

two parts, (1) construction of the analytical model (2) the nozzle enlargement evaluation. The analytical model was derived to achieve the geometric and dynamic similarity between the analytical model and the prototype experiment. The melting of wax is assumed that happen according to (amount), temperature contour in the nozzle. Some the crack progresses according to the crystal face of the material in case of micro-crack in general [4]. The transient calculation is carried out, and the temperature contour is obtained after several seconds when the temperature around the nozzle exit become stable.

It is difficult to reproduce a transient behavior of melting the wax by the reaction heat, a stepwise numerical procedure are devised.

Step I: determine an initial nozzle size. To determine the nozzle width, SWAT-2 experiment data was used. To achieve dynamic similarity between the SWAT experiment and the numerical analysis, Reynolds number of the numerical analysis was determined to be equal to that of the SWAT-2 experiment. The geometric similarity is also considered by setting the aspect ratio of the nozzle has the same value of the SWAT experiment.

Step II: perform a transient calculation up to a few seconds until the reaction gets to be stable

Step III: In this analysis, we assume that the wax melts according to its contour of the melting point. When the calculation reaches stable condition, temperature contour around the exit of the nozzle is obtained.

Step IV: the new mesh grid is produced by replacing the solid area where the temperature exceeds 319.26 K to liquid cells along the isothermal line of the wax melting point.

Step V: iterate the computation from the step II to the step IV until the enlargement reached the HCl side.

Step VI: Evaluate the size of the enlarged Nozzle.

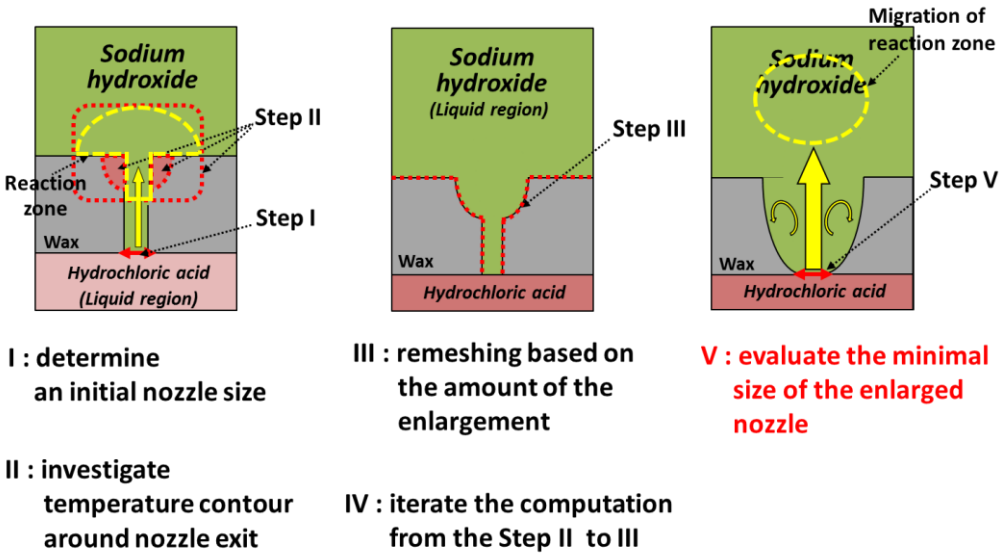

Figure 4.2-1 Numerical procedure of feasibility analysis

4.2.3 Numerical conditions

Figure 4.2-2 shows two-dimensional analytical area and its mesh arrangements. The region consists of the reaction tank, the paraffin wax, and the nozzle. The height of the computational region (reaction tank) is decided to take an enough margin to evaluate the phenomena. Thus, the height of the computational domain of the reaction tank is 150 mm, the width of that is 100 mm. As regards with the nozzle, it is decided to have a high ratio like the SWAT experiment. Since the aspect ratio of the nozzle is about 1:100 to 1:200, the width of the simulant experiment is decided to be 0.2 mm, and the height of the nozzle thickness is 2.0 mm [8]. As shown in Fig.4.2-2, only the mesh of the width of the initial nozzle with the Cartesian coordinates is adopted and is divided equally into 11 (I). The meshes of the other region are divided into 111 (I) × 59 (J) for reaction tank, 50 (I) × 42 (J) for the wax, and each element increases with the ratio of 1.1. The total number of the meshes is approximately 12,000.

For the boundary condition, the constant inlet velocity is applied to the inlet and the constant pressure condition was adopted for the outlet boundary. The inlet velocity is decided to have the same Reynolds number of the SWAT-2 experiment so that the similarity of the flow behavior in the computation is ensured. The heat conduction at the

surface of the wax is considered to evaluate the temperature increase by the reaction heat. Further computational conditions are summarized in Table 4.2.1.

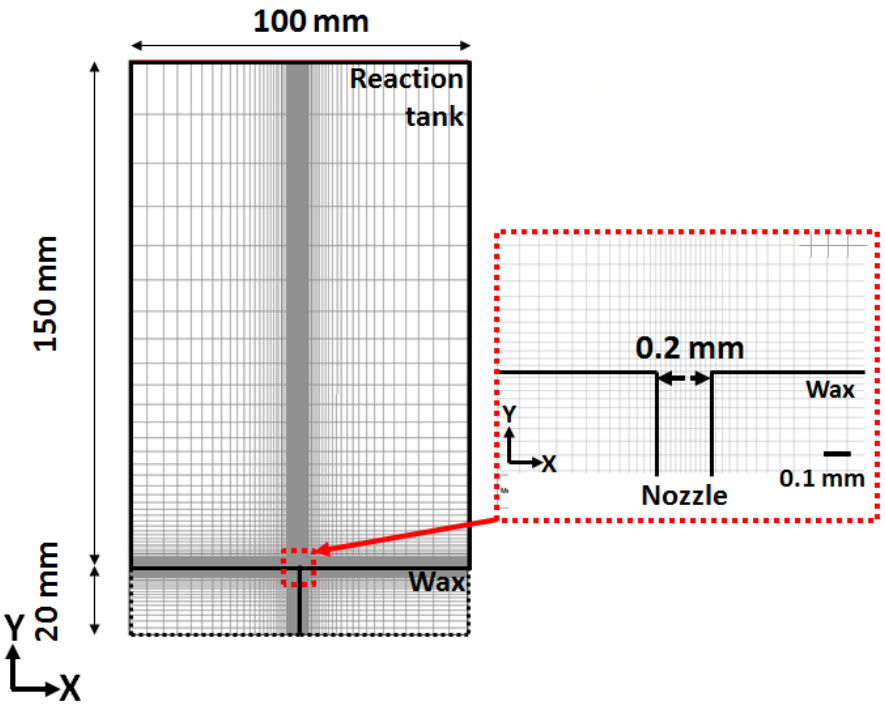

Figure 4.2-2 Numerical mesh grid for feasibility analysis

4.3 Numerical results

4.3.1 Mesh sensitivity analysis

Before carrying out an initial analysis, the preliminary analysis is carried out to check mesh sensitivity. Three different mesh grids are used as shown in Fig.4.3-1. All these 3 meshes have the same nozzle width and number of the cell for the nozzle (10 meshes). However, each mesh grid has 6, 10 and 16 division for the same length in the vicinity of the nozzle.

Figure 4.3-2 shows the temperature distribution at the surface of the nozzle top of the three meshes. In this figure, the red dot-dashed line represents the melting point of the paraffin wax. The temperature is averaged over 5 seconds. For all meshes, the temperature at the surface has almost same distribution. All mesh have the same maximum temperature (331.2K) at the same place. Therefore, the mesh grid that has less cell is decided to be used for the analysis.

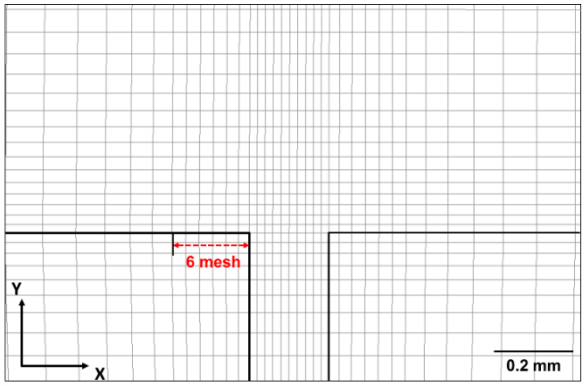

(a) 6 mesh

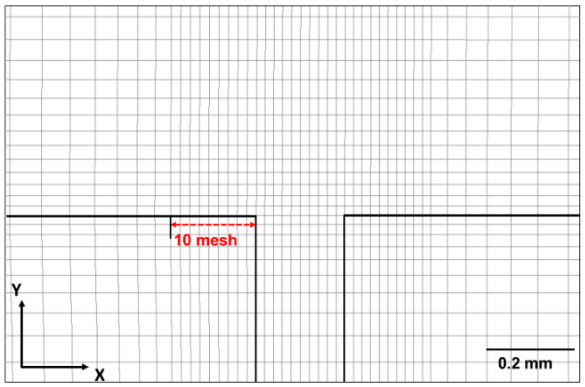

(b) 10 mesh

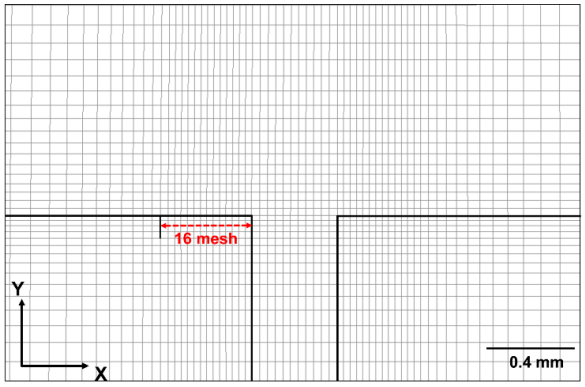

Figure 4.3-1 Three different mesh grids for mesh sensitivity evaluation

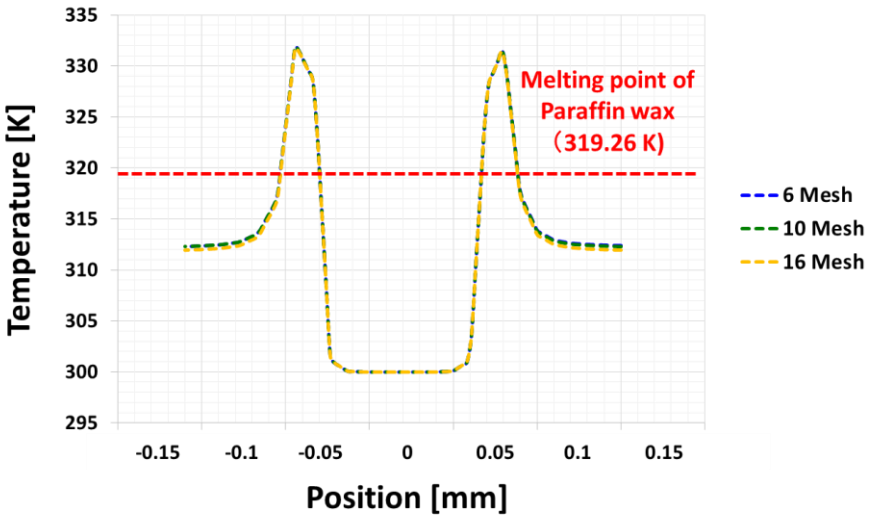

Figure 4.3-2 Temperature distribution of 3 different mesh grid at wax top

4.3.2 Initial analysis

Figure 4.3-3 shows temperature contour around the nozzle exit at different times.

The red line on the temperature contours indicates the melting point of the paraffin wax (319.26K). Thus a white-colored region inside the red line, indicates the region where the temperature exceeds the melting point of paraffin wax. Here, we called this area as 'Meting region'. Accordingly it is expected that the wax in this area would be melted by the reaction heat. As time passes, it is shown that the melting region becomes smaller and locates beside the nozzle exit. It indicates that in an early stage the neutralization reaction occurs inside the nozzle and move toward downstream, and later the reaction take place at the nozzle exit. After 1 sec, it seems that the melting region does not change. Thus, it is expected that the neutralization reaction reaches a stable state. To check that the calculation reaches a stable state, the transient temperature distribution on the top of the wax was obtained in Fig. 4.3-4.The temperature slight changes less than 0.5 sec; however, temperature change on the top of the wax does not distinguish from 0.5 sec to 10.0sec.

Molar fraction, reaction rate and velocity vector around the nozzle exit at 10 seconds are given in Fig. 4.3-5. It shows that the place where neutralization reaction takes place and the melting zone are coincident. Figure 4.3-6 shows the temperature distribution on the top of the wax at 10 sec. In this figure, the red dot-dashed line indicates the melting point of the paraffin wax and green dotted area indicates the width of the nozzle (0.2mm). It is shown that the surface temperature of the wax right beside the nozzle increases over the melting point. The width of this area is approximately 0.035 mm. Since we assume that the wax would melt along the temperature contour line of the melting point, according to the contour line of the melting point, the meshing procedure is carried out (Fig. 4.3-7-a). As a result, an enlarged mesh grid is obtained (Fig. 4.3-7-b). Using the new mesh grid, the further numerical calculation is carried out according to the numerical procedure.

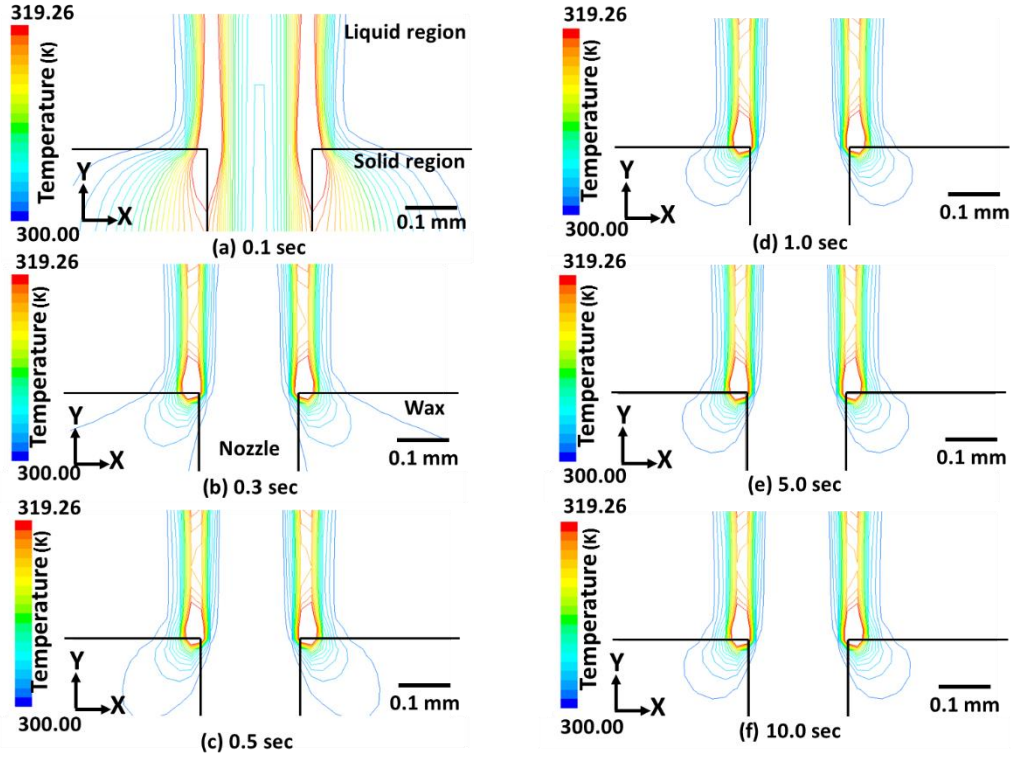

Figure 4.3-3 Temperature contour around the nozzle at different time

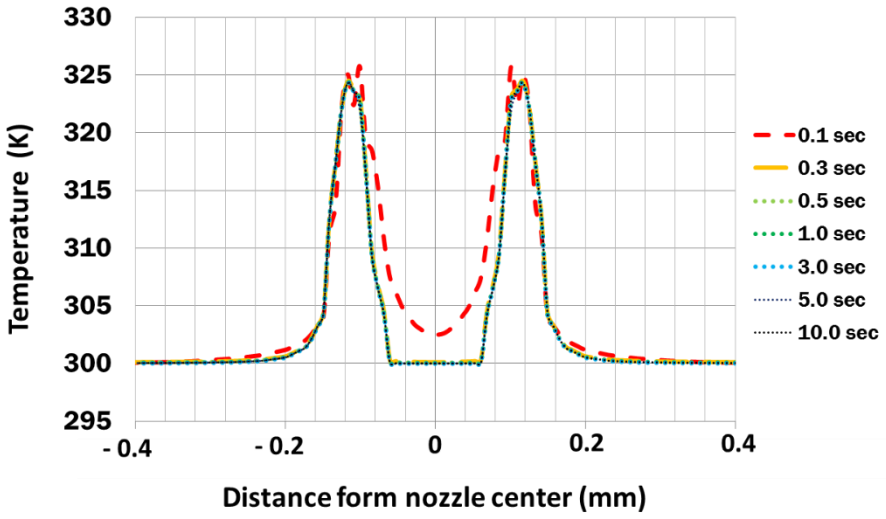

Figure 4.3-4 Temperature distribution on wax top at different times

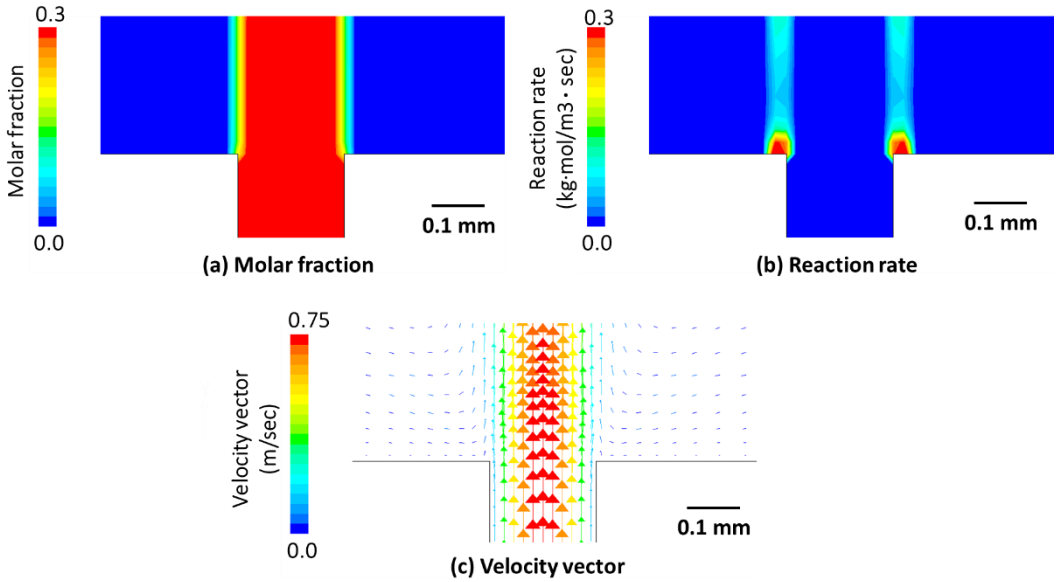

Figure 4.3-5 Molar fraction, reaction rate and velocity vector

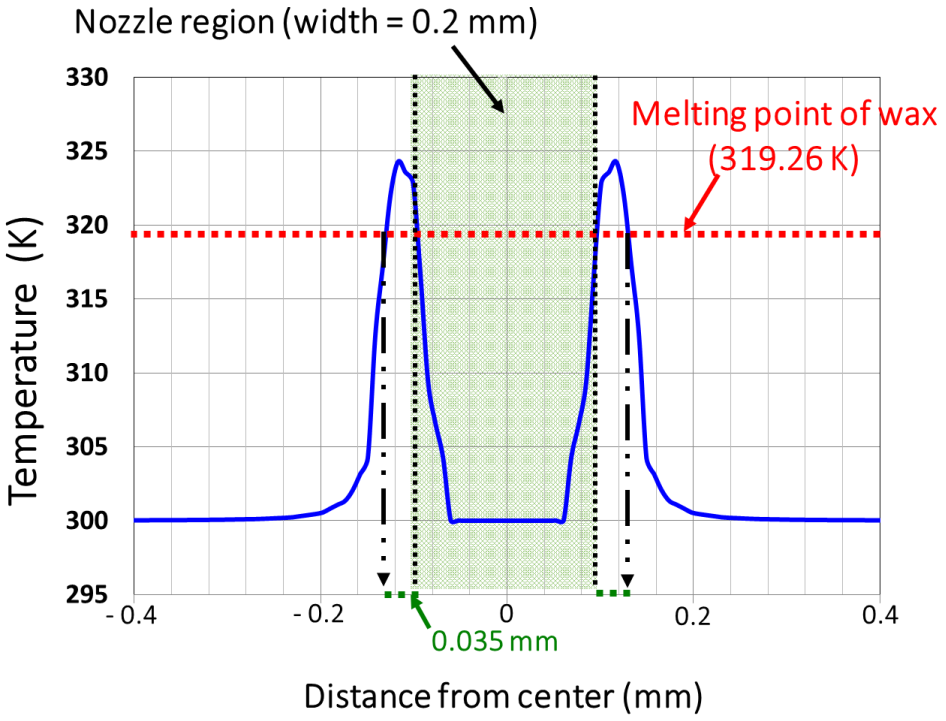

Figure 4.3-6 Temperature distribution at surface of wax top

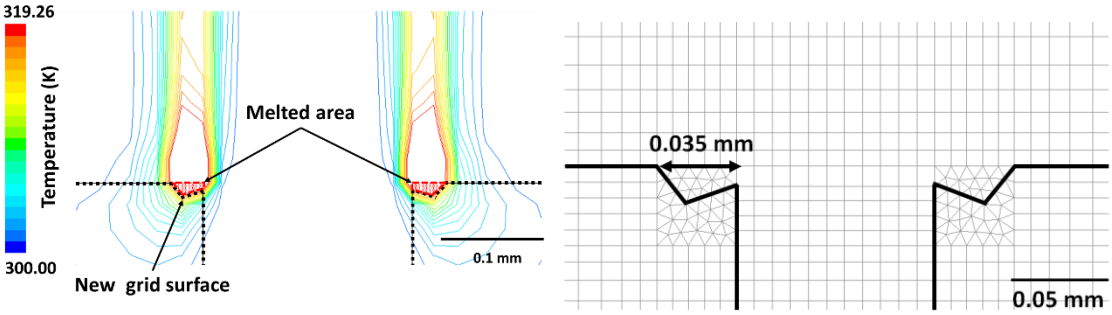

(a) Temperature contour (b) Mesh grid after remeshing

Figure 4.3-7 Remeshing procedure

4.3.3 Further analysis

Using the remeshed grid in Fig.4.3-7, further calculations are performed under the same numerical condition of the initial calculation. In total 75 calculations until the thickness of the remained wall on sodium side become 3 mm. Figure 4-3-8 shows the temperature contour around the nozzle in an early stage. The black-dotted line is the melting point of the paraffin wax. Thus, the contour represents the surface of the newly enlarged nozzle. As we can see, the nozzle enlargement takes place toward both horizontal and vertical direction by having a symmetric concave shape. However, as the simulation goes further, the results of the outline of enlarged nozzle show that the nozzle enlarges in an unsymmetrical way (Fig. 4.3-9). In other words, the nozzle enlargement takes place dominantly in one side. This result is brought due to the direction change of flow. As shown in Fig. 4.3-10, at first, in the early stage of the self-enlargement, the injected HCl has a stable flow pattern, flow straightly toward downstream.

However as the wax is enlarged, the injected flow of HCl was fluctuated by the reaction, these bring the unsymmetrical shape of the enlarged nozzle. As the calculation proceeds, it seems that the shape of the enlarged nozzle looks like almost symmetric. Since almost every cross section of enlarged nozzle have a symmetric geometry in the experiment. We assume that until the enlargement of the nozzle reaches a certain size, the nozzle would be melted in having a symmetric shape. However, when the enlarged nozzle exceeds a certain scale, the flow of injected HCl is disturbed, and it brings an unsymmetric enlargement of the nozzle. Hence, as calculation goes on, the disturbance of the flow brings another almost symmetric surface of the enlarged nozzle. Accordingly from the 40th calculation, even though the estimated enlarged nozzle shape is unsymmetrical, it is assumed that the enlarged nozzle has a symmetric shape.

After carrying out 75 calculations, it is found that the enlargement advances until 15 % of the initial tube thickness. As mentioned earlier, in the real condition high-pressure is working on the steam side (inside of the tube), so that when the remaining tube wall reaches certain thickness, the remaining diaphragm of the wall would be removed by the steam jet. As a result, the width of the crack will be enlarged, and the remaining wall thickness will also be increased. In this study, it is assumed that the when the remaining wall thickness become 15% of the original thickness, nozzle

enlargement on HCl side take place, and the nozzle is regarded as penetrated. Figure 4.3.-11 shows the shape of the completely enlarged nozzle. It has a funnel shape that the diameter of nozzle increase toward the downstream. The enlarged diameter of the nozzle is 35.2 mm.

We put the surface of enlarged nozzle together in Fig. 4.3-12. As shown in the figure, it is notice that the nozzle enlargement takes place along the nozzle wall toward the inlet direction. At first the nozzle enlargement takes places toward almost equally toward the both horizontal and vertical direction. Once the outlet diameter become larger than a certain scale, horizontal enlargement is almost twice faster than vertical enlargement. The maximum horizontal enlargement is 35.0 mm, and the maximum vertical enlargement is 17.0 mm.

There exist only a few measured data of the enlarged outer diameter in the SWAT-2 experiment. It is reported that a large-scale corrosion was observed at the surface of the tube wall in outside, and the diameter of the area is approximately a few millimeters. Since the width of initial crack is about 10 ~ 50 micrometer, the enlargement ratio is about 20 ~ 500. In this study, the ratio of the enlarged nozzle width and the initial width was 176. It is hard to say that the simulant experiment is correctly evaluated the self-wastage phenomena, however, also concerning the geometry of enlarged nozzle, the simulant material experiment has some possibility to reproduce the self-wastage phenomena (Fig.4.3-13)

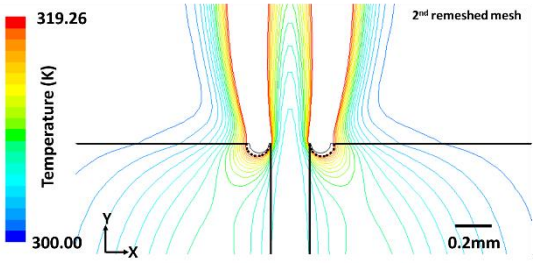

2nd remeshed grid

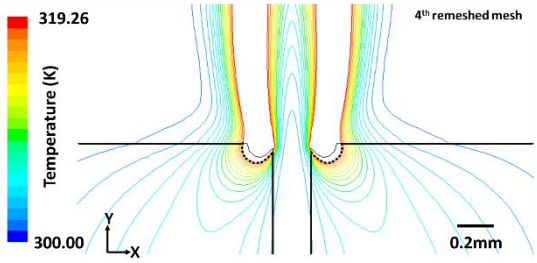

4th remeshged grid

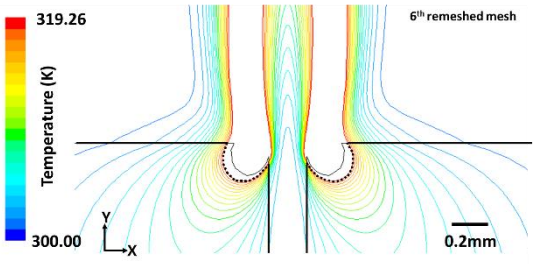

6th remeshed grid

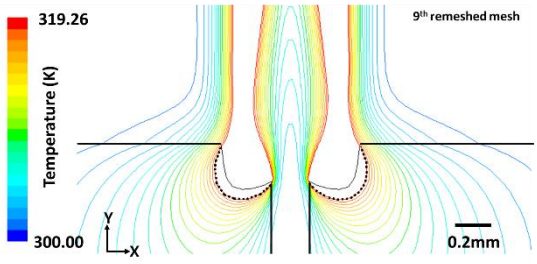

9th remeshed grid

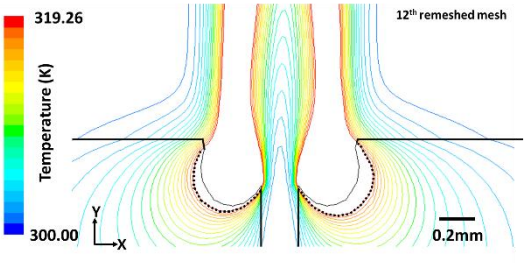

12th remeshed grid

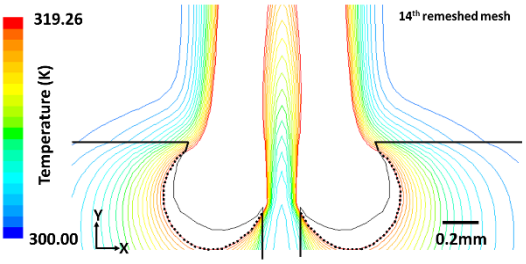

14th remeshed grid

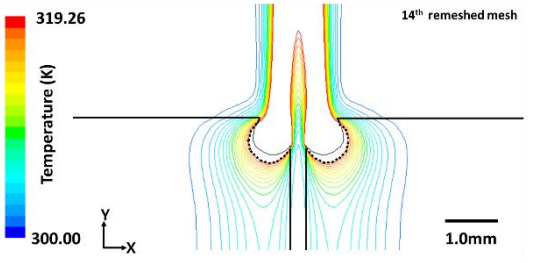

14th remeshed grid (wide view)

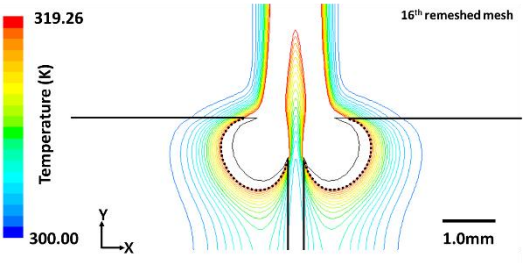

16th remeshed grid

Figure 4.3-8 Temperature contour and nozzle enlargement propagation (2nd to 16th grid)

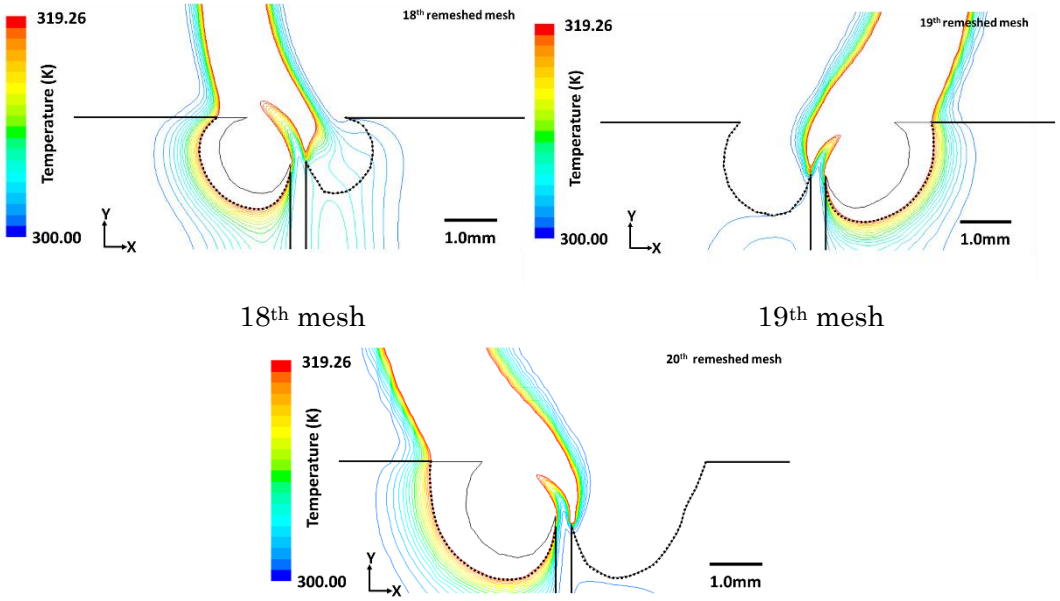

18th mesh　　19th mesh

20th mesh

Figure 4.3-9 Temperature contour and nozzle enlargement propagation (18th to 20th grid)

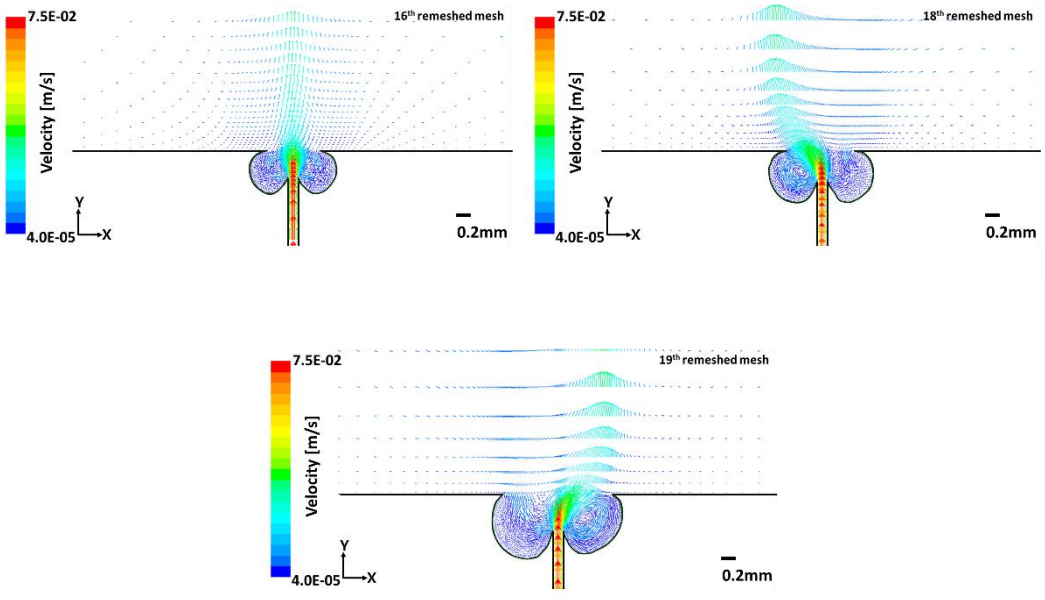

Figure 4.3-10 Velocity vector distribution around the nozzle exit

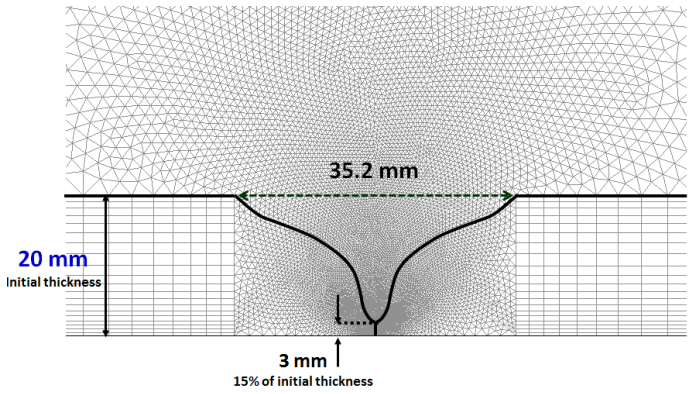

Figure 4.3-11 Mesh grid of completely enlarged nozzle

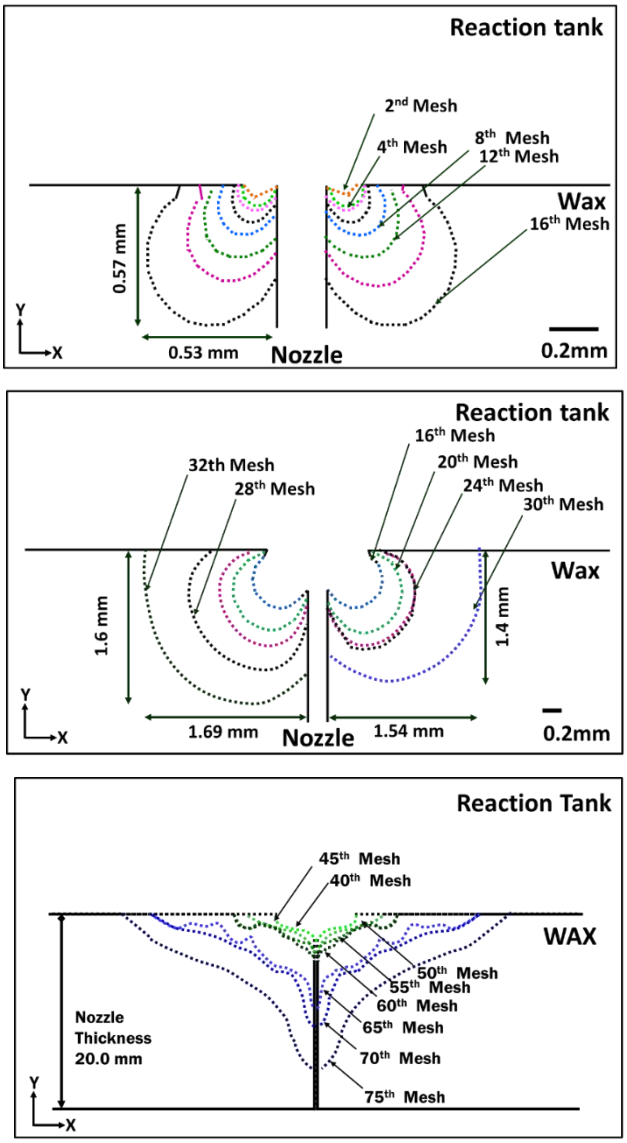

Figure 4.3-12 Outline of enlarged nozzle (45th mesh to 75th mesh)

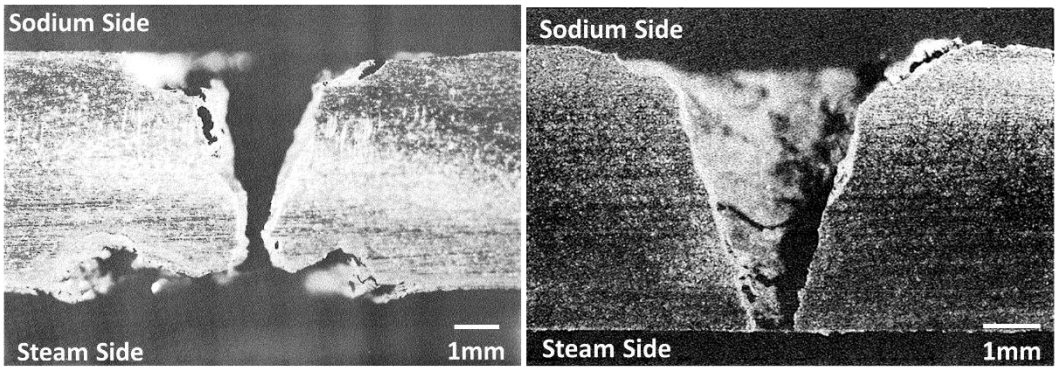

Microscopic view of cross section for completely enlarged nozzle

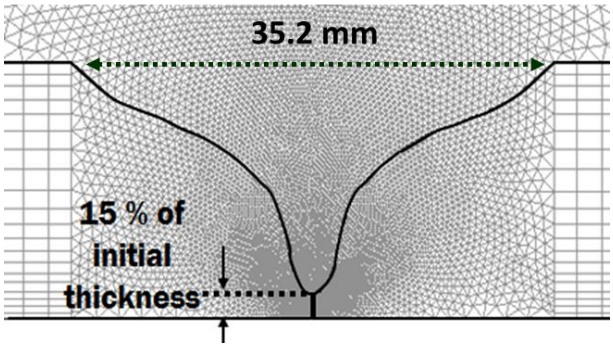

Numerical mesh for completely enlarged nozzle

Figure 4.3-13 Comparison of cross section of the enlarged nozzle

[REFERENCES]

[1] Hori, M. "Sodium/Water Reactions in Liquid Metal Fast Breeder Reactions," Atomic Energy Review, 183, pp.707-778, 1980.

[2] M. Eigen, “Untersuchungen über die kinetik der neutralization I,” Z. Elektrochem., 59, pp.986-993, 1955.

[3] Nippon Seiro Co.,Ltd. “Products guide”.(Http://seiro.co.jp/e/product.html#t01)

[4] S. Jang, T. Takata and A. Yamaguchi, “A Preliminary Numerical Analysis of Self-wastage Phenomena of Micro Leak Caused by Sodium-water reaction in Sodium-cooled Fast Breeder Reactor through Simulant Experiment”, The 10th International Topical Meeting on Nuclear Thermal-Hydraulics, Operation and Safety (NUTHOS-10), NUTHOS10-1252, Okinawa, Japan, 2014.

[5] Fluent, “Fluent 6.3 User’s Guide,” Fluent Inc. Lebanon, New Hampshire, USA , 2006.

[6] Y.Ohnishi, T.Takata and A.Yamaguchi, “Numerical Approach of Self-Westage Phenomenon in Steam Generator of Sodium-Cooled Fast Reactor”, NTHAS8: The Eighth Japan-Korea Symposium on Nuclear Thermal Hydraulics and Safety , N8P1070, Beppu, Japan, 2012.

[7] Flory, M., and T. Gimmi, Solute diffusion, in Methods of Soil Analysis, Part 4, Physical Methods, Soil Science Society of America, Madison, pp. 1323-1351, 2002.

[8] M. Kuroha, K. Sasaki, H. Kawabe, T. Yamada and M. Sato, "Study of Micro-Defect Self-Wastage Phenomena on LMBR Prototype Steam Generator’s Tube." *PNC report,* PNC TN941 82-101, 1982.

5 Conclusion

In this study, two alternative way to evaluate the self-wastage phenomena are devised. At first, the self-wastage evaluation model using the SERAPHIM code is devised. The self-wastage evaluation model consists of five stepwise procedures. A transient calculation is carried out using the SERAPHIM code and the gas temperature and NaOH concentration at the tube surface are investigated. These two properties are used by the self-wastage depth evaluation equation to estimate the self-wasted depth at the surface. The new mesh grid that reflects the self-enlargement is obtained by replacing the solid cells to liquid cell according to self-wastage amount depth. This newly remeshed grid is used again for the further analysis. And the above procedures are iterated. Through these procedures, self-wastage phenomena can be reproduced.
A benchmark analysis of SWAT experiment is carried out with a nozzle of the same shape as the experiment under the same condition. Numerical results regarding thermo-physical properties around the nozzle shows that the SWR is well reproduced by the SERAPHIM code. Also, self-wastage propagation is found that it starts from the sodium side advances to the steam side through the tube wall. As a result of the analysis, the enlarged nozzle is obtained. The enlarged nozzle appeared to taper inward to a significantly smaller opening on the inside of the tube wall. The outer diameter is 4.72 mm. These results show good agreement with SWAT-2 results regarding the enlarged crack width (4.96 mm) on the sodium side and the shape. The numerical benchmark analysis demonstrates the applicability of the self-wastage evaluation model to evaluate the self-wastage phenomena.

Secondly, the influence of parameters on the self-wastage phenomena are considered. Among many parameters, the influence of the averaged leak rate and initial leak diameter are considered. It is found that enlarged orifice diameter is in the range of 0.4 mm to 1.4 mm. It seems that the enlarged diameter does not affect the averaged leak rate and the initial leak diameter. However, the enlargement ratio and the average leak rate, the initial leak diameter has a negative reciprocal relationship. Especially initial leak diameter has a strong negative reciprocal relationship with the enlargement ratio. Self-wastage rate and the average leak rate has a strong positive correlation.
Thus, quantification of the influence of this parameter on the self-wastage phenomena is needed to be evaluated.

Finally, simulant experiment is devised to understand the self-wastage phenomena. HCl, NaOH solution, and paraffin wax are adopted as simulant materials. Melting of nozzle surface of paraffin wax by the reaction heat released by the neutralization reaction represents the self-wastage phenomena. Through a feasibility analysis, it is demonstrated that the maximum temperature at the surface is high enough to melt a surface of paraffin wax. Like the self-wastage phenomena propagation, a propagation of also melting take place around nozzle exist then, it advances through the tube wall toward the inlet direction. The enlarged nozzle also to taper inward to a significantly smaller opening on the inside of the tube wall. Feasibility of the simulant experiment is confirmed.

These studies consider two different alternative way of evaluating the self-wastage phenomena. Quantification of each method is necessary to consider to improve an accuracy of these approaches.

ACKNOWLEDGEMENT

One day in 2008, I heard about Monju prototype fast breeder reactor for the first time during my class in Osaka University, it was the beginning of this dissertation. This dissertation would not have been possible without the help of so many people in so many ways.

I would like to express the deepest appreciation to Professor. Akira Yamaguchi for his guidance and sincere supports. For 5 years, it is really great opportunity for me to learn from him as his students. I could learn necessary knowledge and refinement as a researcher by watching his fine examples. Especially I could develop an ability that how I devise and conduct a research which has its own originality.

I also would like to express my sincere gratitude to Associate Professor Takashi Takata. Without his full and kind supports, I could not finish my dissertation. I also appreciate his generosity and endurance that he showed me for 5 years. It is also good example for me how I take care of students and give them some advice and comments. He generally teaches me about Japanese academic culture, manners and etiquette. It becomes valuable asset for me and helps me a lot in my future carrier.

I also thank to my committee member, Professor Takeshi Fukuda for his kind backing. Even though I made a big mistake while I am preparing my dissertation, He sincerely tried to help me to redeem my errors. I also would like to express my appreciation to my committee member, Associate Professor Eiji Hoashi.

In addition, I would like to thank to Dr. Hiroyuki Ohshima, Dr. Akikazu Kurihara and Dr. Akihiro Uchibori of Japan Atomic Energy Agency for their academic guidance regarding Sodium-water reaction research. I thank to Ms. Azuma and Ms. Matsubara for their kind helps and supports regarding office works.

Also I am happy to spend my academic years in Quantum Engineering and System Design laboratory with my colleague.

A special thanks to my family in Korea and Japan, especially to Masumi for her sincere and loyal supports. I also really want to say thank you to my father who are in now deep sleep. When I meet him again in near future, I really want to show my great appreciation and affection to him.

I hope that my research and work become contributions to achieve a practical application of Sodium-cooled Fast Reactor technology.

List of Published Paper

[Full paper]

1. S. Jang, T. Takata and A. Yamaguchi, "Numerical Analysis of Self-wastage Phenomena Caused by Sodium-water reaction in Sodium-cooled Fast Reactor through Simulant Experiment", *Journal of Energy and Power Engineering*, Vol. 9 No.6, pp. 539-547, 2015.

2. S. Jang, T. Takata, A. Yamaguchi, A. Uchibori, A. Kurihara and H. Oshima, "Numerical Approach for Quantification of Self-wastage Phenomena in Sodium-cooled Fast Breeder Reactor", *Nuclear Engineering and Technology*. (Accepted)

3. S. Jang, T. Takata and A. Yamaguchi, "Numerical Design Study of Self-wastage Experiment Using Simulant Material in Sodium Fast Reactor", *Nuclear Engineering and Technology*. (Under review)

[International conference]

1. S. Jang, T. Takata and A. Yamaguchi, "Numerical Investigation of Self-wastage Phenomenon using a Simulant Materials", 8th KSME-JSME Thermal and Fluids Engineering Conference (TFEC8), TFEC8-GSF24-016, Mach 18-21, 2012, Incheon Korea

2. S. Jang, T. Takata and A. Yamaguchi, "Numerical Investigation of Experimental Methodology for Simulating Self-wastage Phenomenon using Simulant Materials", *8th Japan-Korea Symposium on Nuclear Thermal Hydraulics and Safety (NTHAS-8),* NTHAS8-N8P1118, December 9-12, 2012, Beppu, Japan.

3. S. Jang, T. Takata, A. Yamaguchi, A. Uchibori, A. Kurihara and H. Oshima, "Numerical Quantification of Self-wastage Phenomena in Sodium-cooled Fast Reactor", *9th Japan-Korea Symposium on Nuclear Thermal Hydraulics and Safety (NTHAS-9)*, NTHAS9-N9P0078, November 16-19, 2014, Buyeo, Korea.

4. S. Jang, T. Takata and A. Yamaguchi, "Analysis of Self-wastage Phenomena of Micro Leak Caused by Sodium-water reaction in Sodium-cooled Fast Breeder Reactor through Simulant Experiment", *10th International Topical Meeting on Nuclear Thermal Hydraulics, Operation and Safety (NUTOHS-10)*, NUTHOS10-1252, December 14-18, Okinawa, Japan.

5. S. Jang, T. Takata, A. Yamaguchi, A. Uchibori, A. Kurihara and H. Oshima, "Numerical Investigation of Self-wastage Phenomena in Steam Generator of Sodium-cooled Fast Breeder Reactor, *16th International Topical Meeting on Nuclear Reactor*

Thermalhydraulics, NURETH16- 13852, August 30-Septemper 4, 2015, Chicago, USA.